Copy 2

NATIONAL ADVISORY COMMITTEE FOR AERONAUTICS

TECHNICAL NOTE

No. 939

THE INWARD BULGE TYPE BUCKLING OF MONOCOQUE CYLINDERS

II - EXPERIMENTAL INVESTIGATION OF THE BUCKLING IN COMBINED BENDING AND COMPRESSION

By N. J. Hoff, S. J. Fuchs, and Adam J. Cirillo
Polytechnic Institute of Brooklyn

Washington
October 1944

NATIONAL ADVISORY COMMITTEE FOR AERONAUTICS

TECHNICAL NOTE NO. 939

THE INWARD BULGE TYPE BUCKLING OF MONOCOQUE CYLINDERS

II - EXPERIMENTAL INVESTIGATION OF THE BUCKLING IN COMBINED BENDING AND COMPRESSION

By N. J. Hoff, S. J. Fuchs, and Adam J. Cirillo

SUMMARY

This paper is the second part of a series of reports on the inward bulge type buckling of monocoque cylinders. It presents the results of an experimental investigation of buckling in combined bending and compression. In the investigation it was found that the theory developed in part I of the present series predicts the buckling load in combined bending and compression with the same degree of accuracy as the older theory does in pure bending. In the realm covered by the experiments no systematic variation of the parameter n was observed. The analysis of the test results afforded a check on the theories of buckling of a curved panel. The agreement between experiment and theory was reasonably good. In addition, the effect of the end conditions upon the stress distribution under loads and upon initial stresses was investigated.

INTRODUCTION

Large monocoque fuselages reinforced with closely spaced stringers and rings are likely to buckle, when loaded, in a pattern which involves simultaneous distortions of the stringers, the rings, and the sheet covering. This type of buckling is known as general instability. The details of the pattern vary with the loading. When the maximum stress in the fuselage is caused mainly by a bending moment, which may be accompanied by a small shear force, compressive force, or torque, the characteristic feature of the distorted shape is an inward bulge extending

symmetrically from the most highly compressed stringer. In some cases there is a single inward bulge; in others several appear along the most highly compressed stringer, and these may occur when the bending moment is constant over a uniform portion of considerable length of a monocoque cylinder. Often a few shallower secondary bulges appear alongside the main bulges, or the main bulge is displaced slightly because of inaccuracies of manufacture and load application, but in every case so far observed all these distortions were restricted to the general neighborhood of the most highly compressed stringer. This type of general instability is denoted as inward bulge type buckling.

The purpose of the experimental investigation presented here was the verification of the theory of inward bulge type buckling in combined bending and compression as developed in reference 1. Reinforced monocoque cylinders of 20-inch diameter and 33.5-inch length - four cylinders in the preliminary and nine in the final test series - were tested in the Aircraft Structures Laboratory of the Polytechnic Institute of Brooklyn. For their contribution to the development of the manufacturing and testing technique credit is due to Albert J. Cullen and Joseph Kempner. Similarly, the contribution of Bruno A. Boley in participating in the final tests and the evaluation of the test results must be acknowledged.

In the third section of this report the test specimen and the test rig are described. In the fourth section the test results are analyzed. For the calculation of the theoretical buckling stress corresponding to the inward bulge pattern the effective width of the curved panels of sheet must be known. The determination of the effective width in turn presupposes the knowledge of the buckling stress of the curved panels. Moreover, deviations from the theoretical stress distribution influence the magnitude of the load under which the inward bulge develops and it was established in the experiments that at least the location of the bulge is influenced by the initial stresses in the test specimen.

Because of these complex interrelations it was necessary to analyze the various items separately and to proceed systematically from the discussion of the linearity of the strain distribution in bending through the analyses of the uniformity of strain in compression, the initial stress, the buckling of the sheet covering, the

equilibrium of forces and moments, and the strain-bending moment curves of the stringers to the discussion of the critical stress in inward bulge type buckling proper.

The fifth section contains the principal conclusions drawn from the analysis.

This investigation, conducted at the Polytechnic Institute of Brooklyn, was sponsored by, and conducted with financial assistance from, the National Advisory Committee for Aeronautics.

SYMBOLS

A_{str}	cross-sectional area of stringer plus effective width
d	stringer spacing measured along circumference
E	Young's modulus
$f_{c\ cr}$	buckling stress of curved panel
f_{curved}	buckling stress of circular cylinder
f_{flat}	buckling stress of flat panel
F_{cy}	yield-point stress
I_r	moment of inertia of ring plus effective width
I_{str}	moment of inertia of stringer defined in equation (7)
$I_{str\ r}$	moment of inertia of stringer plus effective width for bending in radial direction
$I_{str\ t}$	moment of inertia of stringer plus effective width for bending in tangential direction
k	constant in formula for buckling stress of flat panel
L_1	ring spacing
n	number of rings involved in buckling

n	parameter characteristic of wave length in circumferential direction
P	axial force in cylinder
r	radius of cylinder
t	thickness of sheet
$2w$	effective width of flat panel
$2w'$	effective width of curved panel
ϵ_{cr}	critical strain in general instability
ϵ_{curved}	buckling strain of circular cylinder
ϵ_{flat}	buckling strain of flat panel
ϵ_{max}	observed strain in most highly compressed stringer
ϵ_{str}	strain in stringer
μ	Poisson's ratio
ν	compressive load divided by perimeter

TEST SPECIMEN AND TEST RIG

The test specimen is shown in figure 1. It consisted of a circular sheet metal cylinder of 20-inch outside diameter and 33½-inch over-all length reinforced with 5 equidistant rings of 3/8- by 1/8-inch rectangular section and with 16 equidistant longitudinals of 3/8-inch square section. In order to simplify manufacture stringers were attached internally and rings externally to the cylindrical sheet. Rings and stringers were connected by 1/8-inch round head machine screws. Machine screws of the same size, spaced 0.714 inch apart, secured the sheet to the stringers.

Ring butt splices were arranged alternately to the right and the left of the top stringer. Segments of the ring stock were used as butt straps extending as far as the adjacent stringers and bolted to them. Two more

bolts between the stringers fastened the strap to the ring and the sheet. Rings were made of 24S-T aluminum alloy. Stringers were of 17S-T aluminum alloy except in cylinder No. 13, where they were of 24S-T aluminum alloy.

Cylinders Nos. 9, 10, and 11 were manufactured of four sheets each which were attached to one another by lap joints along top, bottom, and extreme right and left stringers. In these cylinders the sheets had a nominal thickness of 0.012 inch. Actually this thickness ranged from 0.0119 to 0.0122 inch. The material was 24S-T alclad. All the other cylinders were constructed of two sheets each with lap joints along the extreme right and left stringers. The nominal thickness of the sheets for these cylinders was 0.020 inch, while the actual values varied from 0.0199 to 0.0203 inch. The material was 24S-T aluminum alloy.

The test rig is shown schematically in figure 2. The base of the rig consisted of two pairs of 8-inch channels 30 inches apart. The end stand, built of channel sections, was braced to the base by ties and struts. The loading arm was a tripod. It rested on three ball bearings which were free to roll on the supporting table.

The external load was applied by a screw jack which exerted a downward force on the bottom of a rectangular frame suspended from the apex of the tripod loading arm. The reaction to the force was taken up by a second rectangular frame pinned to the base of the rig.

A heavy machined steel ring was fitted to each end of the cylinder. Ring No. 1 was bolted to the end stand, ring No. 2 to the loading head, which like the end stand was a grid composed of steel channels and angles. The considerable weight of the loading head was balanced by means of a counterweight suspended from an overhead frame by a steel cable guided over sheaves. Two parallel links connected the loading arm to the loading head and transmitted to the test specimen the couple caused by the applied load. Front and rear views of the test arrangement are presented in figures 3 and 4.

The test specimen was connected to the end rings by means of the stringer grip fittings shown in figure 5. Each fitting was attached to the ring by two 1/2-inch steel bolts. The surface of contact between stringer and fitting was serrated, and the pressure exerted by the

bolts was found sufficient to maintain an adequate grip.

The compressive force required for the tests in simple compression and in combined bending and compression was applied by means of the compression load bar indicated in figure 2 and shown in the photograph of figure 6. The bar was machined of chromium-molybdenum steel. At one end it was attached to the loading head, at the other, to the end stand. The latter attachment was effected by means of a buttress thread and nut. By tightening the nut with a large ratchet lever the required compressive force was applied to the test cylinder.

The compressive force in the test cylinder was equal to the tensile force in the load bar. The latter was measured by two Baldwin-Southwark SR-4 metalectric strain gages type A-1, cemented to plane surfaces machined at the middle of the load bar. The load applied to the loading arm was measured by the same type of strain gages attached to a load link inserted between the loading arm and the rectangular frame. In all strain measurements the pairs of gages were connected in series in order to obtain average-direct strain values.

The pairs of gages used for measuring strain in the test cylinders were cemented to the stringers. They were arranged in two sections of the cylinder denoted in figure 2 as Band A and Band B, respectively. At each section the strain was measured in every other stringer.

Two Baldwin-Southwark SR-4 control boxes were used to obtain simultaneous readings of bending moment and compressive force. Switching was effected by means of a tapered brass plug and matching brass sockets. All wiring was done with rubber insulated single conductor No. 18 wire. Separate dummy gages were provided for the load link, the compression load bar, and the stringers.

The compression load bar and the load link were calibrated in a Riehle Bros. lever type testing machine.

ANALYSIS AND DISCUSSION OF TEST RESULTS

Presentation of Test Results

The results of the tests are presented in the diagrams of figures 7 to 63. The diagrams may be subdivided

into four main groups. In the first, figures 7 to 28, the measured direct strain is plotted against distance from the horizontal center line of the cylinder. In the second group, figures 29 to 34, the direct strain caused by the compression alone is indicated in polar coordinates. In the third, figures 35 to 45, the initial strains in the cylinders are given in similar polar form, with the exception of the last diagram, figure 45 in this group, which presents the variation of the initial strain in the axial direction. The fourth group, figures 46 to 63, shows the variation of the stringer strain with increasing bending moment.

Linearity of the Stress Distribution in Bending

In the course of the first pure bending tests of the present investigation it was noticed that the direct strain measured deviated greatly from the straight-line law usually assumed to prevail in structures subjected to bending. In order to obtain a better agreement with the assumptions of theory, the loading head was systematically reinforced and the effect of these reinforcements on the strain distribution was observed. The improvement attained may be judged on the basis of a comparison of figures 24 to 25 and 7 to 8, representing the strain distribution in cylinders Nos. 2 and 5, respectively. In cylinder No. 2, although the greater part of the reinforcements already had been added, the deviations from linearity are seen to be still excessive. By contrast, cylinder No. 5, which was the first of the final test series, yields a close agreement with the theoretical assumptions in the A band and a satisfactory agreement in the B band. The strain lines corresponding to high bending moments are slightly concave on the compression side of the B band.

A review of all the strain diagrams reveals that as a rule the strain curves are straight up to about one-half the failing load. In the later stages of loading, when buckling of the sheet becomes pronounced, deviations from linearity appear, especially on the compression side of the cylinder. In most cases these deviations make the compression side of the strain curves convex when the bending moment is accompanied by a high compressive force, and concave when bending moments are applied alone. For each cylinder tested in combined bending and compression, a control test in pure bending was run before the main

test was made. The results of the control test are shown by a dotted line which in no case deviates appreciably from a straight line.

In order to illustrate more clearly the deviations from linearity, figures 26 to 28 are included. These figures show experimental strain curves for typical cases of combined bending and compression at various stages of loading superimposed upon the theoretical straight lines constructed for the corresponding loads.

The development of a linear strain distribution may be interpreted by the principle of least work. A linear distribution corresponds indeed to the least strain energy in a cylinder subjected to pure bending if Hooke's law applies and if the ends of the cylinder are attached to perfectly rigid bodies. In many experimental setups it may be inconvenient to provide very rigid and thus heavy and cumbersome structural arrangements for transmitting the applied forces to the ends of the cylinders. The least work principle then requires that the total strain energy stored in both the cylinder and the attaching structural members be a minimum. The resulting strain distribution may deviate considerably from linearity in such cases. Moreover, the relative rigidity of test specimen and attaching structural elements changes with the type and the magnitude of the loading. Consequently, ideal straight-line strain curves are not likely to be obtained in experiments carried out with a single test rig under various conditions of loading, unless very heavy attaching structural elements are used.

The deviations from the straight-line law obtained in the present experiments were considered permissible in view of the results of the calculations presented under The Effect of Nonlinear Direct Stress Distribution in reference 1. However, the conclusion is drawn from the foregoing investigations that a careful survey of the strain distribution in a monocoque structure subjected to bending is a necessary preliminary to the use of a new test rig or of a new type of test specimen.

It is noted that the compressive forces listed in the diagrams for tests of bending combined with compression are nominal values. The exact values at the various stages of loading are listed in table I.

Uniformity of the Strain Distribution in Compression

After the first successful tests in pure bending were accomplished, the testing of the cylinders in combined bending and compression was undertaken. Trial compressive tests applied to cylinder No. 6 resulted in great deviations from a uniform strain distribution. This may be seen from figure 34. The magnitude of the deviations was unexpected since the satisfactory strain curves obtained in bending had been interpreted as a proof of an adequate rigidity of the loading rig for all types of loading. The fallacy of this conclusion became apparent when the incorporation in the test rig of additional differently arranged stiffening elements and a systematic application of shims, resulted in strain curves sufficiently uniform for practical purposes. Apparently the strain energy balance discussed in the preceding article changes materially from one loading condition to the other.

As a preliminary of the combined bending and compression tests a simple compression check test was run with each of the subsequent cylinders except No. 13. The results of the check runs are shown in figures 29 to 33, and the maximum deviations from the uniformity of the strain are listed in table II. The maximum deviation from the average strain was 8.17 percent for the four cylinders having the thick sheet, 15.31 percent for the two having the thin sheet.

Initial Strains

In the simple bending and the combined bending and compression tests it was observed that buckling of the sheet covering almost invariably started near stringer No. 7, although theoretically the maximum compressive strain should have occurred at stringer No. 9. The possibility that this phenomenon had been caused by initial stresses was investigated in a series of systematic experiments. The results obtained in the experiments carried out on cylinder No. 13 are presented in figures 40 to 44.

First the strain gages were cemented to the stringers before any of the bolts which served for attaching test specimen, end rings, and test rig were tightened. With the cylinder resting on the floor, strain gage readings

were made to serve as zero readings. Next the bolts in the stringer grip fittings of end ring No. 1 were tightened and a new set of strain readings was taken. The strains calculated from these readings are shown in figure 40. They are predominately tensile, the maximum value being 2.25×10^{-4}. In the following steps the cylinder was fastened to the end stand, the stringer grip fittings tightened at the other end of the cylinder, and finally the loading head was bolted to end ring No. 2. After each of these steps the strains were measured and recorded. They are shown in figures 41 to 43. The diagrams reveal the characteristic features and the relative importance of the strains caused by each operation. Figure 44 presents the total initial strain in cylinder No. 13.

Figures 35 to 39 show the strains caused in cylinder No. 10 by a similar sequence of operations in which, however, the order of the first two steps was reversed. Because of this change, and possibly because of the difference in the thickness of the sheet, the effect of the individual operations differed from that observed in the experiments carried out with cylinder No. 13. Nevertheless, the curves representing the total initial strains in the two cylinders show marked resemblance. The same is true of the total initial strain curves of cylinders Nos. 8 and 9, which are not reproduced in this report.

The total initial strain distribution corresponds basically to a warping group with a vanishing resultant force and a vanishing moment about any axis. The strains caused by an operation undertaken at one end ring decrease rapidly in the direction of the other end ring, as may be seen from figure 45. This is in agreement with Saint Venant's principle. It should be noted, however, that the distance at which the effect of a disturbance becomes negligibly small is likely to be equal to two or three times the diameter of the cylinder.

In the initial strain measurements undertaken, the greatest tensile strains occurred generally at stringers Nos. 1 and 9, and comparatively large compressive strains at stringers Nos. 7 and 13. The maximum total initial stress was of the order of 3000 pounds per square inch. Moreover, the curves of distribution of strain in compression (figs. 29 to 33) also indicate some excess over the average of compressive strain. These findings completely explain why the first buckles in the sheet

appeared near stringer No. 7 rather than near stringer No. 9. On this basis the development of the inward bulge along stringer No. 7 near end ring No. 1 in some of the tests also can be understood. It does not appear likely, however, that the initial stress could have appreciably influenced the magnitude of the critical stress in inward bulge type buckling. This opinion is based on the fact that there was no systematic variation in the buckling stress to correspond with changes in the location of the inward bulge. It appears advisable, however, to pay more attention in the future to initial stresses in experimental investigations on semimonocoque cylinders than was usual in the past.

The Buckling of the Sheet Covering

The determination of the effective width of sheet, needed in the comparison of experiment with the theory of general instability, depends on a correct estimate of the strain (or of the stress) at which the sheet covering buckles. In the calculation of the critical stress $f_{c\ cr}$ of the curved panels of sheet Redshaw's formula was used:

$$f_{c\ cr} = (f_{flat}/2) + \sqrt{f^2_{curved} + (f_{flat}/2)^2} \qquad (1)$$

In this equation f_{flat} stands for the critical stress of the corresponding flat sheet. Its value is given by the formula

$$f_{flat} = k \frac{\pi^2 E}{12(1-\mu^2)} (t/d)^2 \qquad (2)$$

where t is the thickness of the sheet, d the width of the panel measured along the perimeter of the cylinder, E Young's modulus, and μ Poisson's ratio. The value of k depends upon the length-to-width ratio of the panel and upon the edge conditions. In the test specimens the length-to-width ratio was high because of the absence of intermediate attachment between rings and sheet. If the difference in the elastic restraint exerted by the stringers upon the thick and the thin sheet is taken into account, it appears reasonable to choose $k = 4$ for the thick and $k = 5$ for the thin sheet.

Equation (2) then gives 987 and 445 pounds per square inch for the critical stress of the thick- and the thin-walled specimens, respectively.

The buckling stress of the circular cylindrical sheet was denoted f_{curved} in equation (1). It can best be calculated from Donnell's formula:

$$f_{curved} = 0.6E\,(t/r)\,\frac{1 - 1.7 \times 10^{-7}(r/t)^2}{1 + 0.004\,(E/F_{cy})} \qquad (3)$$

where r is the radius of the cylinder and F_{cy} the compressive yield-point stress of the material. Equation (3) gives $f_{curved} = 5890$ pounds per square inch for specimens having the thick sheet, and $f_{curved} = 3250$ pounds per square inch for those having the thin sheet. For the critical stress of the curved panels equation (1) then gives:

$f_{c\,cr} = 6400$ pounds per square inch (for the 0.020-in.-thick sheet), and

$f_{c\,cr} = 3480$ pounds per square inch (for the 0.012-in.-thick sheet).

In the course of the experiments these theoretical values were checked in four ways. First, the appearance of the first buckle was visually observed and the strain at its location was determined from the strain-gage readings. Secondly, use was made of the strain against bending moment curves drawn for stringer No. 9. The curves are straight until the sheet begins to buckle. Consequently, the first deviations from the initial slope mark the bending moment at which the sheet buckles. A third indication of the critical strain of the sheet covering was found in plots of the observed shift of the neutral axis in bending, since there cannot be any shift until the sheet buckles. Finally, the slope of the strain curves of figures 7 to 28 was determined at the neutral axis and plotted against the bending moment. The slope of these curves also changes when the sheet begins to buckle.

The data obtained by the methods just outlined are collected in table III. Correction of the data for initial strain was not considered warranted for the purposes of the present investigation. In spite of the considerable

scatter of the values one conclusion, at least, is inevitable: the sheet buckled at much higher strains when the specimen was acted upon by a bending moment than in the case when the load was pure compression. This phenomenon had been noted by Lundquist in reference 2, but is disregarded as a rule in the stress calculation of semimonocoques. It would be desirable to develop methods of analysis that take this effect into account. With no such method yet available, however, a constant value of the buckling strain all along the circumference of the cylinder was assumed for the subsequent calculations. From the comparison of theory and experiment the following round numbers were chosen for use in later analysis:

$$\begin{aligned} \epsilon_{flat} &= 1 \times 10^{-4} \text{ (for the 0.020-in.-thick sheet)} \\ \epsilon_{flat} &= 0.5 \times 10^{-4} \text{ (for the 0.012-in.-thick sheet)} \\ \epsilon_{curved} &= 6 \times 10^{-4} \text{ (for the 0.020-in.-thick sheet)} \\ \epsilon_{curved} &= 3 \times 10^{-4} \text{ (for the 0.012-in.-thick sheet)} \end{aligned} \tag{4}$$

Force and Moment Equilibrium

In order to obtain an independent check of the accuracy of the load and strain measurement, as well as of the methods used in the analysis, the applied forces and moments were compared with the force and moment resultants of the measured internal direct stresses. In this comparison Hooke's law was assumed valid, and the modulus of elasticity was taken as 10.5×10^6 pounds per square inch for both sheet and stringers over the whole range of strains measured. For the stringers in which the strain had not been measured it was determined by interpolation. The effective width $2w'$ of the curved panels was taken as the total width wherever the panel was in a nonbuckled state. In the buckled state it was calculated from the following formulas:

$$\begin{aligned} 2w' &= 2w + (\epsilon_{curved}/\epsilon_{str})(d - 2w) \\ 2w &= [\epsilon_{flat}/(\epsilon_{str} - \epsilon_{curved})]^{1/3}d \end{aligned} \tag{5}$$

where ϵ_{str} is the strain in the stringer. These equations are quoted from reference 3. The values given in

in equations (4) were used for the buckling strains.

Calculated values of forces and moments are listed in table IV for a number of loading conditions and for various test cylinders. The agreement is good between the external and the internal moment, especially under small and moderate loads. For the higher stages of loading the internal moment slightly exceeds the external moment. The agreement between the internal and the external compressive force is also good in the low load range, but the values deviate considerably for the higher stages of loading. The discrepancies can be explained by the reduction in the value of the modulus of elasticity of the material.

It was shown in reference 4 that the tangent modulus of 24S-T extruded sections begins to decrease at stresses between 22,000 and 30,000 pounds per square inch in compression, while its value remains constant up to a range from 38,000 to 47,000 pounds per square inch in tension. The value of the tangent modulus of alclad 24S-T experiences a drop even at a stress of 10,000 pounds per square inch. Evaluation of the pure compression tests made with the monocoque test cylinders during the present investigations at the Polytechnic Institute of Brooklyn also showed a decrease in the apparent modulus with increasing load, as may be seen from the data included in table V.

Since exact values of the variation of the modulus with stress were not available for the sheet and the sections used in the experiments, the force and moment equilibrium could not be determined accurately. In one case, however, the calculations were repeated with the assumption of $E = 10.5 \times 10^6$ pounds per square inch for tension and for compression below 10,000-pounds-per-square-inch stress, and of $E = 9.5 \times 10^6$ pounds per square inch for compression above 10,000-pounds-per-square-inch stress. This slight change sufficed to reduce the original discrepancy of 45.6 percent in the compressive force to 12.2 percent. The corresponding change in the value of the moment was unimportant. (See table IX.) This example indicates that the variation of the modulus may well be the reason for the discrepancies noted. The effect of such a slight variation is pronounced only in the case of the resultant force which is the small difference of two large quantities - namely, the resultant forces on the tension and the compression sides of the specimen.

Variation of the Strain in the Stringers

Figures 46 to 57 give typical examples of the variation with bending moment of the strain in the three most highly stressed stringers on the tension and on the compression sides. The curves shown represent data obtained with cylinders Nos. 7, 9, and 10, corrected for the weight of the loading arm. In figures 58 to 63 measured values of the compressive strain in stringer No. 9 are compared with the theoretical stringer strain variation curves. This comparison is of importance since in the theory of the inward bulge type buckling a theoretical stringer strain variation is assumed.

The theoretical curves were determined as follows: For different assumed values of the shift of the neutral axis the resultant bending moment was calculated and plotted against the compressive strain in stringer No. 9. In a second diagram the resultant compressive force was plotted against the compressive strain in stringer No. 9 for the same values of the parameter "neutral axis shift." From these two diagrams the variation of the compressive strain in stringer No. 9 with increasing bending moment was determined and plotted for several constant values of the compressive force. Since at each stage of loading the centroid of the effective material of the cross section of the specimen is shifted a different distance from the geometric center of the cylinder while the compressive load is always applied at the geometric center, an additional bending moment arises the effect of which must be taken into account before the theoretical curves can be compared with the experimental values. Figures 58 to 63 present curves which have been corrected for this effect.

In general, the agreement between theory and experiment can be considered good. In some cases at high bending moments the experimental values of the strain exceed those predicted by theory. This discrepancy is probably caused by the variation of the modulus.

General Instability

The correlation of experiment with the theory of the inward bulge type buckling of monocoque cylinders, which is the ultimate objective of these investigations, can best be carried out on the basis of the strains in the most highly compressed stringer at the moment of general

instability. The formula for the maximum compressive strain at collapse ϵ_{cr}, derived from equation (24) of reference 1 with the assumption of the same modulus of elasticity for rings and stringers, is as follows:

$$\epsilon_{cr} = n^2 \sqrt{\frac{d}{L_1}} \frac{\pi^2}{A_{str}} \frac{\sqrt{I_{str} I_r}}{r^2} - \frac{(0.9/n^2)\, \nu d}{A_{str} E} \qquad (6)$$

where n is a parameter, L_1 the ring spacing, A_{str} the cross-sectional area of stringer plus effective width, I_r the moment of inertia of ring plus effective width, ν the compressive load divided by the perimeter of the cylinder, and I_{str} is defined by the equation

$$I_{str} = I_{str\ r} + (5/8)(1/n^2)\, I_{str\ t} \qquad (7)$$

where $I_{str\ r}$ and $I_{str\ t}$ are the moments of inertia of the stringer plus effective width for radial and tangential bending, respectively. The effective width of the sheet acting with the ring was assumed to be equal to the width of the ring.

The forces at collapse in the load link and in the compression load bar were accurately known since they were continuously observed with the aid of the two control boxes while the load was applied. In many cases the strains in the stringers were also measured close to the load at which general instability occurred. Some test specimens, however, collapsed before readings could be taken in the proximity of the buckling load. The strains just prior to instability were not significant, however, since they were obviously influenced by the developing bulge. In many cylinders with the imminent approach of instability the maximum compressive strain suddenly increased in one band, and decreased in the other. Because of this the following procedure was used to determine significant values of the maximum compressive strain at collapse:

Stringer strain variation curves, as obtained for stringer No. 9 in bands A and B, were superimposed. The general trend, established prior to the appearance of irregularities, of the curve representing the average of

the values in bands A and B was extrapolated up to the collapsing load. The strain at collapse obtained by this procedure was considered the experimental critical strain.

Table VI presents the collapsing loads as measured, and as corrected for the weight of the loading arm and for the effect of the shift of the centroid of the effective material from the geometric center of the cylinder. Values of the experimental critical strain are listed in table VII.

From these maximum compressive strains the value of the parameter n was calculated in accordance with the suggestions of reference 3 and satisfying equation (6) of this report. The results are listed in table VIII. It may be seen from the table that n varies but little, its maximum value being 3.21, the average 2.935, and the minimum 2.66. The possibility of a variation of n with compressive force was anticipated in reference 3 but any systematic variation is lacking in table VIII. On the other hand, equation (6) appears to give the influence of the compressive load correctly.

It should be noted that the average value obtained for n is 15 percent smaller than could be predicted from figure 10 of reference 3, which is based on the GALCIT experiments. The reason for this deviation is unknown. There was, however, a slight difference in the way the specimens were constructed. In the GALCIT cylinders the sheet was bolted to the rings and the stringers; while in the cylinders used in the present investigation the sheet was attached to the stringers alone.

In reference 3 it was suggested that the critical strain in general instability could be calculated approximately by neglecting the effective width of the sheet. The accuracy of this suggestion was checked by calculating n from equation (6) using values of the moments of inertia of stringers and rings alone. The values so obtained are also presented in table VIII. There is a systematic deviation between the accurate and the approximate values. The average deviation is 16 percent. Consequently in the present case, the use of the approximate procedure suggested would result in underestimating the critical strain by 26 percent.

The general appearance of the distorted shape after buckling is shown in the photographs of figures 64 to 74.

The pictures agree well with the description of the inward bulge given in the introduction. The values of the parameters n and m characteristic of the bulge could not be determined accurately because the bulge did not terminate sharply. The approximate values are listed in table VIII, together with the theoretical values. The average experimental value of the number m of rings involved in buckling was 3, while theory predicted about 4. The observed mean value of n was near 5 as compared with the theoretical average of 3.

CONCLUSIONS

The series of tests conducted in the Aircraft Structures Laboratory of the Polytechnic Institute of Brooklyn with reinforced monocoque cylinders in combined bending and compression leads to the following conclusions:

1. The pattern of distortion at buckling as realized in the actual tests corresponds in essential features to the deflected shape assumed in the theory.

2. The experimentally established strains in the most highly compressed stringer at buckling are consistent with the values obtained from the theoretical relationship:

$$\epsilon_{cr} = n^2 \sqrt{\frac{d}{L_1}} \frac{\pi^2}{A_{str}} \frac{\sqrt{I_{str} I_r}}{r^2} - \frac{(0.9/n^2)\, \nu d}{A_{str} E}$$

3. No systematic variation was found of the parameter n with compressive force.

4. The average value of the parameter n was 2.935 when calculated from the formula quoted in conclusion 2 using experimental values of the critical strain.

5. The data collected in the course of the experiments afforded fairly close corroboration of the theories of buckling of curved panels.

6. It was established that the elastic properties of the test rig and the manner of attachment of the test

specimens exerted a considerable influence on the nature of the stress distribution and on the initial strains in the specimen.

Polytechnic Institute of Brooklyn
Brooklyn, N. Y., February 1944.

REFERENCES

1. Hoff, N. J., and Klein, Bertram: The Inward Bulge Type Buckling of Monocoque Cylinders. I - Calculation of the Effect upon the Buckling Stress of a Compressive Force, a Nonlinear Direct Stress Distribution, and a Shear Force. NACA TN No. 938, 1944.

2. Lundquist, Eugene E.: Strength Tests of Thin-Walled Duralumin Cylinders in Pure Bending. NACA TN No. 479, 1933.

3. Hoff, N. J.: General Instability of Monocoque Cylinders. Jour. Aero. Sci., vol. 10, no. 4, April 1943, pp. 105-114, 130.

4. Templin, R. L., Hartmann, E. C., and Paul, D. A.: Typical Tensile and Compressive Stress-Strain Curves for Aluminum Alloy 24S-T, Alclad 24S-T, 24S-RT, and Alclad 24S-RT Products. Tech. Paper No. 6, Aluminum Res. Lab., Aluminum Co. of Am., 1942.

Table I. Table of Compressive Forces

Cyl. No.	Nominal Load lb.	Stage 1	2	3	4	5	6	7	8	9	10	11	12
2	0	No Compressive Force											
5	0	No Compressive Force											
6	0	No Compressive Force											
7	17,000	17900	17600	17450	17400	17100	17000	16900	16250	14500			
8	14,500	14700	14660	14440	14250	14750	14440	14900	14500				
9	14,000	13850	13800	13750	13700	13750	13850	12900					
10	14,000	14250	14050	14050	13900	13850	14000						
11	0	No Compressive Force											
12	7,250	7200	7270	7230	7230	7400	7230	7230	7230	7360	7360	7200	
13	7,250	7260	7200	7200	7200	7200	7200	7140	7200	7200	7200	7200	7200

Table II – Maximum Deviation in Compression

Test Cyl. No.	Stage No.	Load lb.	Stringer No.	Average Strain $\epsilon \times 10^4$ (lb./sq.in.)	Maximum Deviation Percentage
7	1	13,000	A-11	3.79	+8.17
	1	13,000	B-5	3.76	-7.44
8	1	6,500	A-5	1.93	-7.25
	1	6,500	B-1	1.89	+6.35
	2	12,700	A-5	3.76	-5.33
	2	12,700	B-5	3.75	+4.26
	3	19,300	A-5	5.65	-5.30
	3	19,300	B-9	5.65	-5.67
9	1	5,000	A-15	1.83	+15.31
	1	5,000	B-13	1.76	+11.93
	2	7,970	A-9	2.95	-10.85
	2	7,970	B-13	2.85	+12.26
	3	11,900	A-9	4.52	-13.72
	3	11,900	B-13	4.45	+12.36
	4	18,000	A-9	7.18	-11.13
	4	18,000	B-9	7.04	-11.93
10	1	3,900	A-11	1.33	+9.03
	1	3,900	B-15	1.33	-3.76
	2	7,860	A-11	2.77	+9.03
	2	7,860	B-11	2.72	+4.78
	3	11,600	A-15	4.07	-12.55
	3	11,600	B-11	4.08	+7.60
	4	15,600	A-7	5.63	+12.43
	4	15,600	B-11	5.69	+8.87
	5	19,800	A-7	7.43	+9.96
	5	19,800	B-11	7.52	+7.85
12	1	7,100	A-1	2.03	+4.92
	1	7,100	B-5	2.00	-4.50
	1	7,100	B-13	2.00	+4.50
	2	14,600	A-11	4.14	+3.86
	2	14,600	B-9	4.05	-5.68

Table III - Experimental Values of Buckling Stress

Cylinder Number	Sheet Thickness in.	Compressive Buckling Stress Observed psi	Bending Buckling Stress psi How Obtained			
			Observed	Change in Slope of Stringer Curve	Change in Slope of Shift Curve	Change in Slope of Slope Curve
5	.020			9,450		
6	.020	3,060	8,900	9,850		10,900
7	.020	4,965	8,050			9,800
8	.020	4,000 (average)	7,500		6,300	7,400
10	.012	1,500 (average)	3,800			
11	.012	1,760 (average)	3,150	4,400	2,100	
12	.020		6,400	10,000	4,100	9,000
13	.020		8,650	9,000	8,100	7,000

Table IV - Force and Moment Equilibrium

Percentage of failing load	No. of Cyl.	6		7		10		11		12		13	
	Source	Mom. in.lb.	Force lb.	Mom. in.lb.	Force lb.	Mom. in.lb.	Force lb.	Mom. in.lb.	Force lb.	Mom. in.lb.	Force lb.	Mom. in.lb.	Force lb.
10%-20%	Actual							34600	0	37400	7270	30000	7250
	Calc.A							31400	-35	36000	7600	34645	7600
	Calc.B												
20%-30%	Actual							72000	0	67600	7230	72000	7250
	Calc.A							66500	-294	64750	7760	78300	7270
	Calc.B												
30%-40%	Actual									106500	7230	108000	7250
	Calc.A									103000	7900	103200	7220
	Calc.B												
40%-50%	Actual							108000	0	142500	7400	144000	7250
	Calc.A							98500	-472	131500	7850	144100	7420
	Calc.B												
50%-60%	Actual							144000	0				
	Calc.A							130500	-682				
	Calc.B												
60%-70%	Actual					151000	13850						
	Calc.A					155000	15600						
	Calc.B					151500	15260						
70%-80%	Actual							212000	0	249000	7230		
	Calc.A							208000	-925	256000	9010		
	Calc.B									250000	8520		
80%-90%	Actual			239000	16250							302000	7250
	Calc.A			257000	20100							326000	10560
	Calc.B			262500	21600							307000	9880
90%-100%	Actual	324000	0	257000	14500					310000	7200	316000	7250
	Calc.A	351000	-2390	273500	17960					352300	12000	343000	10860
	Calc.B	329000	-396	304500	21950					311000	8360	321500	9960

Table V - Stress-Strain Proportionality Factors in Compression

Cyl. No.	Sheet Thick.	P lb.	Δ P lb.	A sq.in.	$\frac{\Delta P}{A}$ 10^{-3} psi	Aver ϵ x10^4	$\Delta\epsilon$ x10^4	$\frac{\Delta P}{A} / \Delta\epsilon \times 10^{-6} = E$ psi
7	.020	13,000	13,000	3.5	3.71	3.78	3.78	9.8
8	.020	6,500	6,500	3.5	1.86	1.91	1.91	9.75
		12,700	6,200	3.5	1.77	3.76	1.85	9.55
		19,300	6,600	3.5	1.89	5.65	1.89	10.0
9	.012	5,000	5,000	3.0	1.667	1.79	1.79	9.3
		7,970	2,970	3.0	.99	2.90	1.11	8.92
		11,900	3,930	2.96	1.33	4.49	1.59	8.36
		18,000	6,100	2.79	2.18	7.11	2.62	8.32
10	.012	3,900	3,900	3.0	1.3	1.33	1.33	9.78
		7,860	3,960	3.0	1.32	2.74	1.41	9.36
		11,600	3,740	2.99	1.25	4.08	1.34	9.32
		15,600	4,000	2.88	1.39	5.66	1.58	8.80
		19,800	4,200	2.76	1.52	7.47	1.81	8.40
11	.012	5,300	5,300	3.0	1.767	1.81	1.81	9.75
12	.020	7,100	7,100	3.5	2.03	2.01	2.01	10.1
		14,600	7,500	3.5	2.14	4.1	2.09	10.2
13	.020	7,300	7,300	3.5	2.09	2.07	2.07	10.1

Table VI - Critical Instability Moments

Test Cyl. No.	Sheet Thick. in.	Type Test *	Actual Collapsing Load lb.		Highest (last) Recorded Load Previous Collapse lb.		Shift of Centroid	Equiv. jack load corr. for shift lb. $\frac{P \times Shift}{72}$	Corr. Collapsing jack load lb.	Total jack Coll. Load Corr. for wght. of loading arm lb.	Total Coll. Moment in. lb.
			Jack load (bending)	Compression	Jack load (bending)	Compression					
5	.020	B	4,150	---	3,960	---		-----		4,275	308,000
6	.020	B	4,870	---	4,510	---		-----		4,995	359,000
7	.020	B & C	3,670	13,000	3,580	14,400	1.75	320	3,990	4,115	296,000
8	.020	B & C	3,460	14,600	3,220	14,500	3.0	610	4,070	4,195	302,000
9	.012	B & C	2,750	13,900	2,650	12,900	1.4	270	3,020	3,145	227,000
10	.012	B & C	3,080	14,200	2,650	14,000	1.28	252	3,332	3,457	249,000
11	.012	B	3,880	-----	3,500	-----		---	3,880	4,005	289,000
12	.020	B & C	4,450	7,400	4,350	7,200	0.85	88	4,538	4,665	336,000
13	.020	B & C	4,750	7,200	4,640	7,200	1.6	160	4,910	5,035	362,000

* B: Pure bending
B & C: Bending and compression combined

VII - Experimental Critical Strains

Test Cyl. No.	Sheet Thick-ness in.	Type Test *	Highest (Last) Recorded Stringer Strain x 10^4 #9(Compression)	#1 Tension	Extrapolated Stringer Strain x 10^4 Average A and B #9 (Compression)
5	.020	B	20.78 20.20	16.2 15.69	21.83
6	.020	B	24.7 20.9	17.9 16.8	25.68
7	.020	B & C	18.6 23.95	11.88 11.06	24.0
8	.020	B & C	28.4 16.C	10.18 9.66	23.28
9	.012	B & C	18.3 18.2	8.68 8.10	21.7
10	.012	B & C	19.2 19.0	7.75 7.28	22.4
11	.012	B	19.1 17.0	15.4 13.65	20.86
12	.020	B & C	27.2 16.6	15.85 15.76	24.38
13	.020	B & C	31.2 25.4	17.3 15.9	28.6

*B - (Pure Bending)
B & C - (Bending and Compression Combined)

Table VIII.- Experimentally Determined Values of Parameters n and m

Cyl. No.	t in.	P lb.	ϵ_{cr} x10^4	n	m	n for 2W=0	Observed n	Observed m
5	.020	0	21.83	2.66	4.93	3.28		
6	.020	0	25.68	2.99	4.05	3.56	4	3
7	.020	13,000	24.0	2.89	4.32	3.44	5.33	3
8	.020	14,600	23.28	2.84	4.45	3.38	6.4	3
9	.012	13,900	21.7	2.99	3.82	3.27	4	3
10	.012	14,200	22.4	3.05	3.70	3.32	6.4	2
11	.012	0	20.86	2.89	4.00	3.2	4.25	4
12	.020	7,400	24.38	2.90	4.27	3.48	5.33	3
13	.020	7,250	28.6	3.21	3.60	3.76	4.57	3

Table IX. Force and Moment Equilibrium.

Cylinder No. 13
Band A

Applied Moment: 302,000 in.-lb.
Calculator: R. Boley

Applied Compressive Force: 7,250 lb.

Stringer No.	Vert. Distance from C.L. h in.	Strain ϵ x 10^4	Eff. cross section A sq. in.	ϵ A x10^4	ϵ Ah x10^4	E x10^{-6} psi	ϵ AE lb.	ϵ AEh in.-lb.
1	9.83	15.0	0.219	3.28	32.3	10.5	3,445	33,900
2	9.08	14.0	0.219	3.07	27.9	10.5	3,220	29,300
3	6.95	10.1	0.219	2.21	15.4	10.5	2,320	16,150
4	3.76	4.0	0.219	0.88	3.3	10.5	925	3,480
5	0	-3.2	0.219	-0.70	0	10.5	-735	0
6	-3.76	-11.1	0.204	-2.26	8.5	9.5	-2,145	8,070
7	-6.95	-17.7	0.190	-3.36	23.4	9.5	-3,190	22,200
8	-9.08	-23.0	0.184	-4.23	38.4	9.5	-4,025	36,500
9	-9.83	-25.0	0.182	-4.55	44.5	9.5	-4,320	42,500
10	-9.08	-23.0	0.184	-4.23	38.4	9.5	-4,025	36,500
11	-6.95	-17.7	0.190	-3.36	23.4	9.5	-3,190	22,200
12	-3.76	-11.1	0.204	-2.26	8.5	9.5	-2,145	8,070
13	0	-3.2	0.219	-0.70	0	10.5	-735	0
14	3.76	4.0	0.219	0.88	3.3	10.5	925	3,480
15	6.95	10.1	0.219	2.21	15.4	10.5	2,320	16,150
16	9.08	14.1	0.219	3.07	27.9	10.5	3,220	29,300
				-10.05	310.6		-8,135	307,580

Total load (E = const): $P = -10.05 \times 10.5 \times 10^2 = -10,550$ lb. Error: 10 x (10,550 - 7,250)/7,250 = 45.5%
Total moment (E = const): $M = 310.6 \times 10.5 \times 10^2 = 326,000$ in.-lb. Error: 10(326-302)/302 = 7.95%

Total load (E variable): P = -8,135 lb. Error: 10(8,135 - 7,250)/7,250 = 12.2%
Total moment (E variable): M = 307,580 in.-lb. Error: 10(307,580 - 302,000)/302,000 = 1.8%

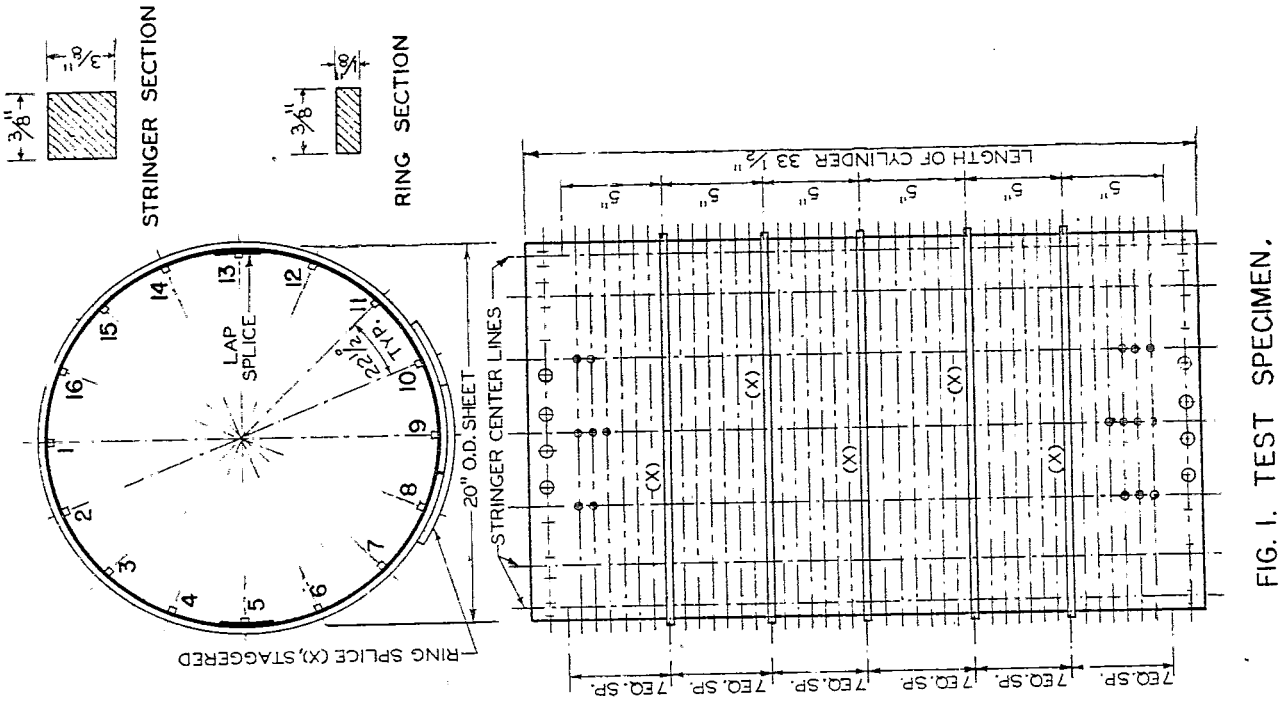

FIG. 1. TEST SPECIMEN.

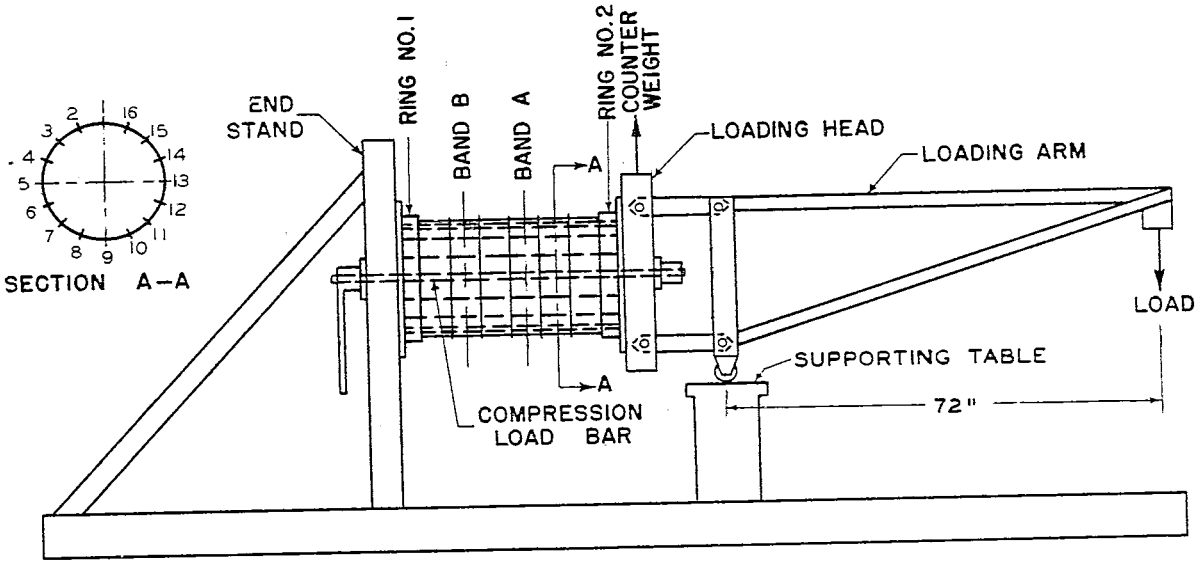

FIG. 2. DIAGRAM OF TEST SET-UP.

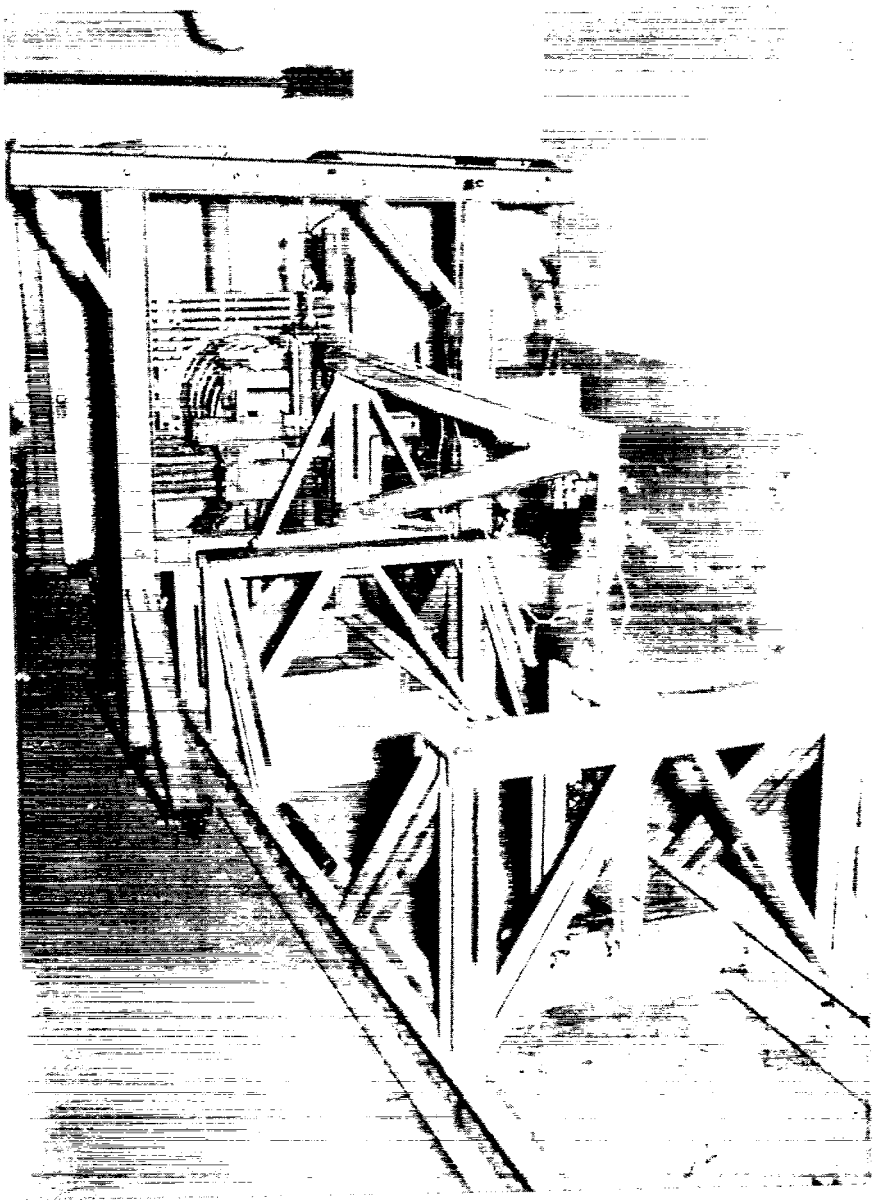

Figure 3. – Forward view of test rig.

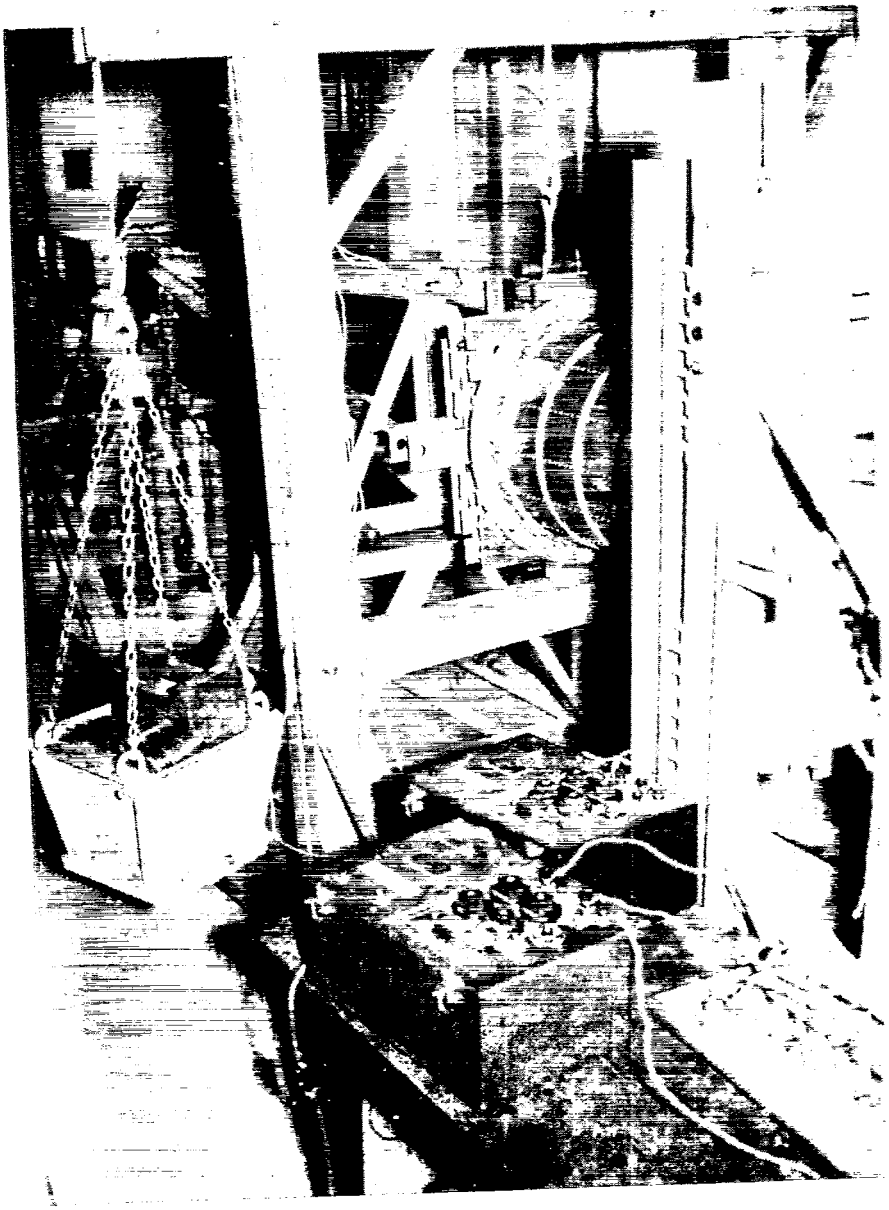

Figure 4. - Rear view of test rig.

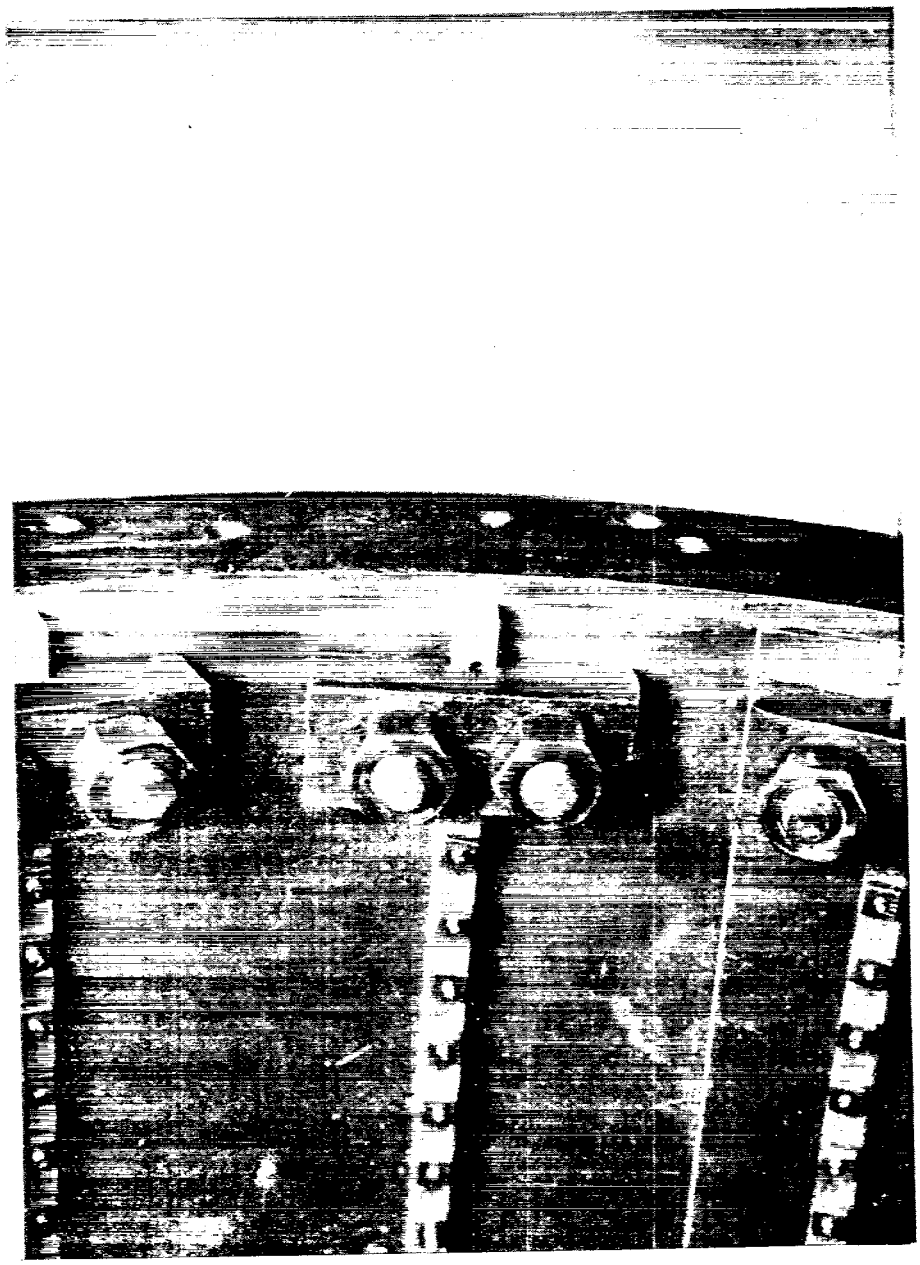

Figure 5. - Stringer grip fittings.

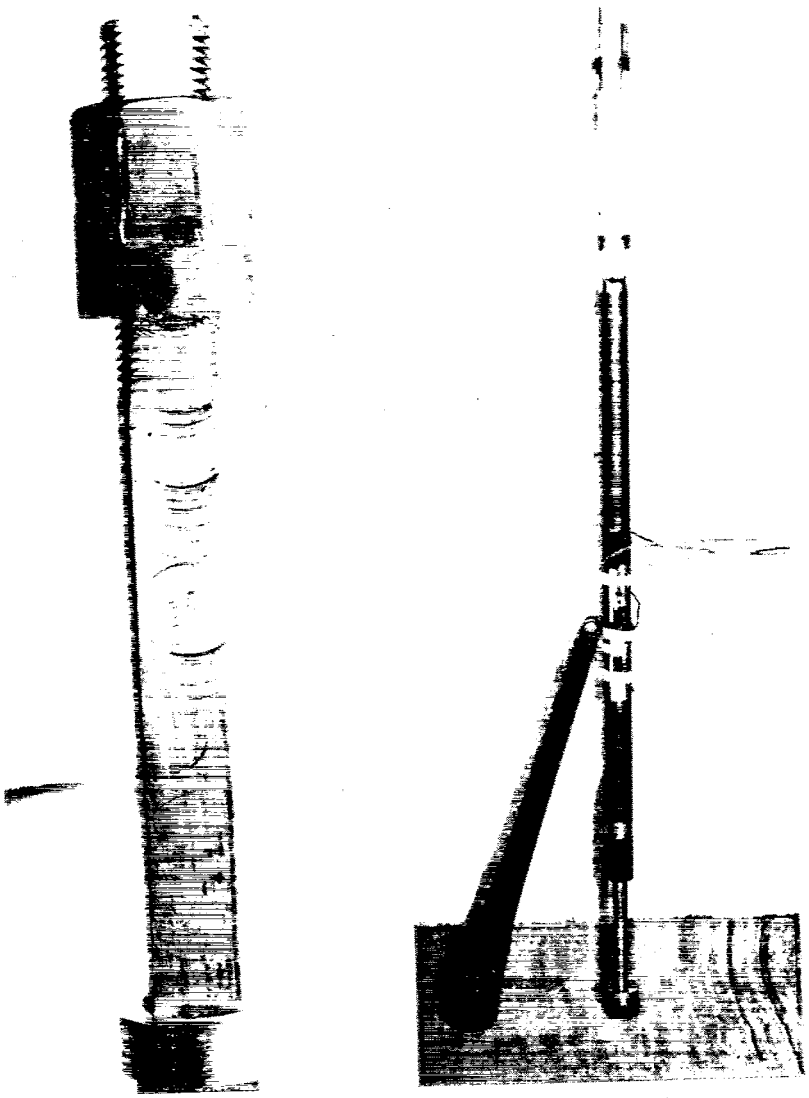

Figure 6. - Compression bar and adjustment end.

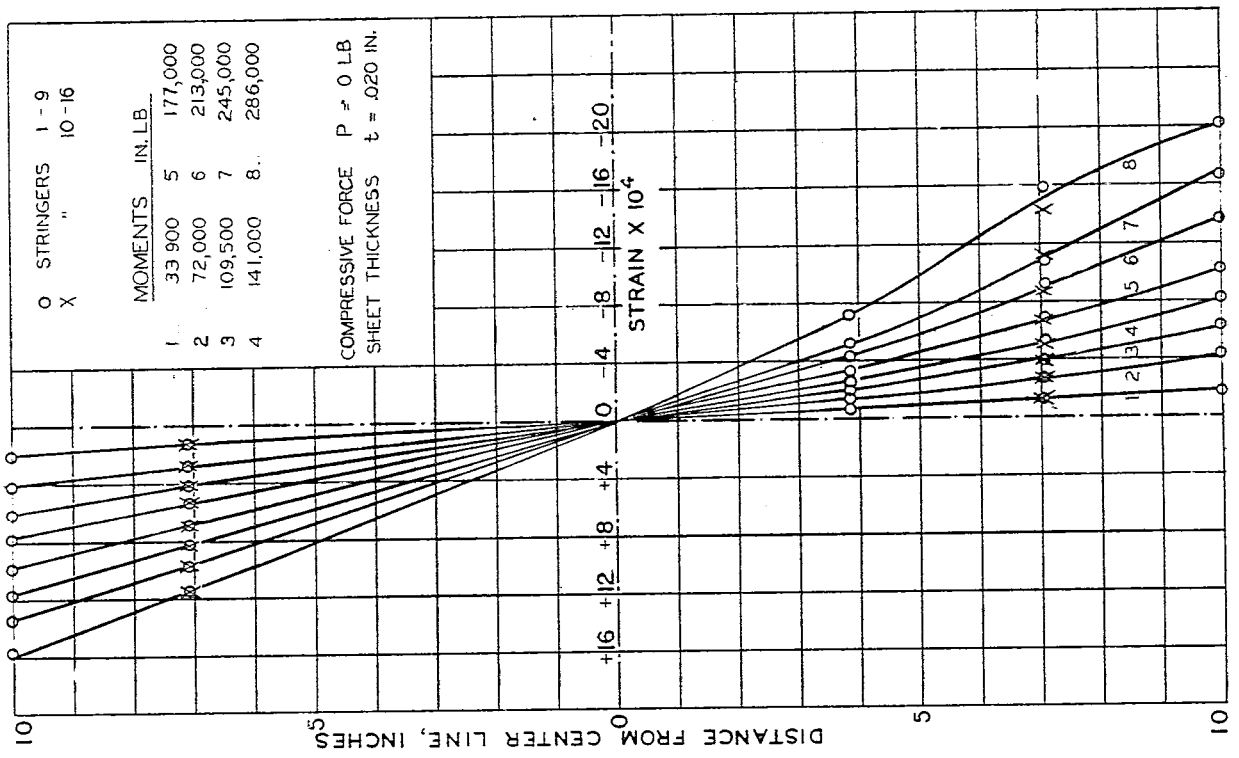

(1 block = 10 divisions on 1/32" Arch. scale)

FIG. 8. STRAIN DIAGRAM OF CYLINDER NO. 5 BAND B.

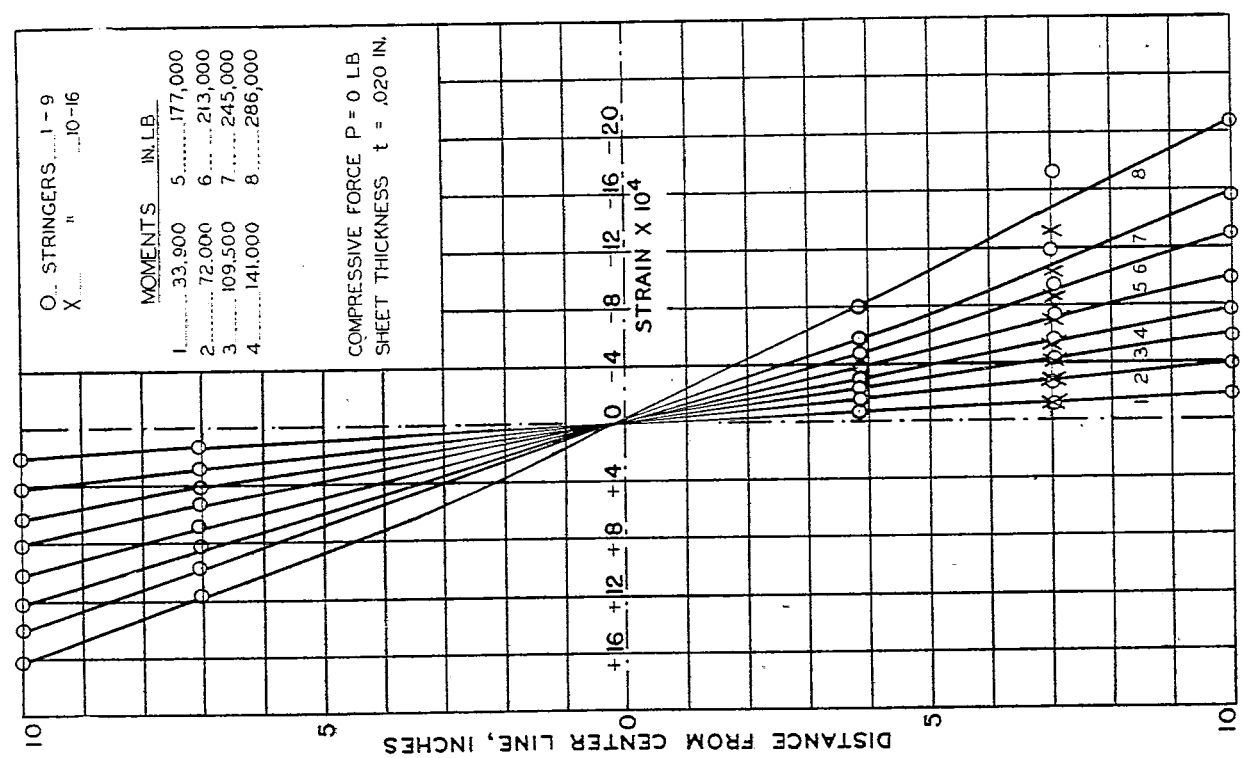

FIG. 7. STRAIN DIAGRAM OF CYLINDER NO. 5 BAND A.

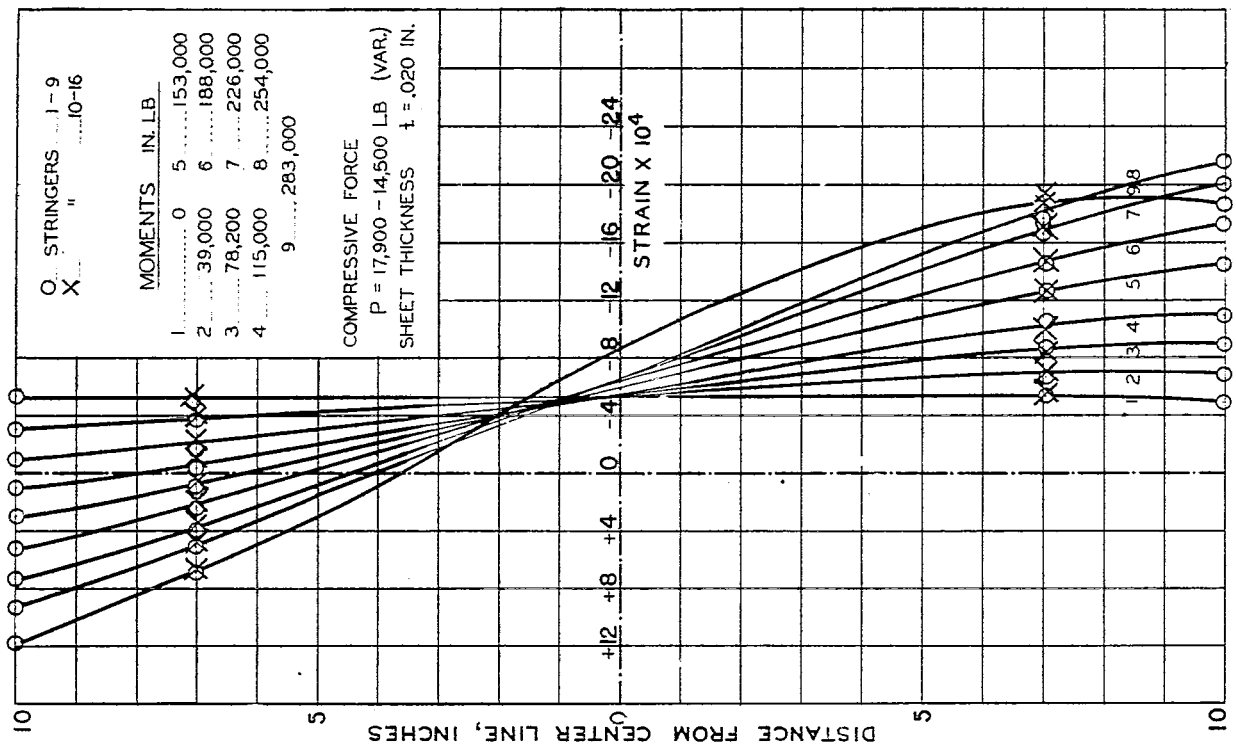

FIG. 10. STRAIN DIAGRAM OF CYLINDER NO. 7 BAND A.

(1 block = 10/32")

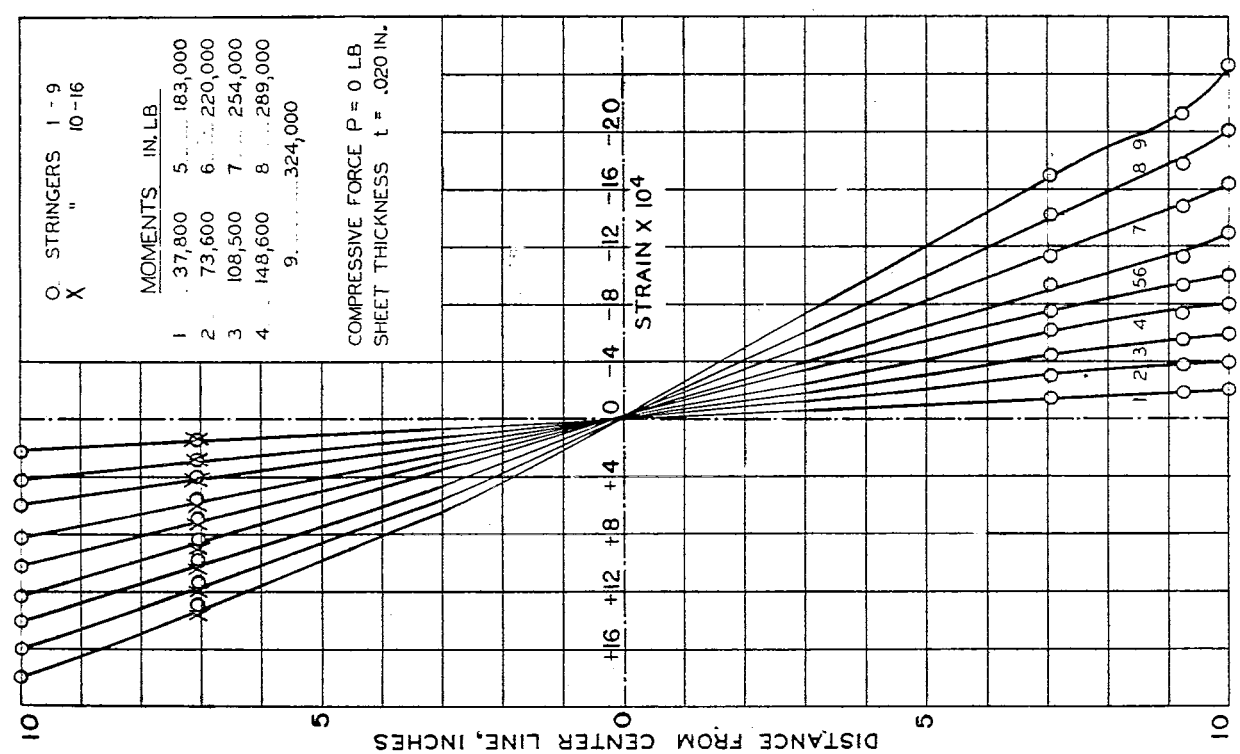

FIG. 9. STRAIN DIAGRAM OF CYLINDER NO. 6 BAND A.

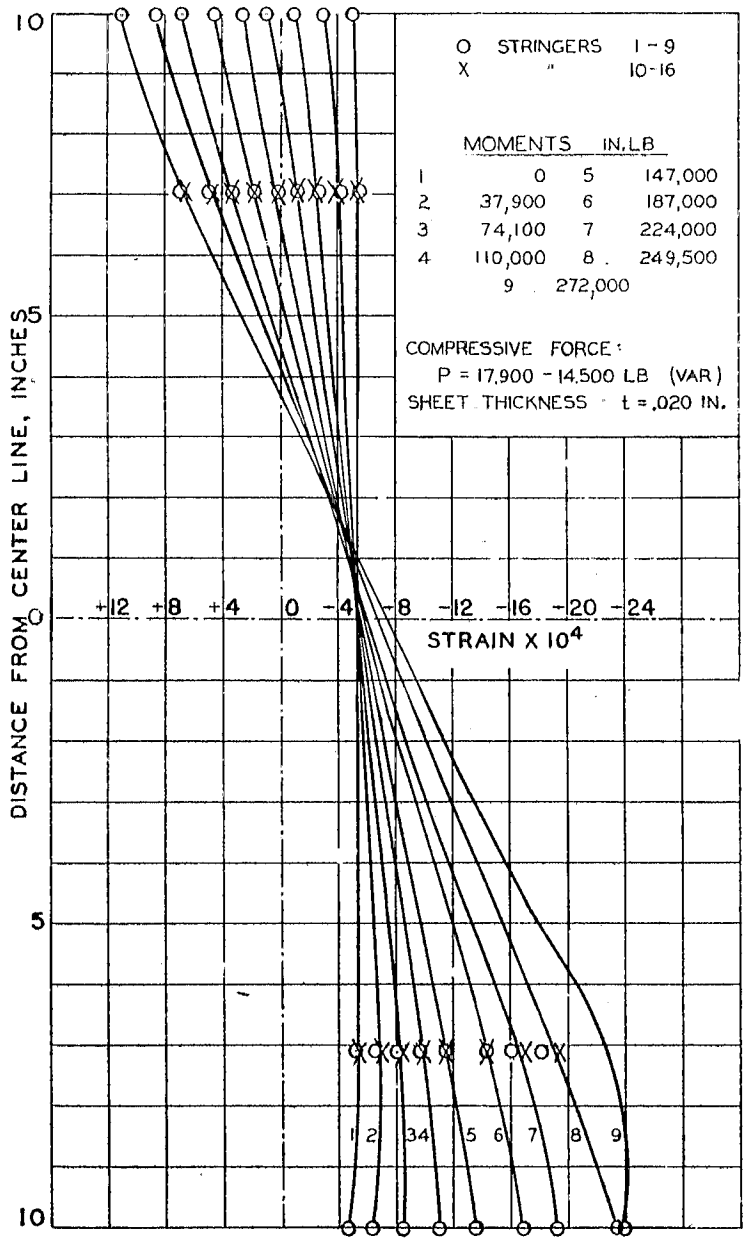

FIG.11. STRAIN DIAGRAM OF CYLINDER NO. 7 BAND B.

(1 block = 10/32")

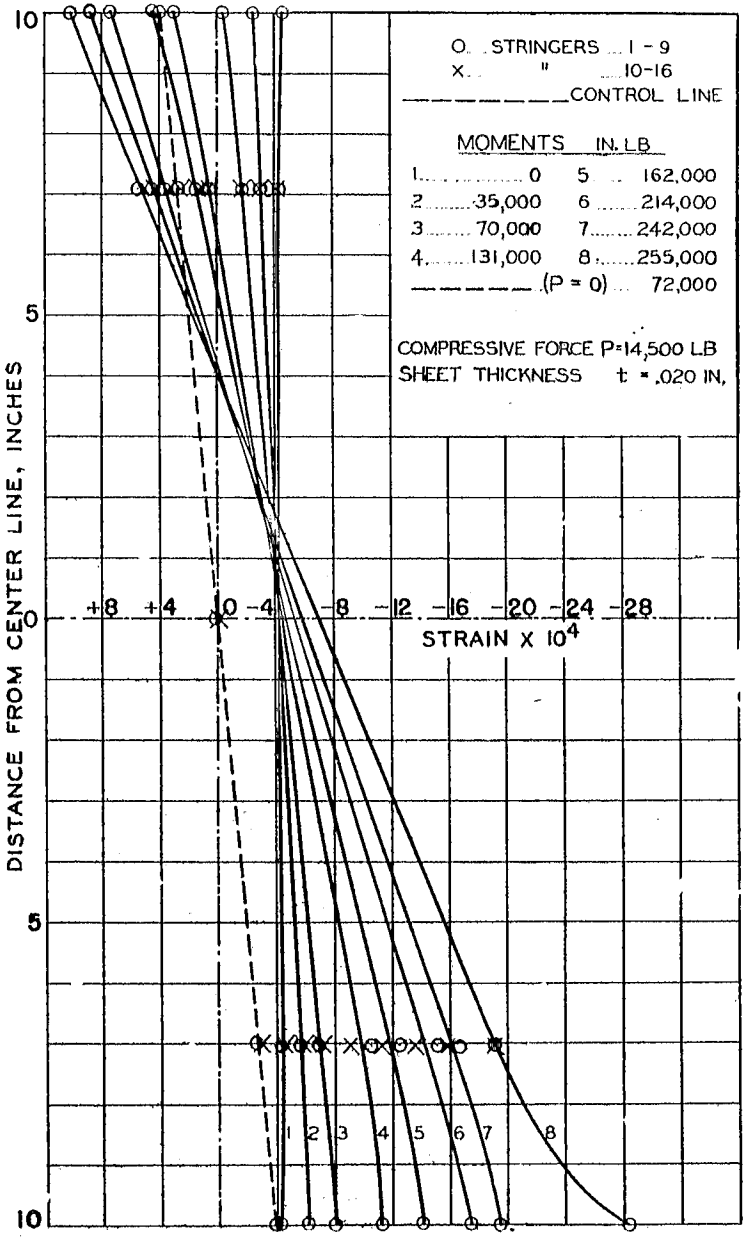

FIG.12. STRAIN DIAGRAM OF CYLINDER NO. 8 BAND A.

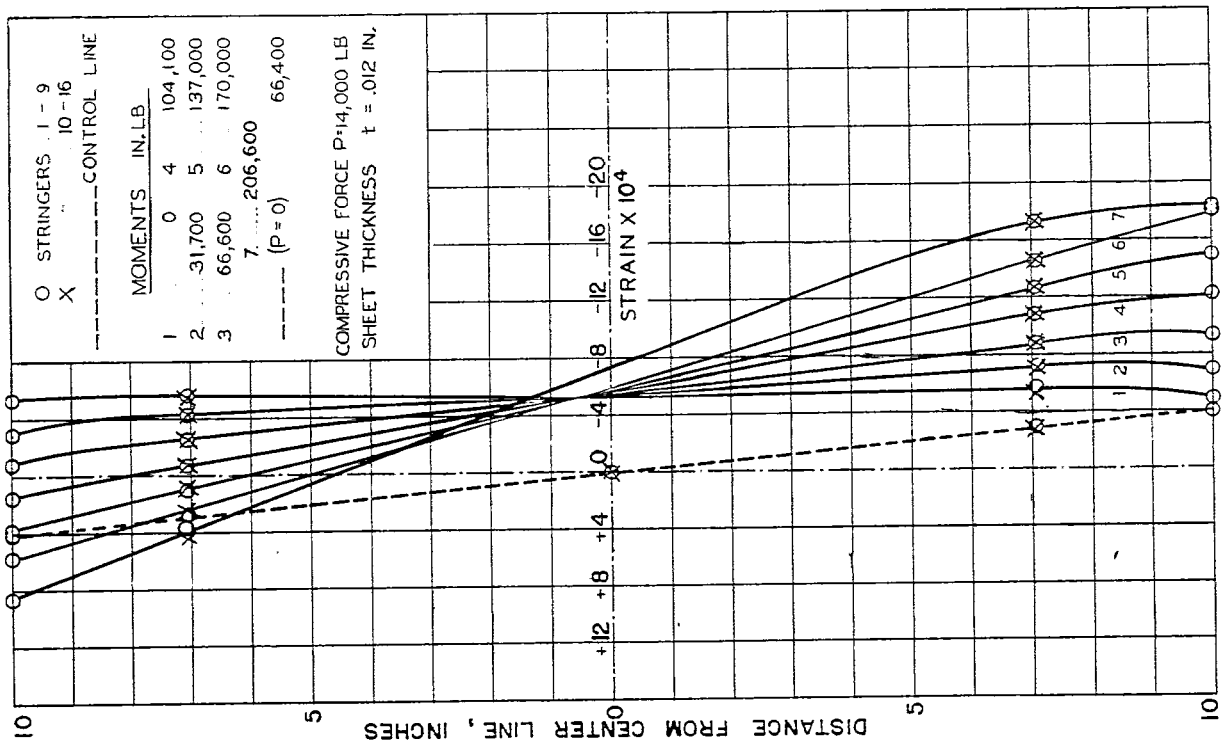

FIG.14. STRAIN DIAGRAM OF CYLINDER NO. 9 BAND A.

(1 block = 10/32")

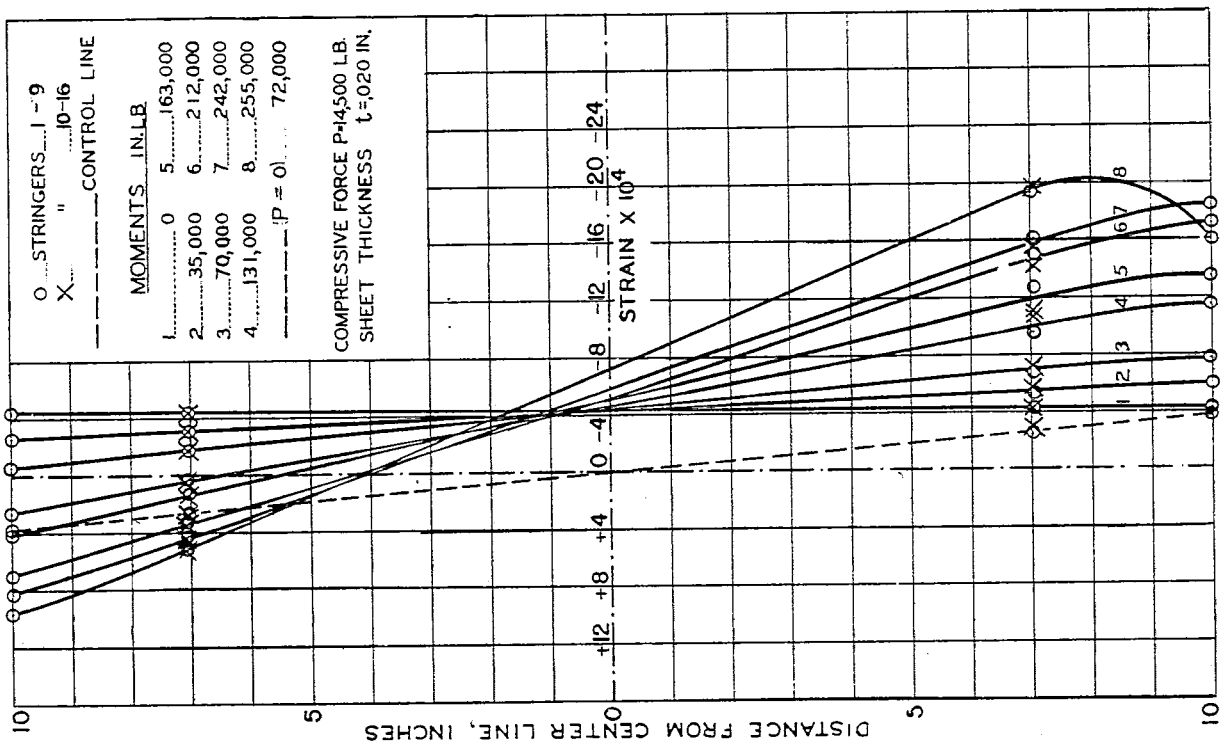

FIG.13. STRAIN DIAGRAM OF CYLINDER NO. 8 BAND B.

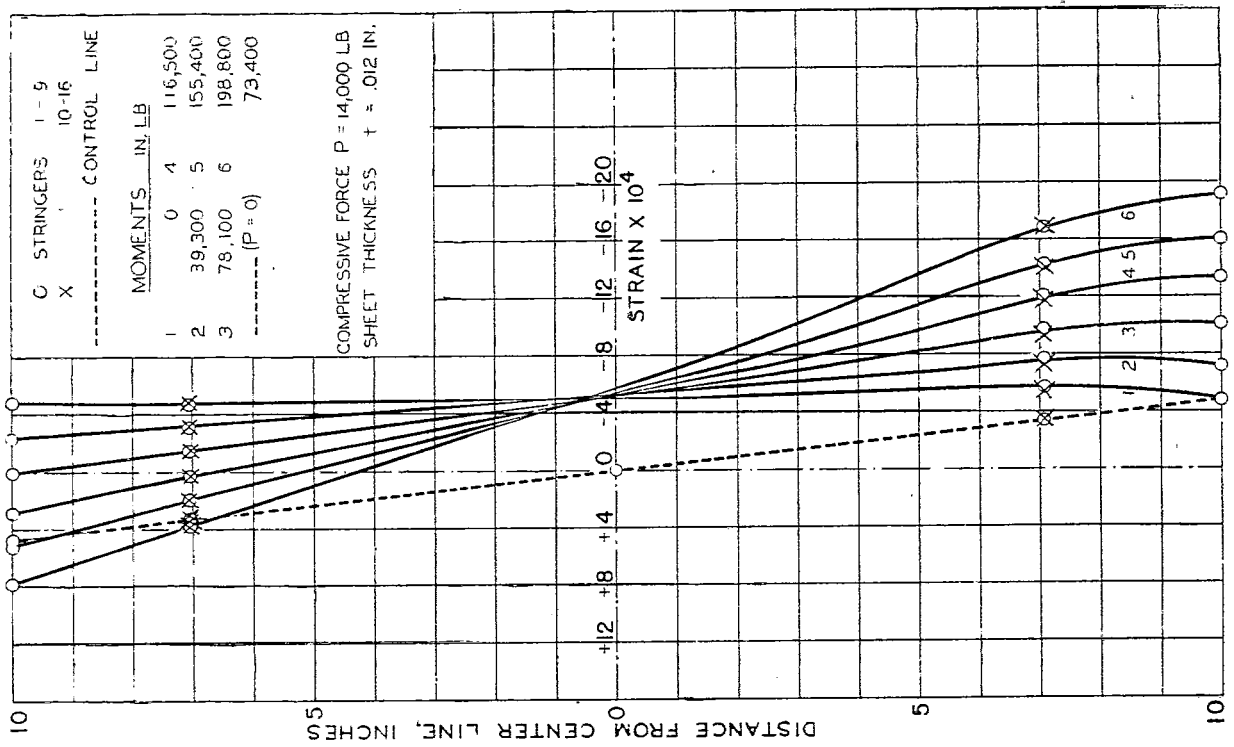

FIG.16. STRAIN DIAGRAM OF CYLINDER NO. 10 BAND A.

(1 block = 10/32")

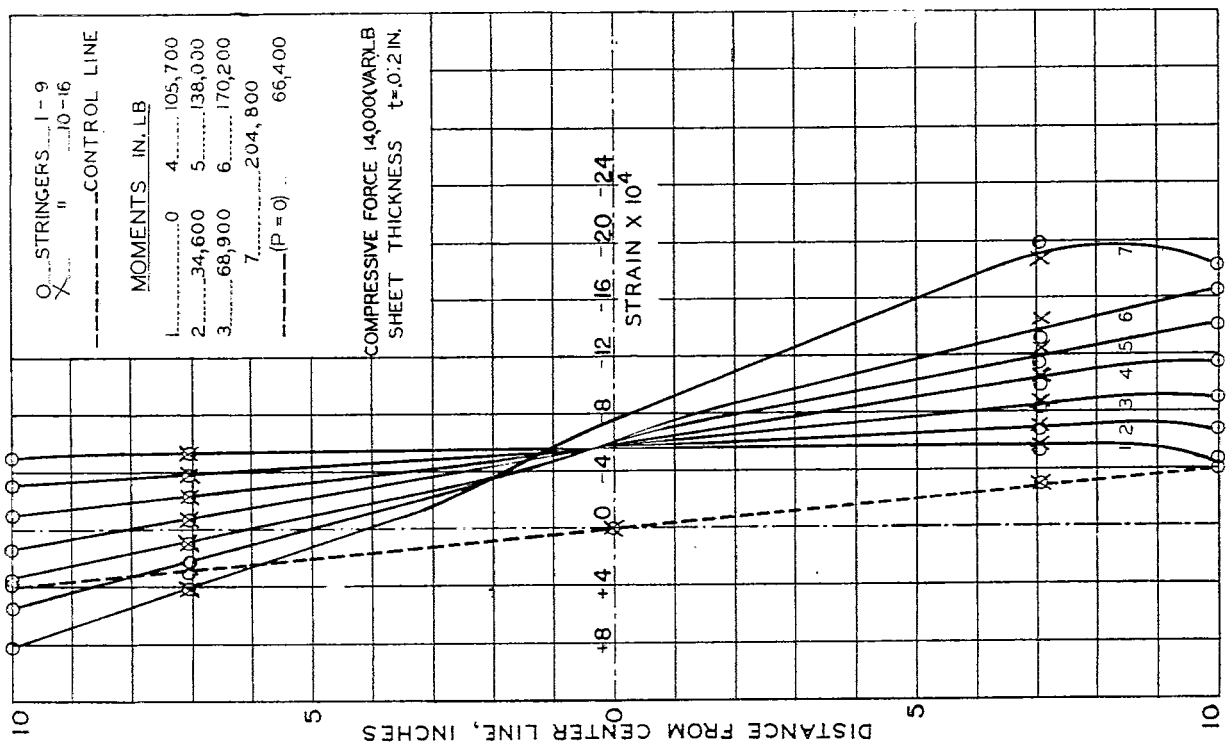

FIG.15. STRAIN DIAGRAM OF CYLINDER NO. 9 BAND B.

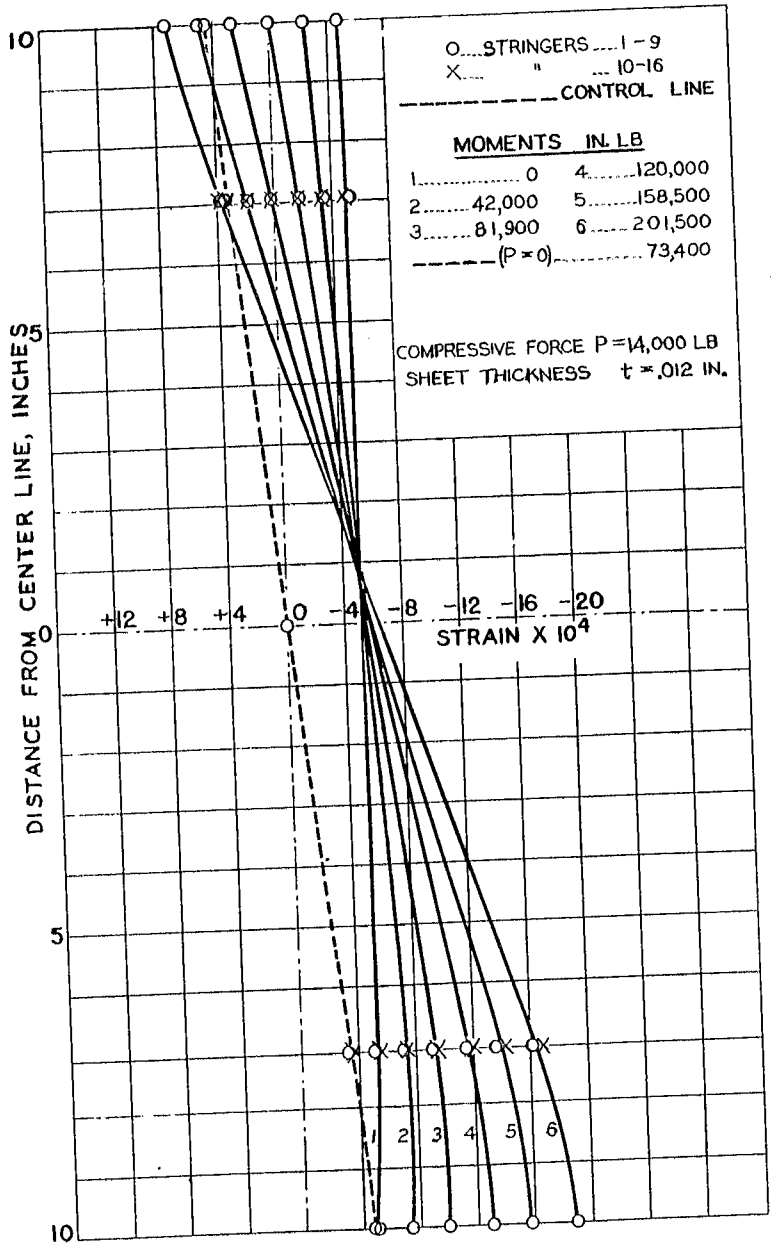

FIG.17. STRAIN DIAGRAM OF CYLINDER NO. 10 BAND B.

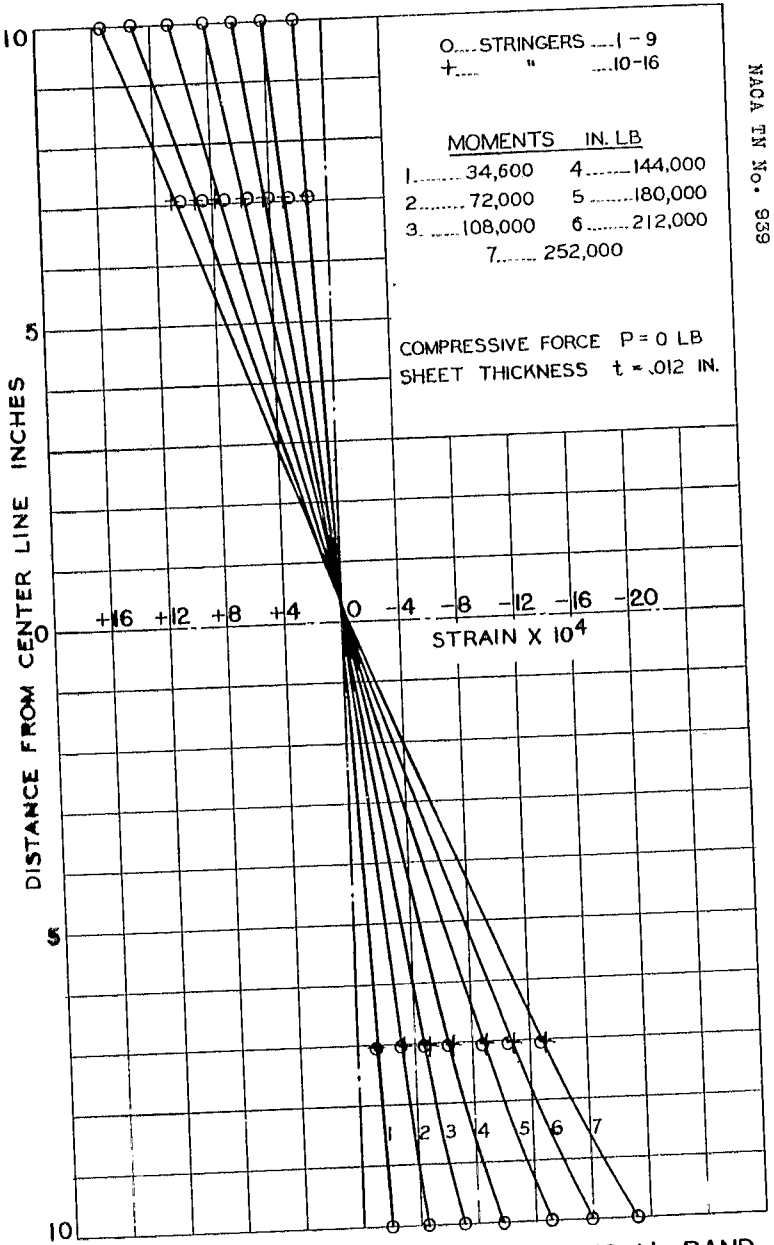

FIG.18. STRAIN DIAGRAM OF CYLINDER NO. 11 BAND A.

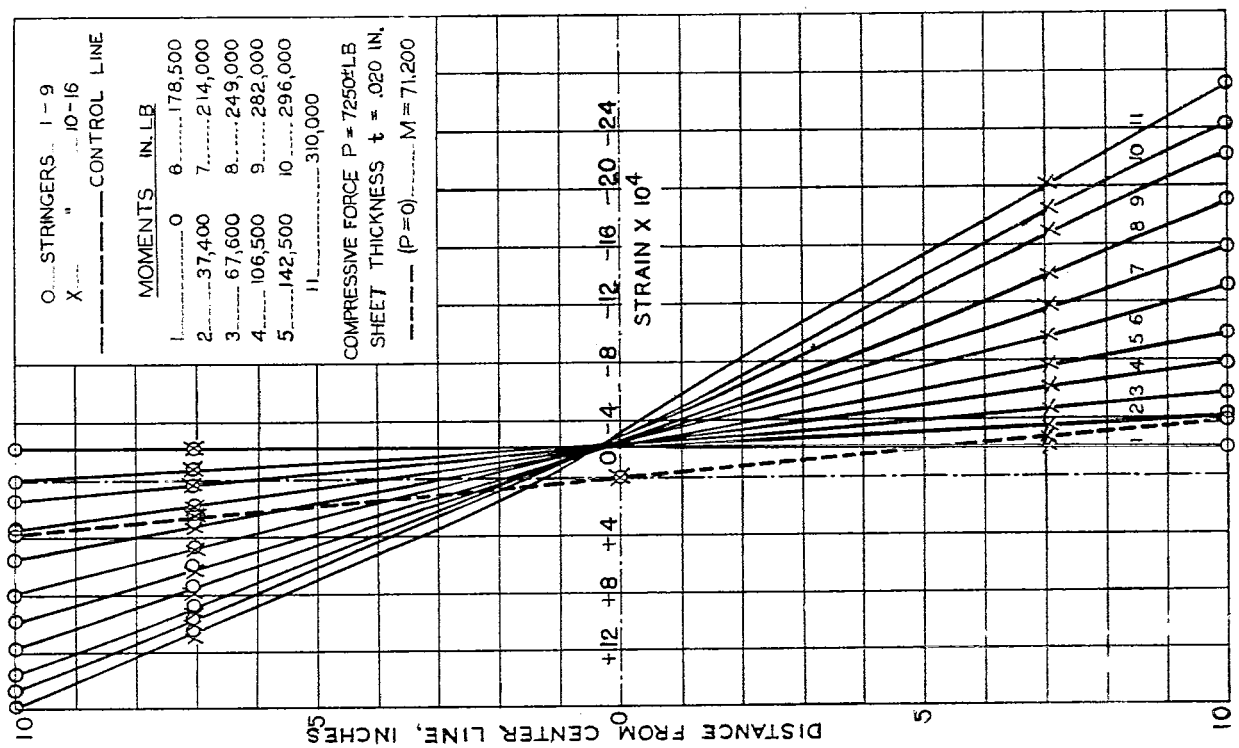

FIG.20. STRAIN DIAGRAM OF CYLINDER NO. 12 BAND A.

(1 block = 10/32")

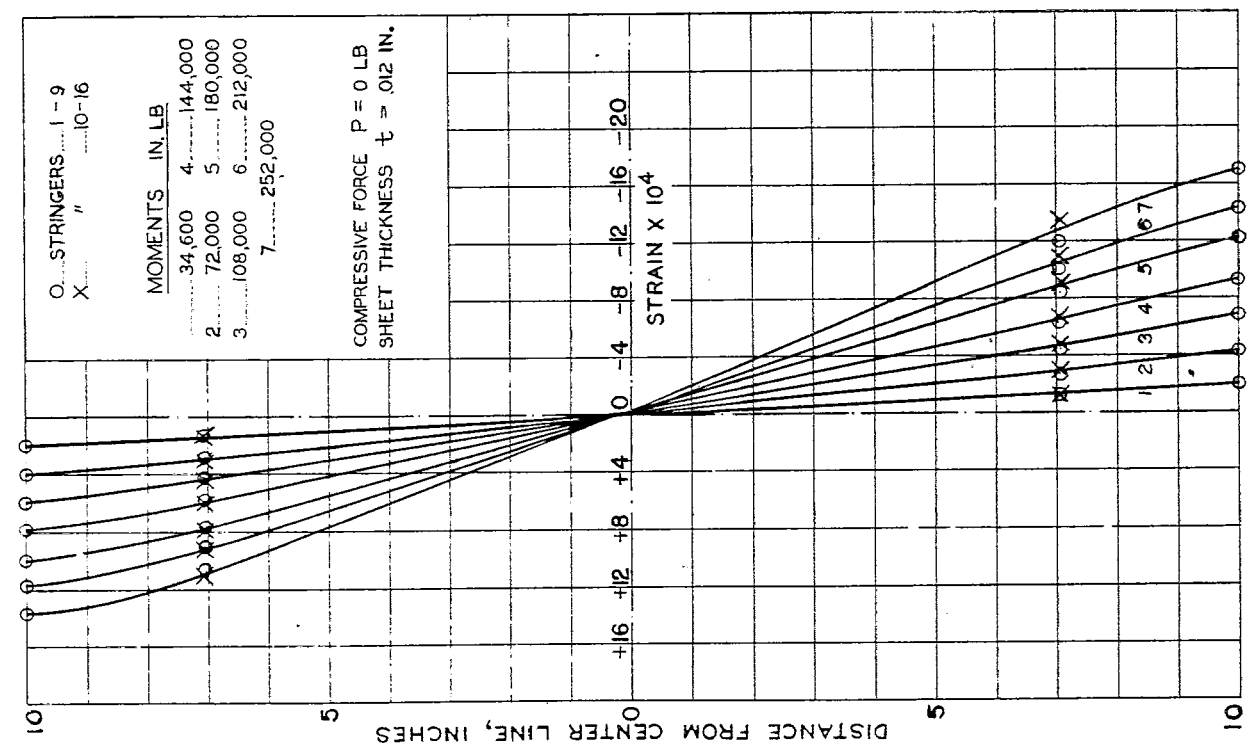

FIG.19. STRAIN DIAGRAM OF CYLINDER NO. 11 BAND B.

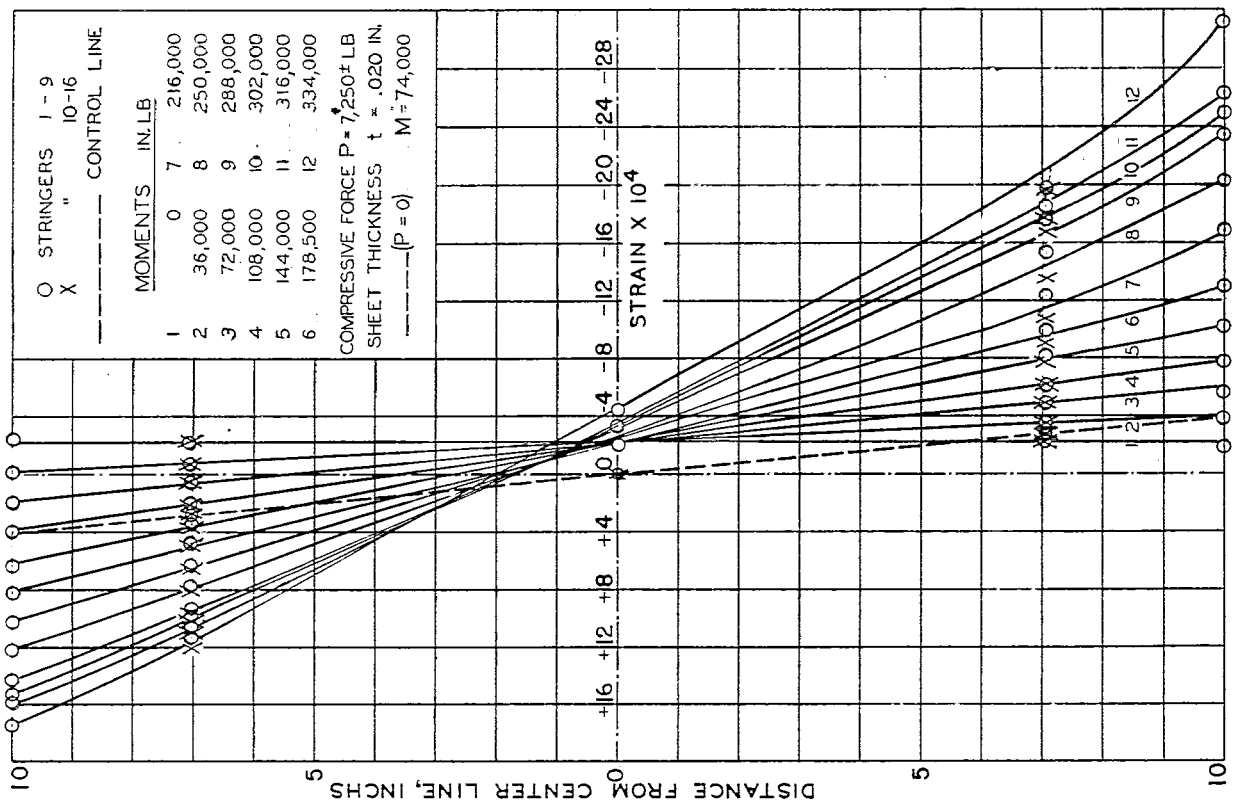

FIG.22. STRAIN DIAGRAM OF CYLINDER NO. 13 BAND A

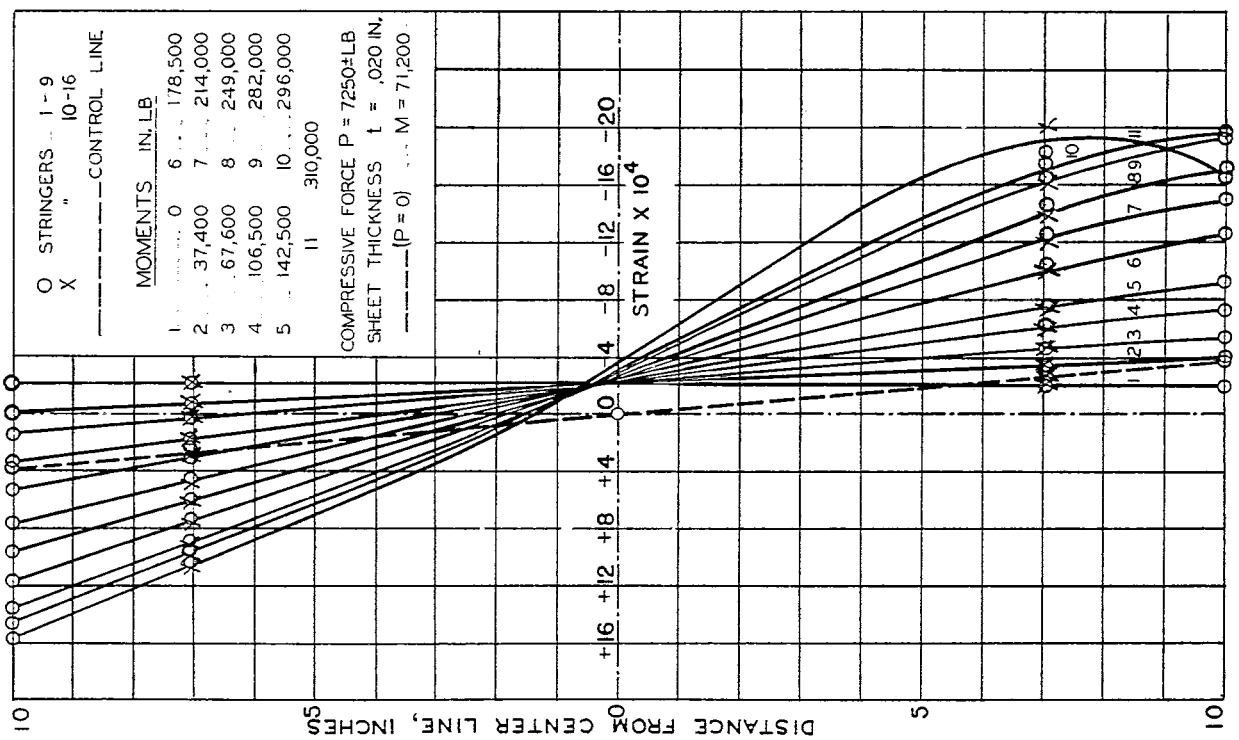

FIG.21. STRAIN DIAGRAM OF CYLINDER NO. 12 BAND B.

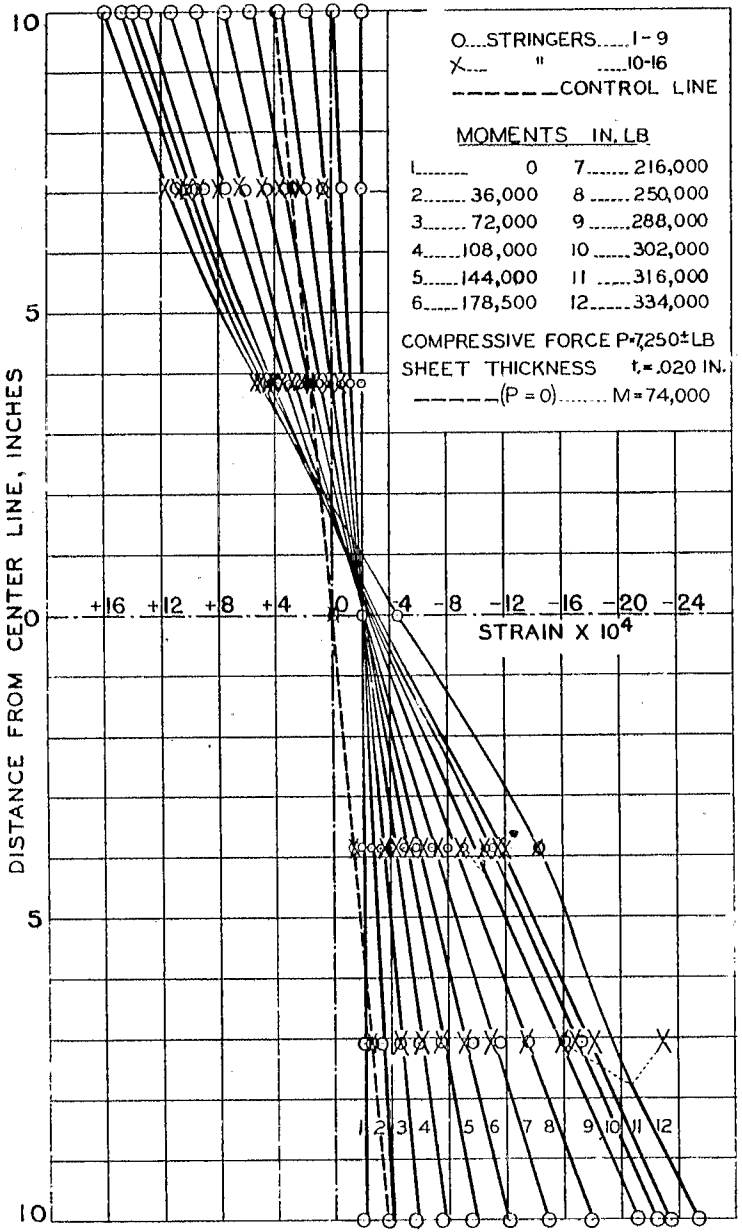

FIG.23. STRAIN DIAGRAM OF CYLINDER NO. 13 BAND B.

(1 block = 10/32")

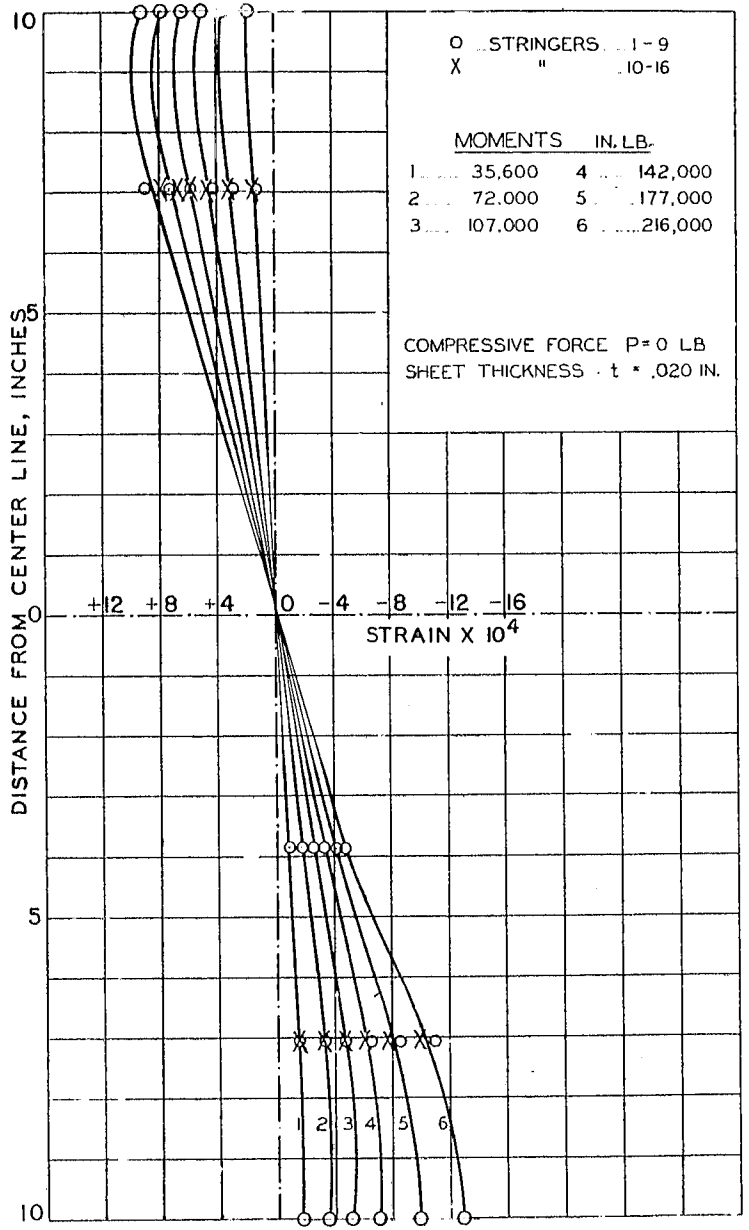

FIG.24. STRAIN DIAGRAM OF CYLINDER NO. 2 BAND A.

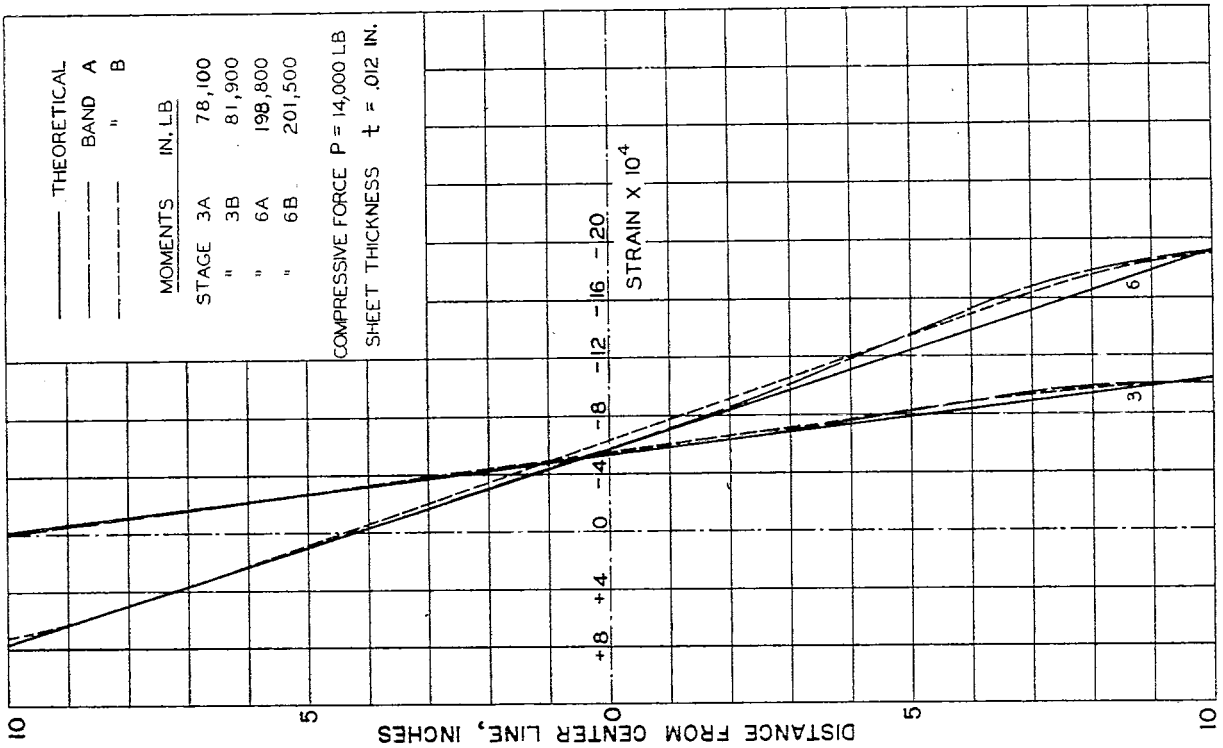

FIG. 26. STRAIN DIAGRAM OF CYLINDER NO. 10
COMPARISON WITH THEORETICAL.

(1 block = 10/32")

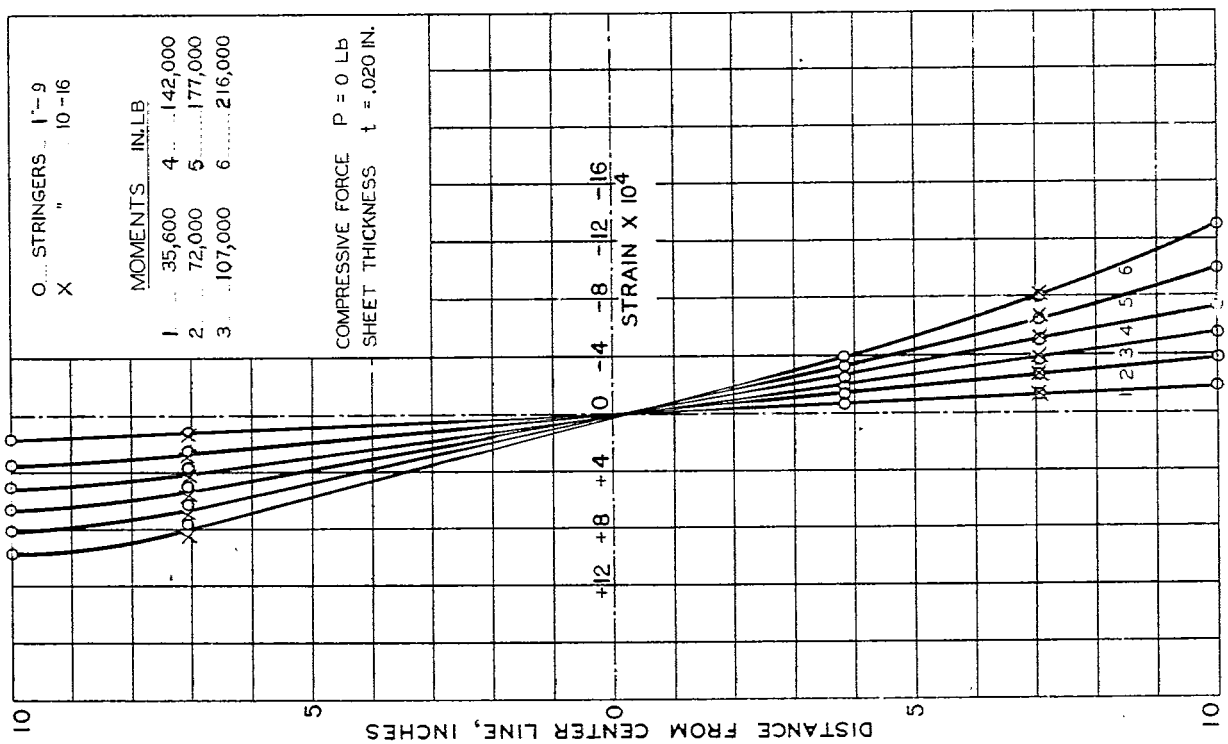

FIG.25. STRAIN DIAGRAM OF CYLINDER NO. 2 BAND B.

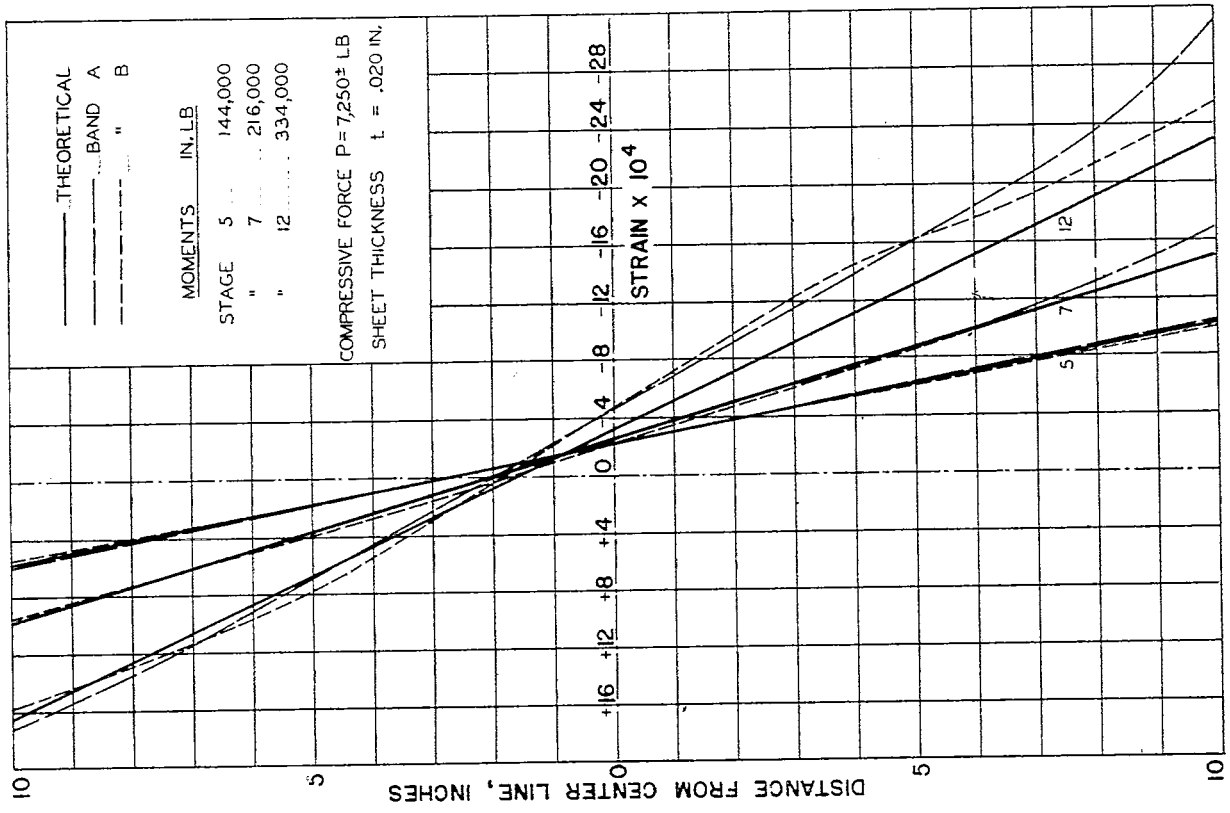

FIG. 28. STRAIN DIAGRAM OF CYLINDER NO. 13
COMPARISON WITH THEORETICAL.

(1 block = 10/32")

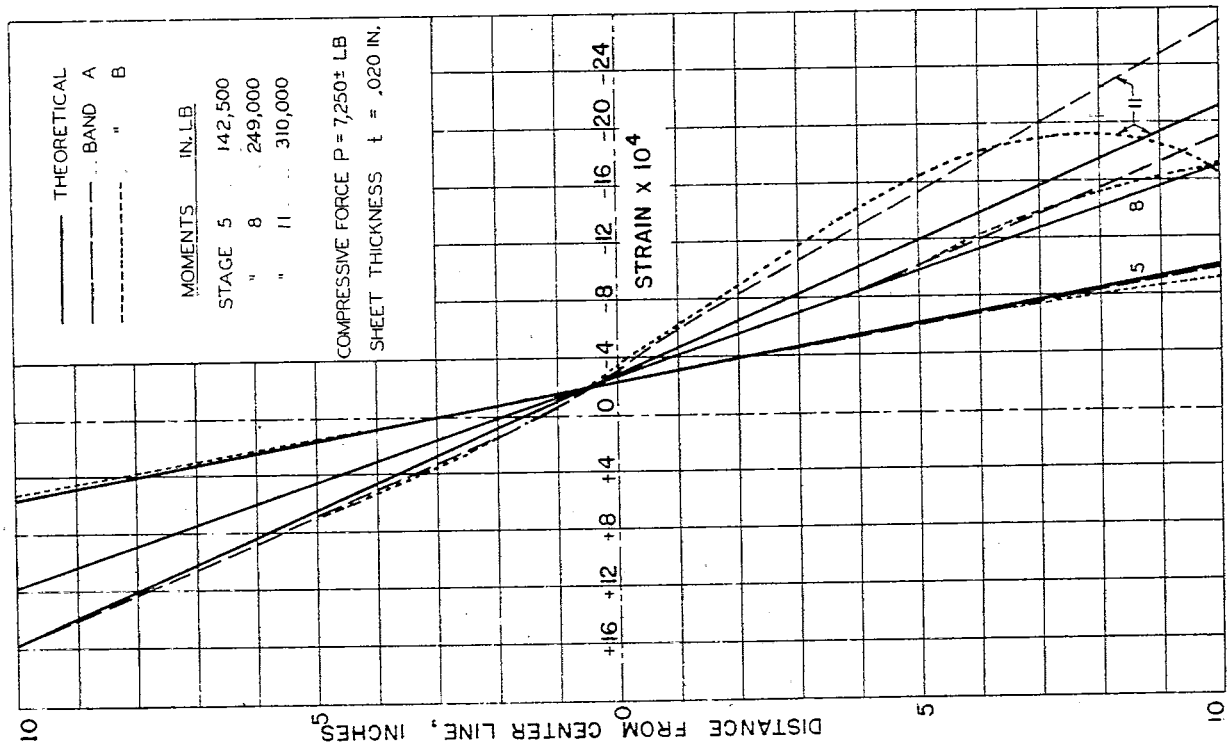

FIG. 27. STRAIN DIAGRAM OF CYLINDER NO. 12
COMPARISON WITH THEORETICAL.

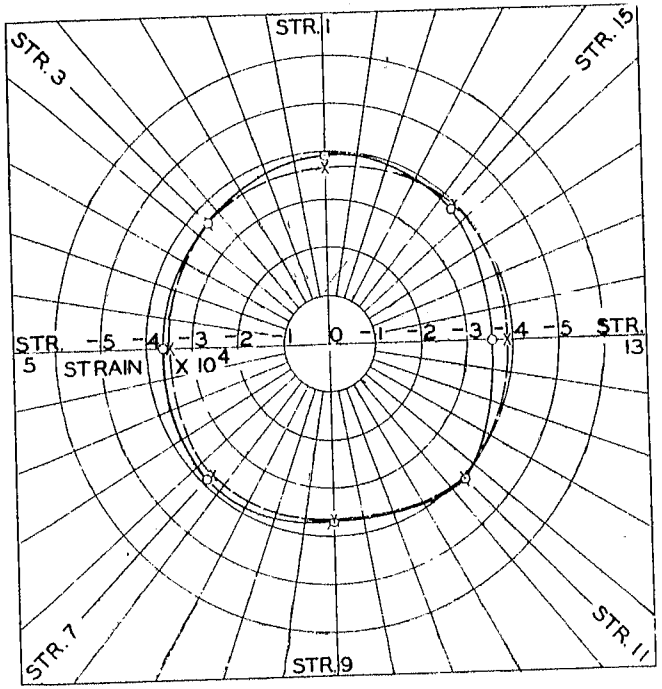

FIG. 29 DISTRIBUTION OF STRAIN IN COMPRESSION.
CYLINDER NO. 7 SHEET THICKNESS t = .020 IN.
—○— BAND A ---×--- BAND B
COMPRESSIVE FORCE P = 13,000 LB

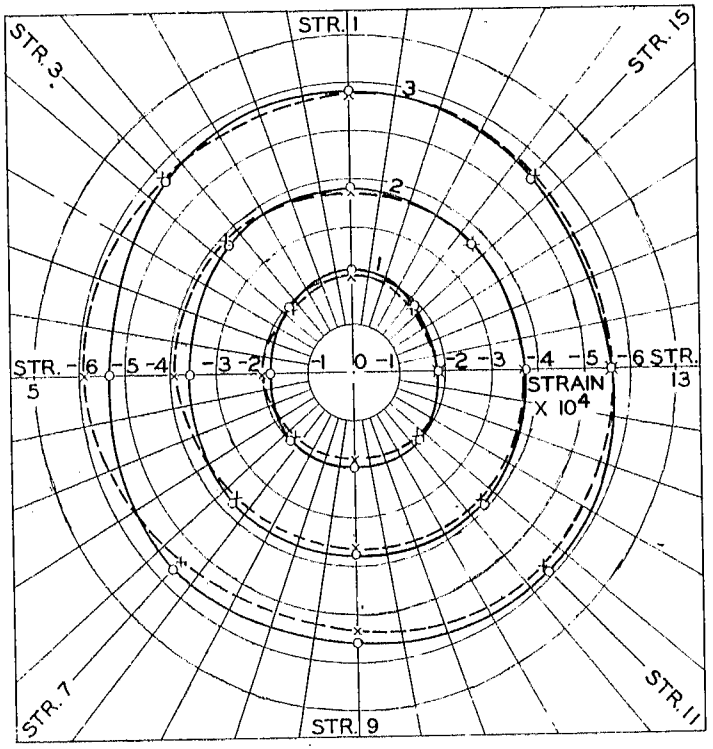

FIG. 30 DISTRIBUTION OF STRAIN IN COMPRESSION
CYLINDER NO. 8 SHEET THICKNESS t = .020 IN.
—○— BAND A ---×--- BAND B
COMPRESSIVE FORCE P LB
1 - 6,500 2 - 12,700 3 - 19,300

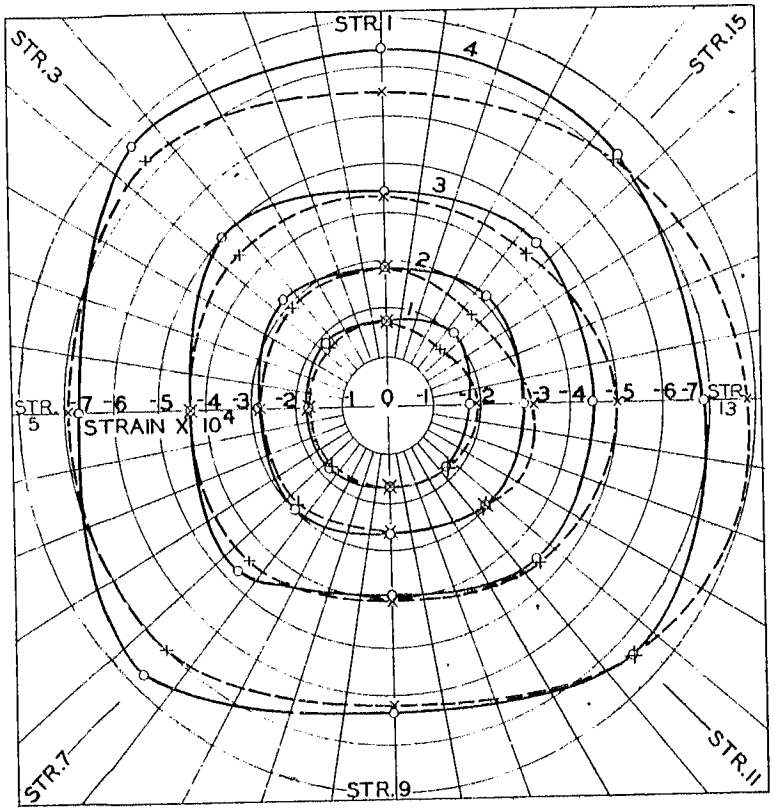

FIG. 31 DISTRIBUTION OF STRAIN IN COMPRESSION

CYLINDER NO. 9 SHEET THICKNESS t = .012 IN.

—o— BAND A - - -x- - - BAND B

COMPRESSIVE FORCE P ... LB

1 - 5,000 2 - 7,970 3 - 11,900 4 - 18,000.

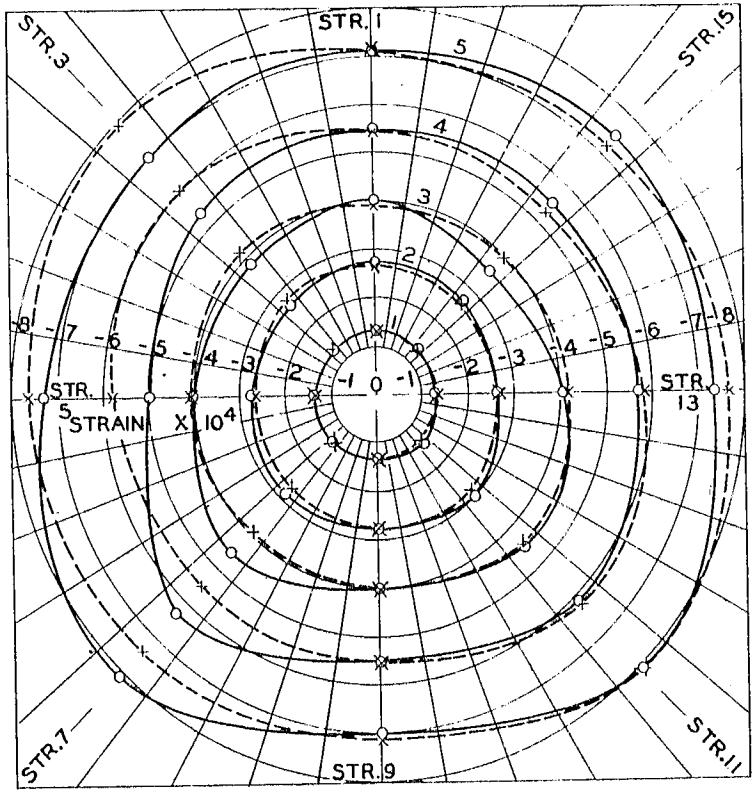

FIG. 32 DISTRIBUTION OF STRAIN IN COMPRESSION

CYLINDER NO. 10 SHEET THICKNESS t = .012 IN.

—o— BAND A - - -x- - - BAND B

COMPRESSIVE FORCE P LB

1 - 3,900 2 - 7,860 3 - 11,600 4 - 15,600 5 - 19,850

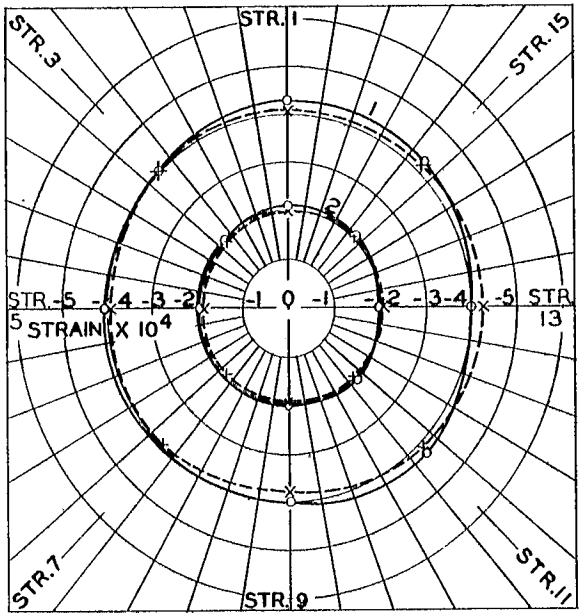

FIG. 33 DISTRIBUTION OF STRAIN IN COMPRESSION

CYLINDER NO. 12 SHEET THICKNESS t = .020 IN.

——o—— BAND A ----x---- BAND B

COMPRESSIVE FORCE P LB

1 - 14,600 2 - 7,100

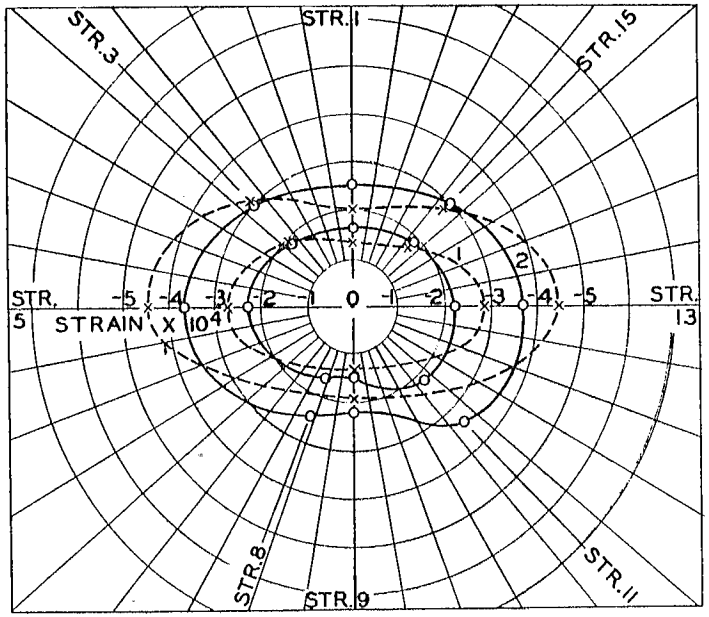

FIG. 34 DISTRIBUTION OF STRAIN IN COMPRESSION

CYLINDER NO. 6 SHEET THICKNESS t = 020 IN.

——o—— BAND A ---x--- BAND B

COMPRESSIVE FORCE P LB

1 - 6,400 2 - 10,000

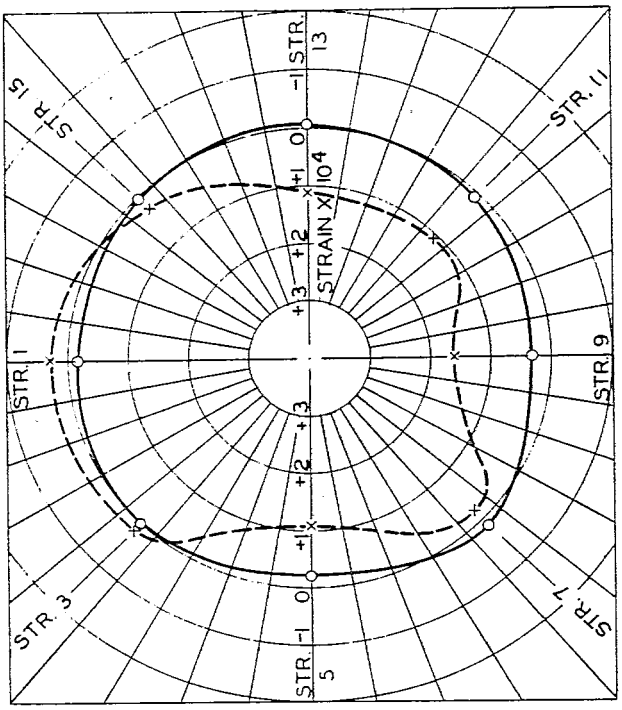

FIG. 36. INITIAL STRAIN IN CYLINDER NO. 10 CAUSED BY TIGHTENING STRINGER GRIP FITTINGS TO RING NO. 1.

—○— BAND A ---x--- BAND B

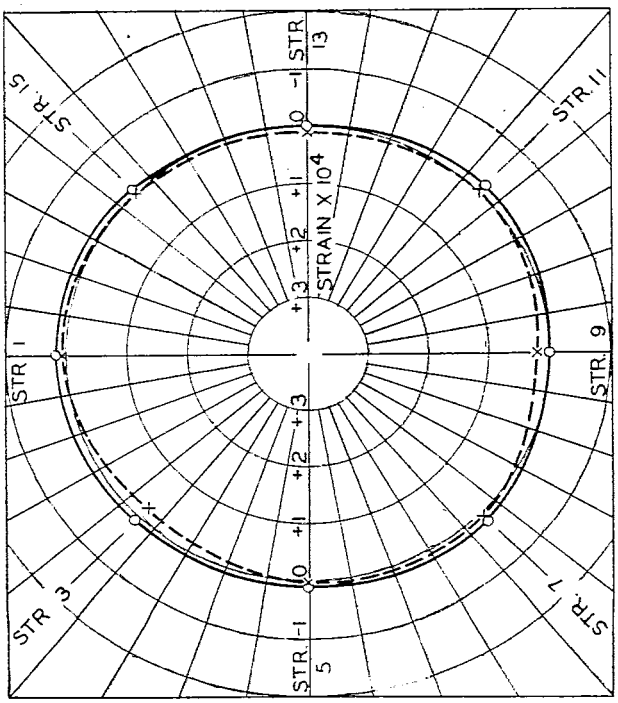

FIG. 35. INITIAL STRAIN IN CYLINDER NO. 10 CAUSED BY TIGHTENING RING NO. 1 TO END STAND.

—○— BAND A ---x--- BAND B

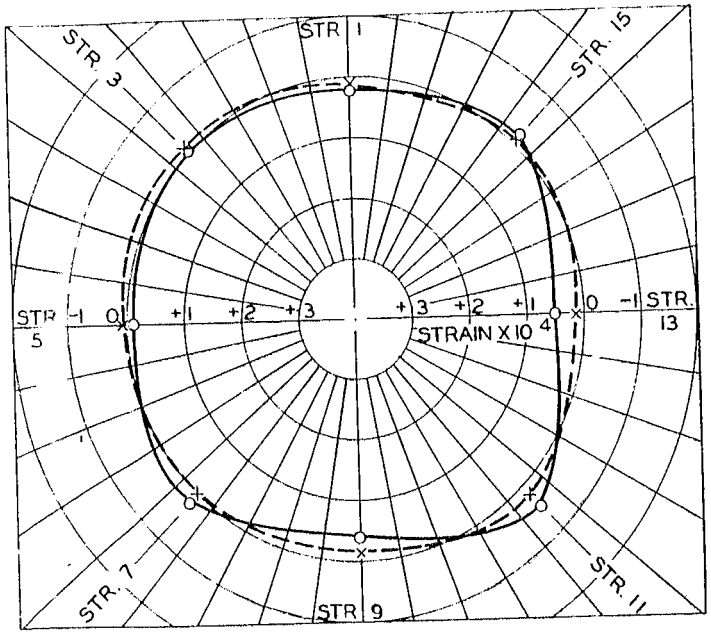

FIG. 37 INITIAL STRAIN IN CYLINDER NO. 10
CAUSED BY TIGHTENING STRINGER GRIP FITTINGS TO RING NO. 2.

——o—— BAND A ---x--- BAND B

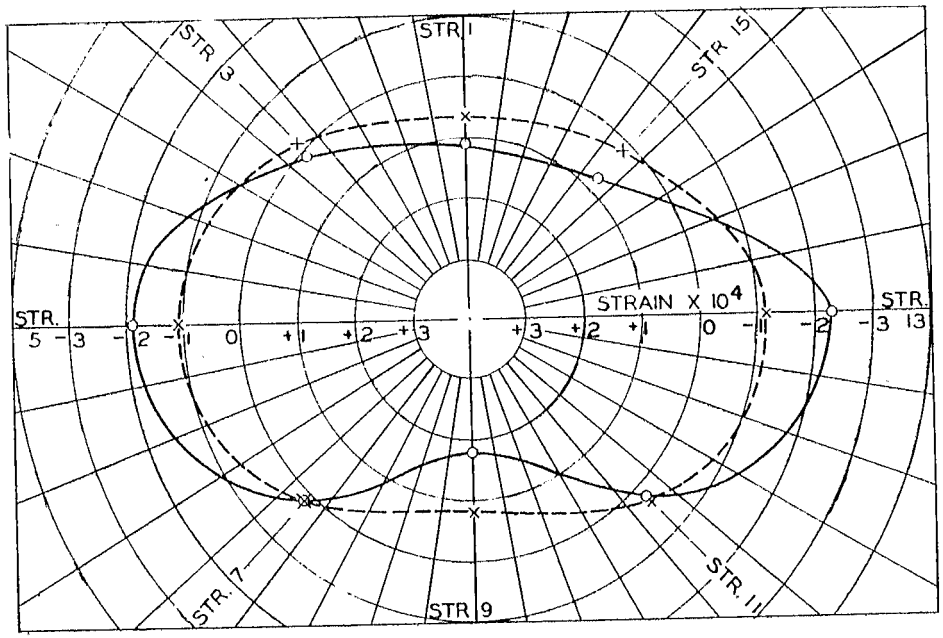

FIG. 38. INITIAL STRAIN IN CYLINDER NO. 10
CAUSED BY TIGHTENING TO LOADING HEAD

——o—— BAND A ---x--- BAND B

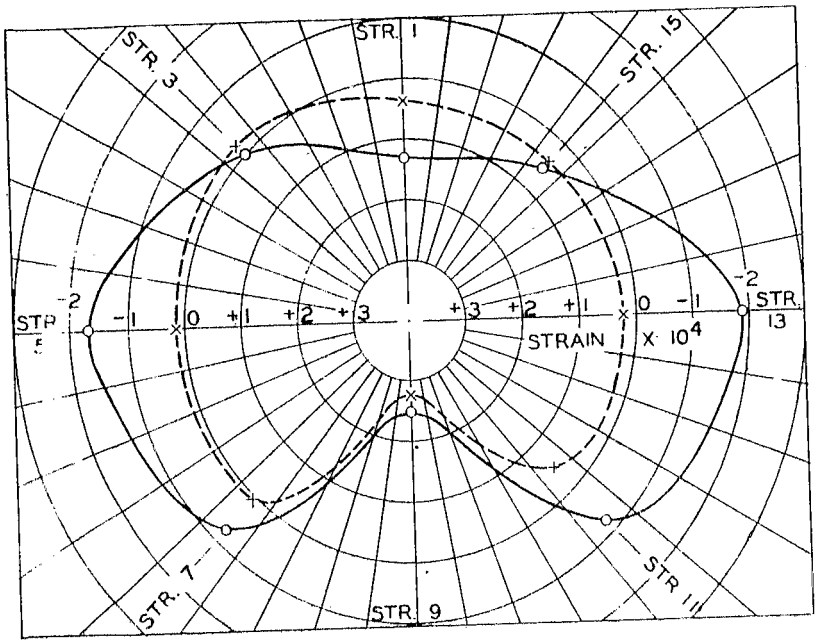

FIG. 39. TOTAL INITIAL STRAIN IN CYLINDER NO. 10

—o— BAND A --x-- BAND B

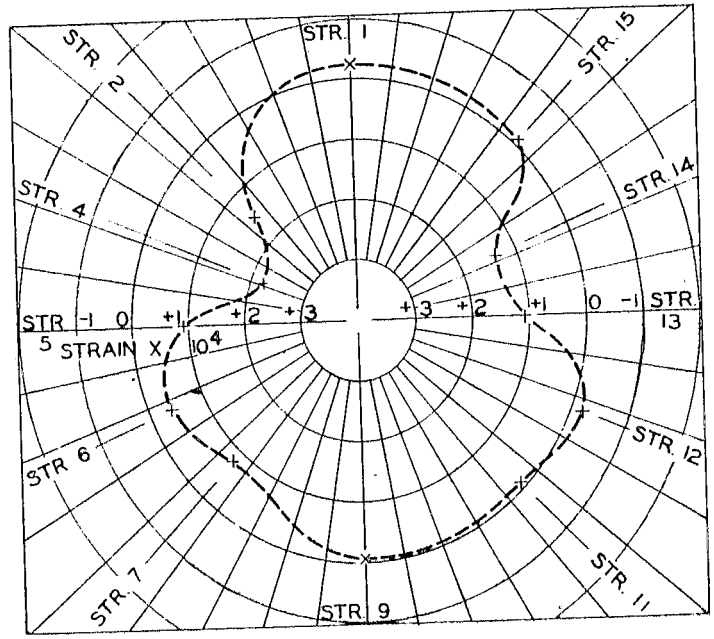

FIG. 40. INITIAL STRAIN IN CYLINDER NO. 13 CAUSED BY TIGHTENING STRINGER GRIP FITTINGS TO RING NO. 1.

---x--- BAND B

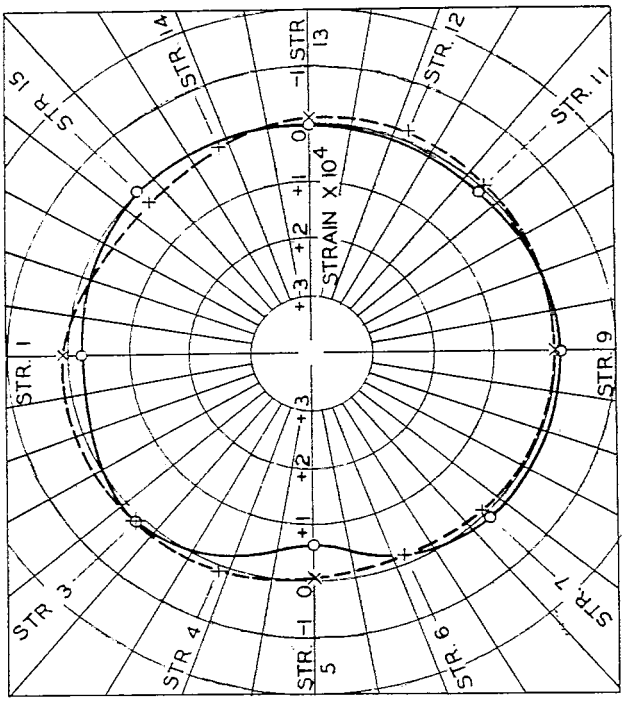

FIG. 42. INITIAL STRAIN IN CYLINDER NO. 13 CAUSED BY TIGHTENING STRINGER GRIP FITTINGS TO RING NO. 2.

—○— BAND A —×— BAND B

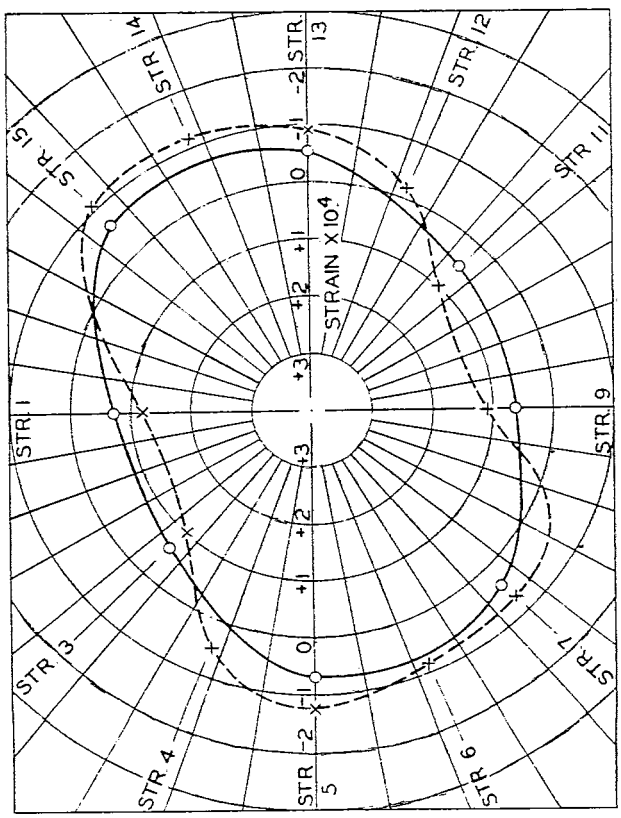

FIG. 41. INITIAL STRAIN IN CYLINDER NO. 13 CAUSED BY TIGHTENING RING NO. 1 TO END STAND.

—○— BAND A —×— BAND B

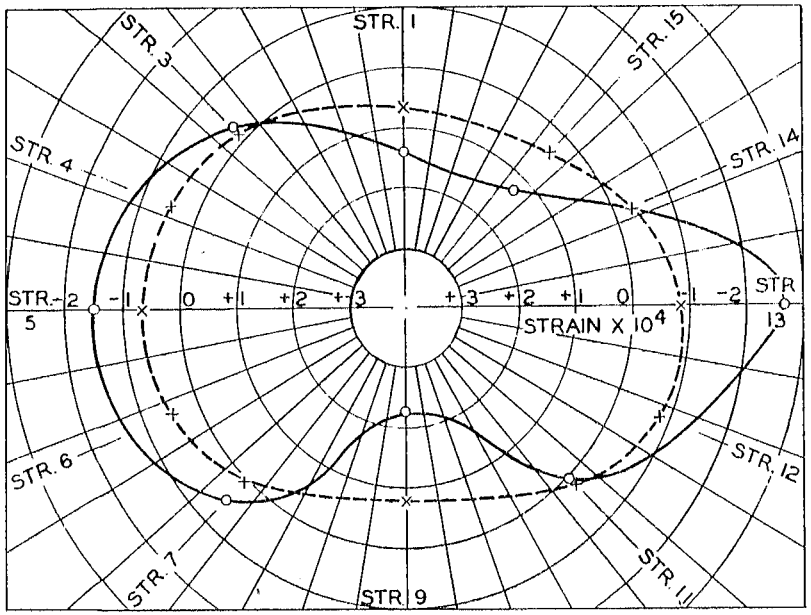

FIG. 43. INITIAL STRAIN IN CYLINDER NO. 13
CAUSED BY TIGHTENING TO LOADING HEAD
—o— BAND A ---x--- BAND B

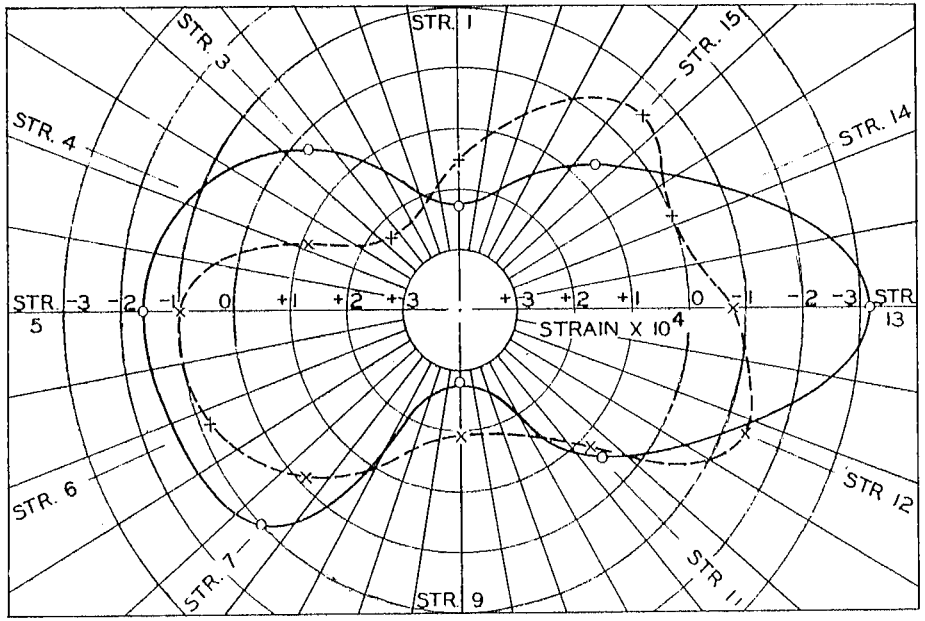

FIG. 44. TOTAL INITIAL STRAIN IN CYLINDER NO. 13
—o— BAND A ---x--- BAND B

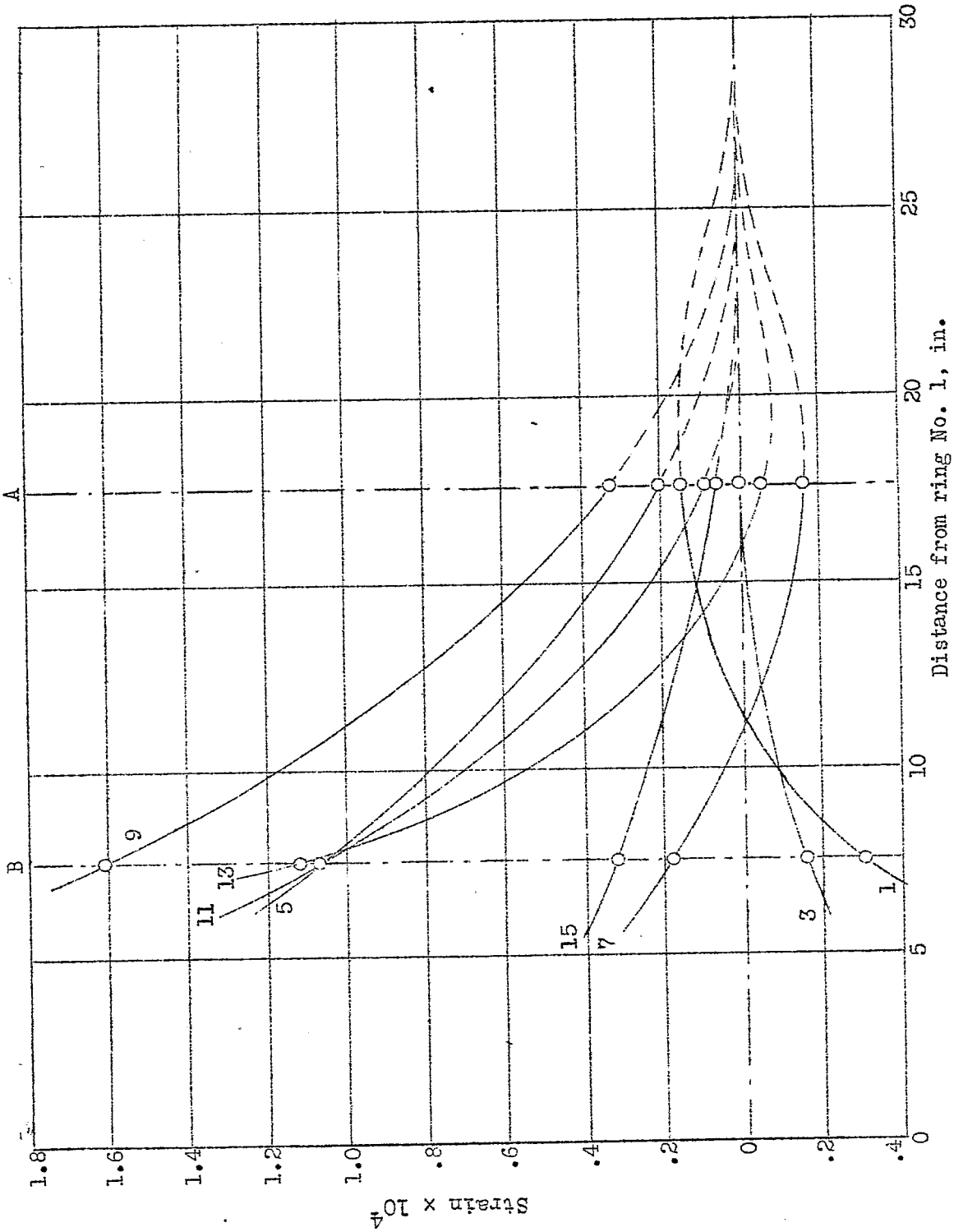

Figure 45.- Axial variation of strain caused by tightening stringer grip fittings to ring No. 1.

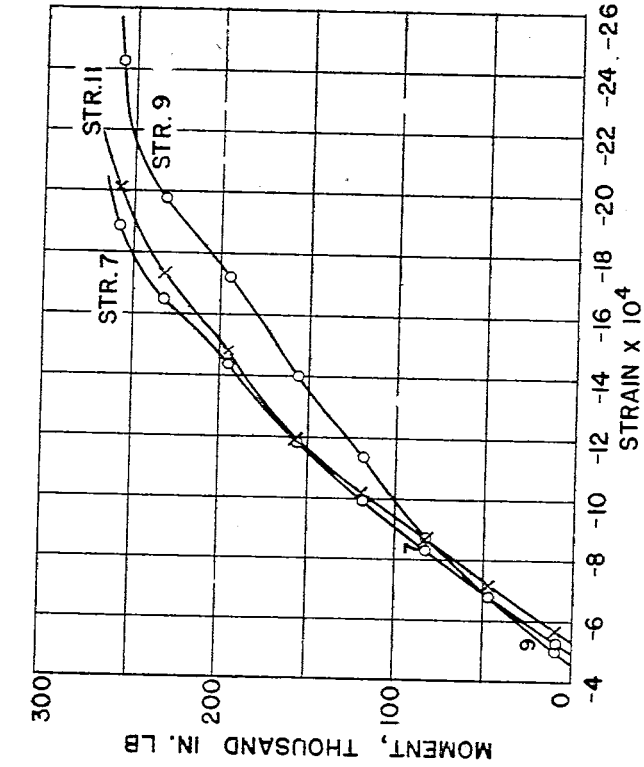

FIG. 47.-STRINGER STRAIN VARIATION.
CYLINDER NO. 7 BAND B.
COMPRESSIVE FORCE P=17,000 LB

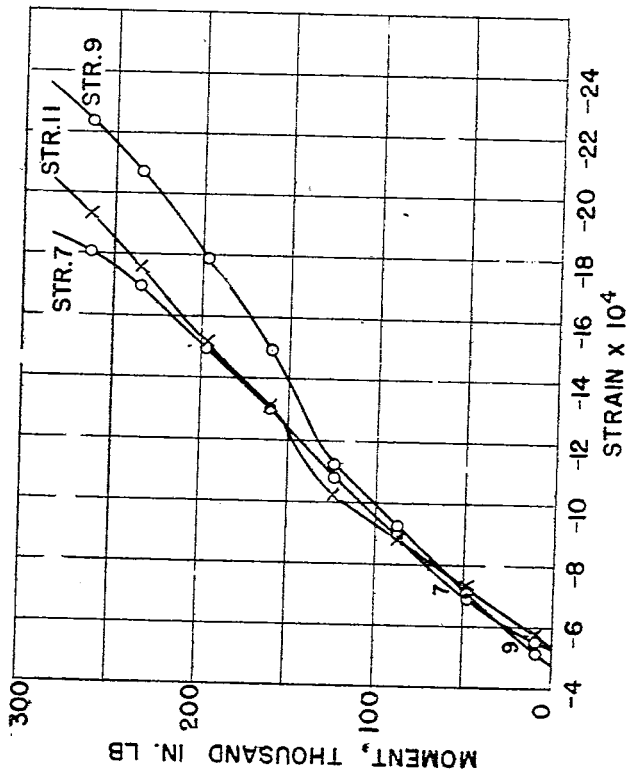

FIG. 46.-STRINGER STRAIN VARIATION.
CYLINDER NO. 7 BAND A.
COMPRESSIVE FORCE P=17,000 LB

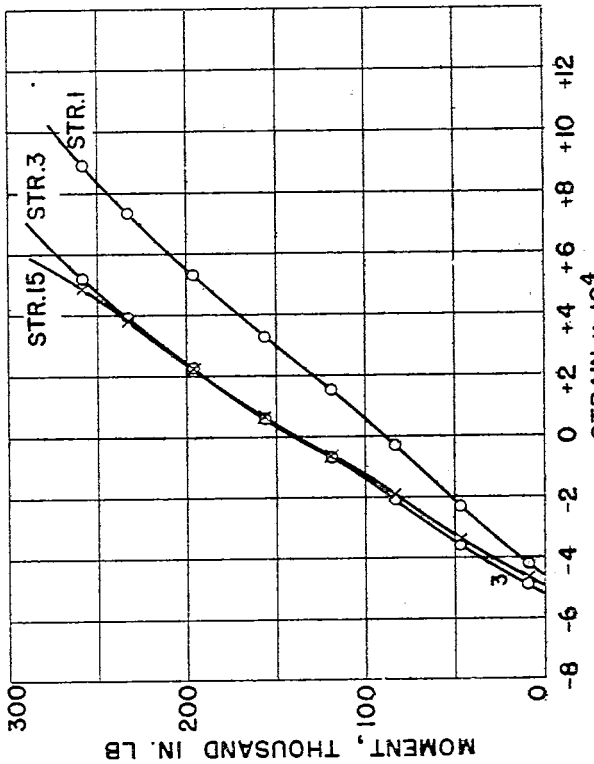

FIG. 49.-STRINGER STRAIN VARIATION
CYLINDER NO. 7 BAND B.
COMPRESSIVE FORCE P=17,000 LB

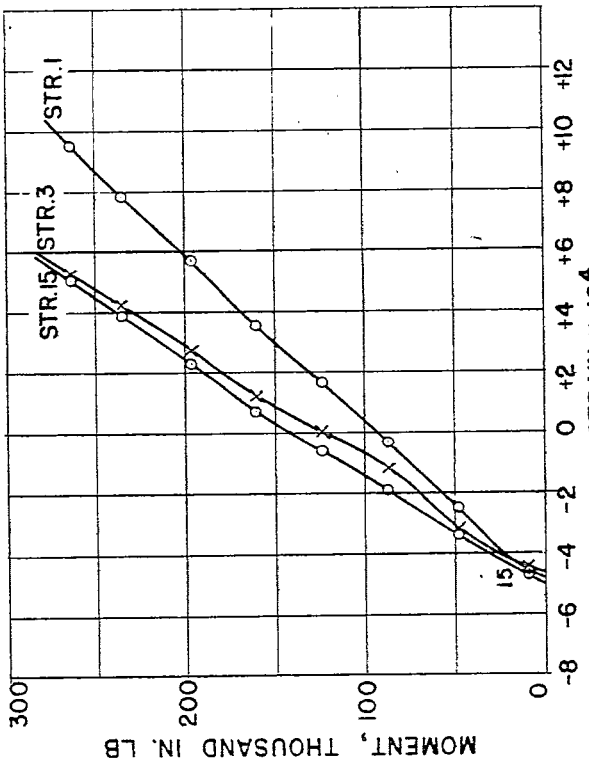

FIG. 48.-STRINGER STRAIN VARIATION.
CYLINDER NO. 7 BAND A.
COMPRESSIVE FORCE P=17,000 LB

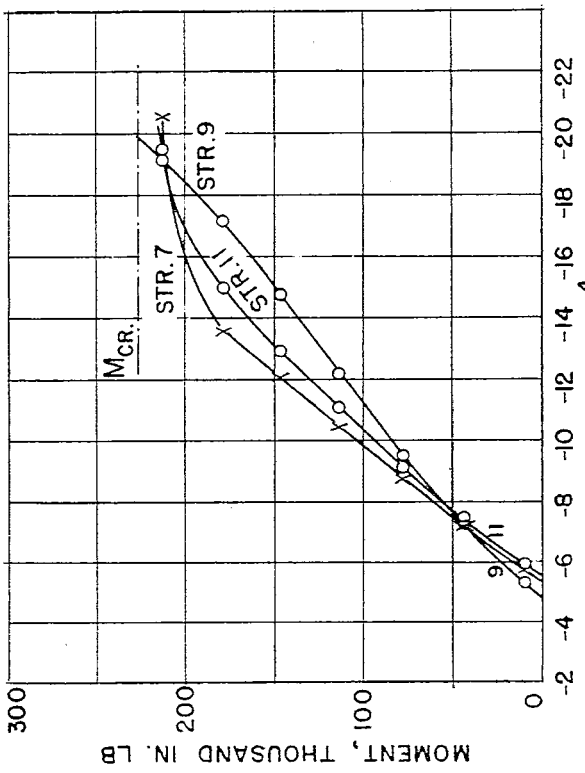

FIG. 51.- STRINGER STRAIN VARIATION.
CYLINDER NO. 9 BAND B.
COMPRESSIVE FORCE P=14,000 LB

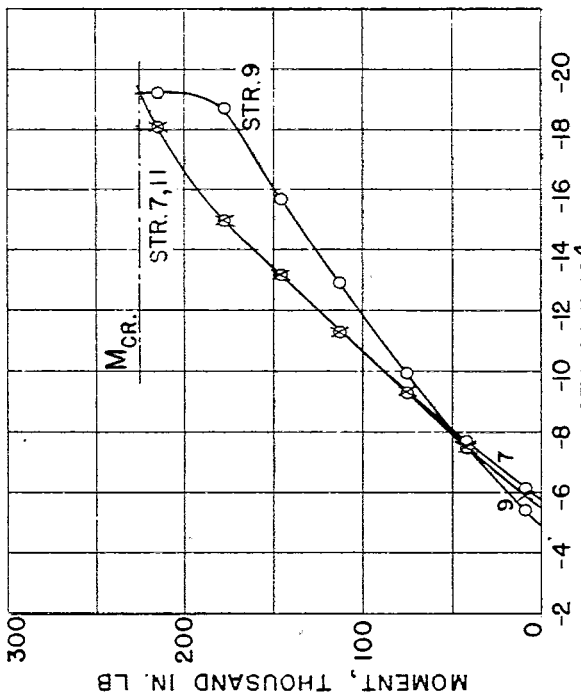

FIG. 50.- STRINGER STRAIN VARIATION.
CYLINDER NO. 9 BAND A.
COMPRESSIVE FORCE P=14,000 LB

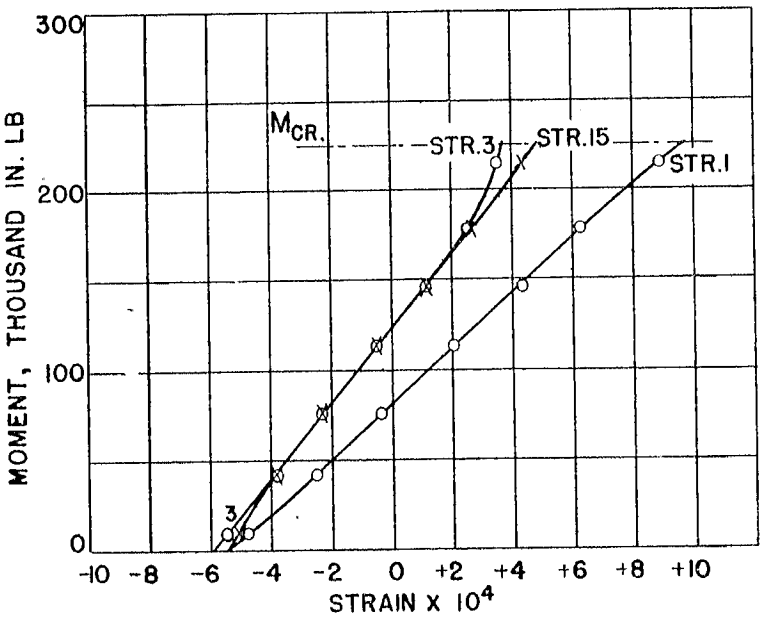

FIG. 52.-STRINGER STRAIN VARIATION.

CYLINDER NO. 9 BAND A.
COMPRESSIVE FORCE P = 14,000 LB

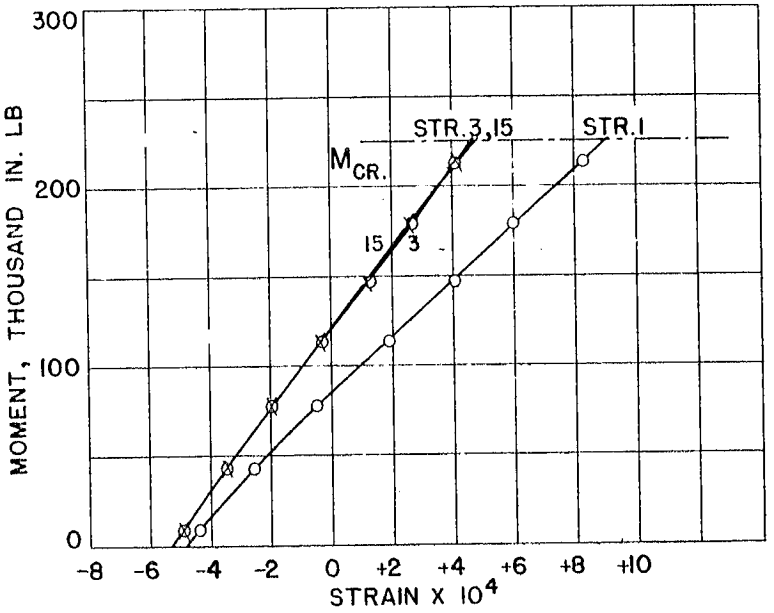

FIG. 53.-STRINGER STRAIN VARIATION.

CYLINDER NO. 9 BAND B.
COMPRESSIVE FORCE P = 14,000 LB

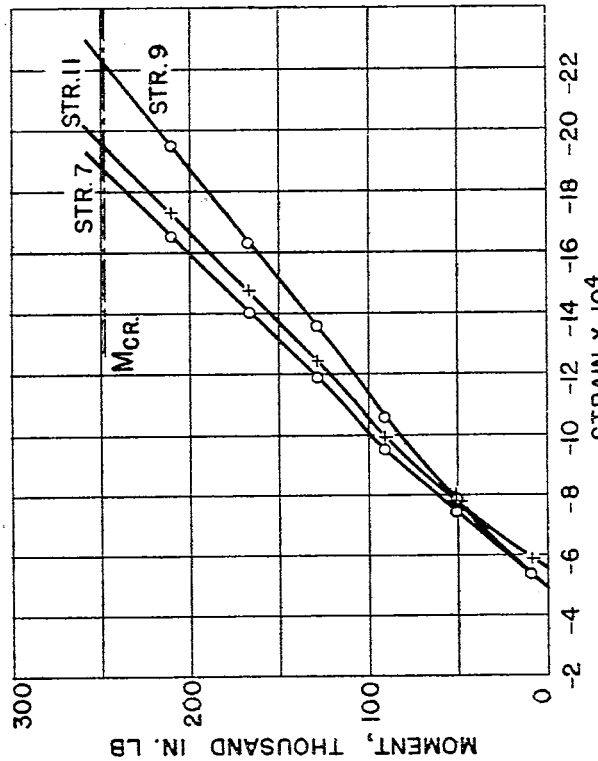

FIG. 55.- STRINGER STRAIN VARIATION.
CYLINDER NO. 10 BAND B.
COMPRESSIVE FORCE P = 14,000 LB

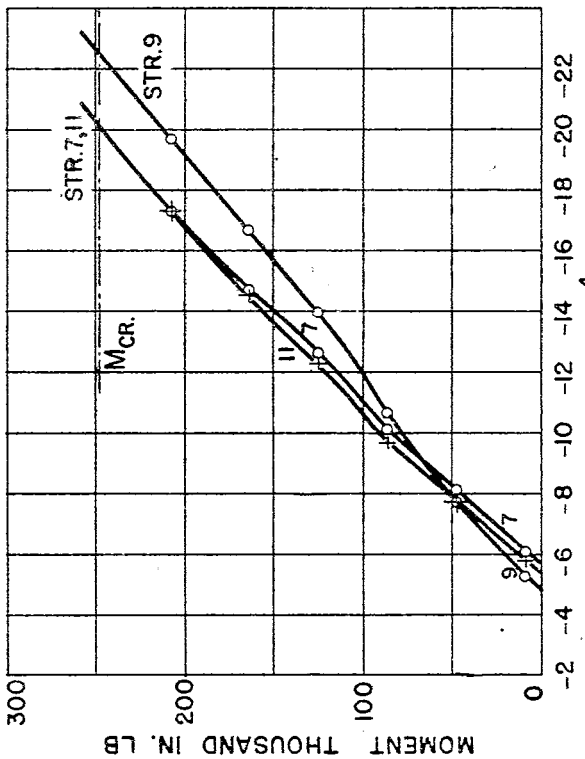

FIG. 54.- STRINGER STRAIN VARIATION.
CYLINDER NO. 10 BAND A.
COMPRESSIVE FORCE P = 14 000 LB

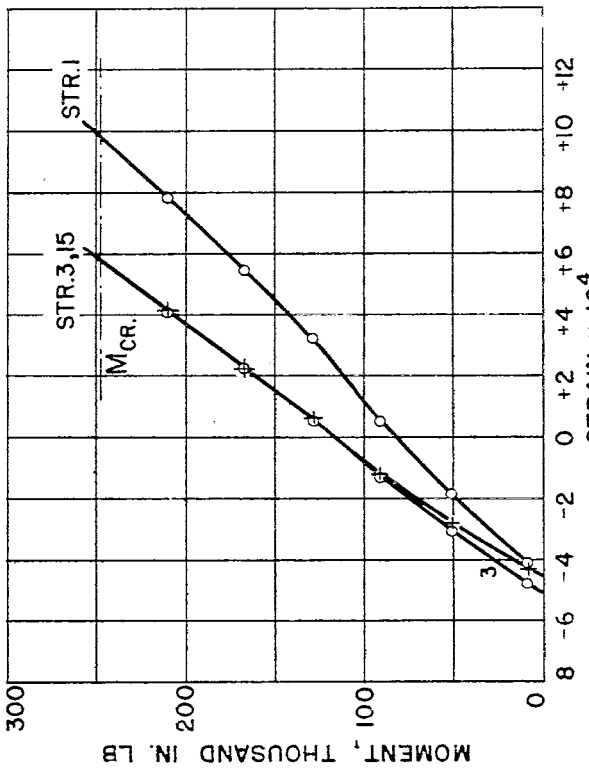

FIG. 57.- STRINGER STRAIN VARIATION.
CYLINDER NO. 10 BAND B.
COMPRESSIVE FORCE P = 14,000 LB

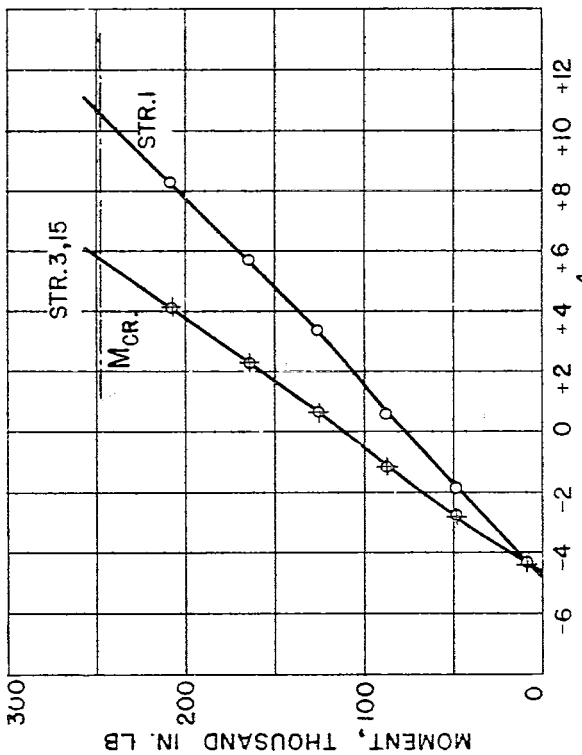

FIG. 56 - STRINGER STRAIN VARIATION.
CYLINDER NO. 10 BAND A.
COMPRESSIVE FORCE P = 14,000 LB

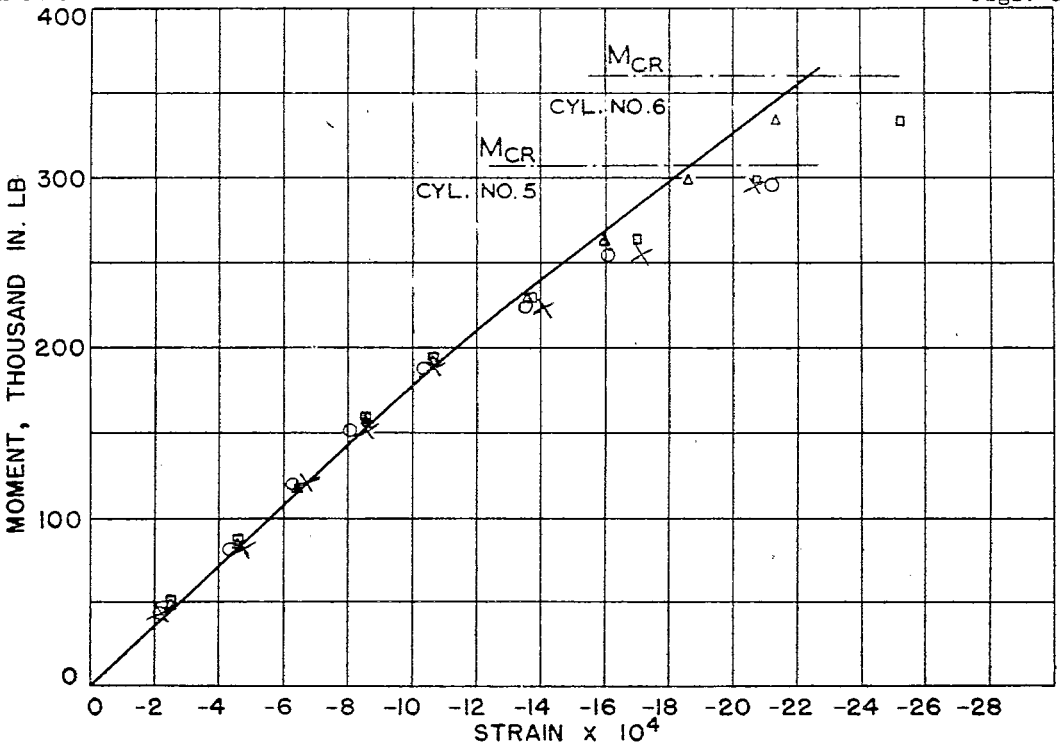

FIG. 58.–MAXIMUM COMPRESSIVE STRINGER STRAIN VARIATION.

COMPRESSIVE FORCE P = 0 LB SHEET THICKNESS t = .020 IN.

THEORETICAL

CYLINDER NO. 5 ○ BAND A × BAND B

" " 6 □ " A △ " B

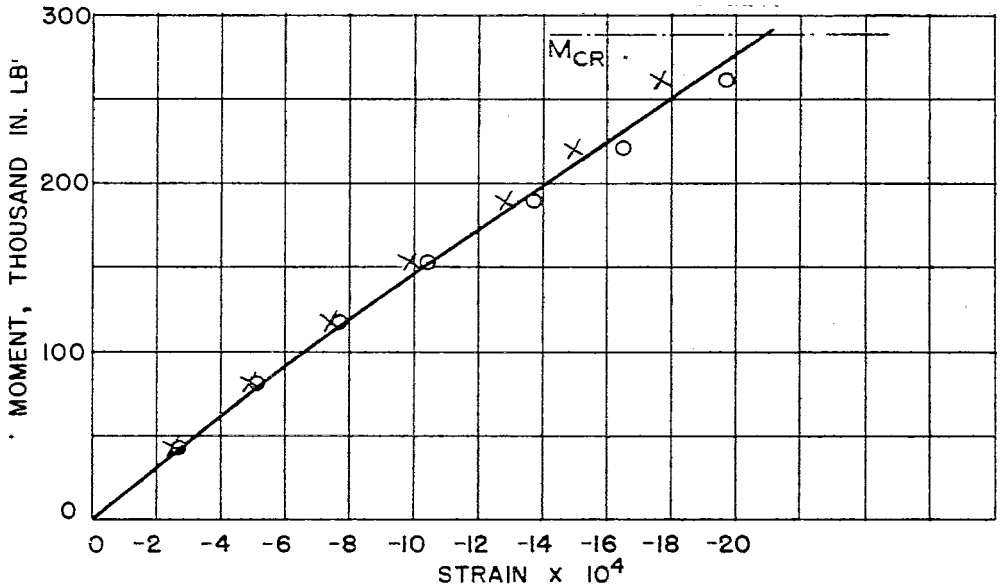

FIG. 59.– MAXIMUM COMPRESSIVE STRINGER STRAIN VARIATION.

COMPRESSIVE FORCE P = 0 SHEET THICKNESS t = .012 IN.

THEORETICAL

CYLINDER NO. 11 ○ BAND A × BAND B

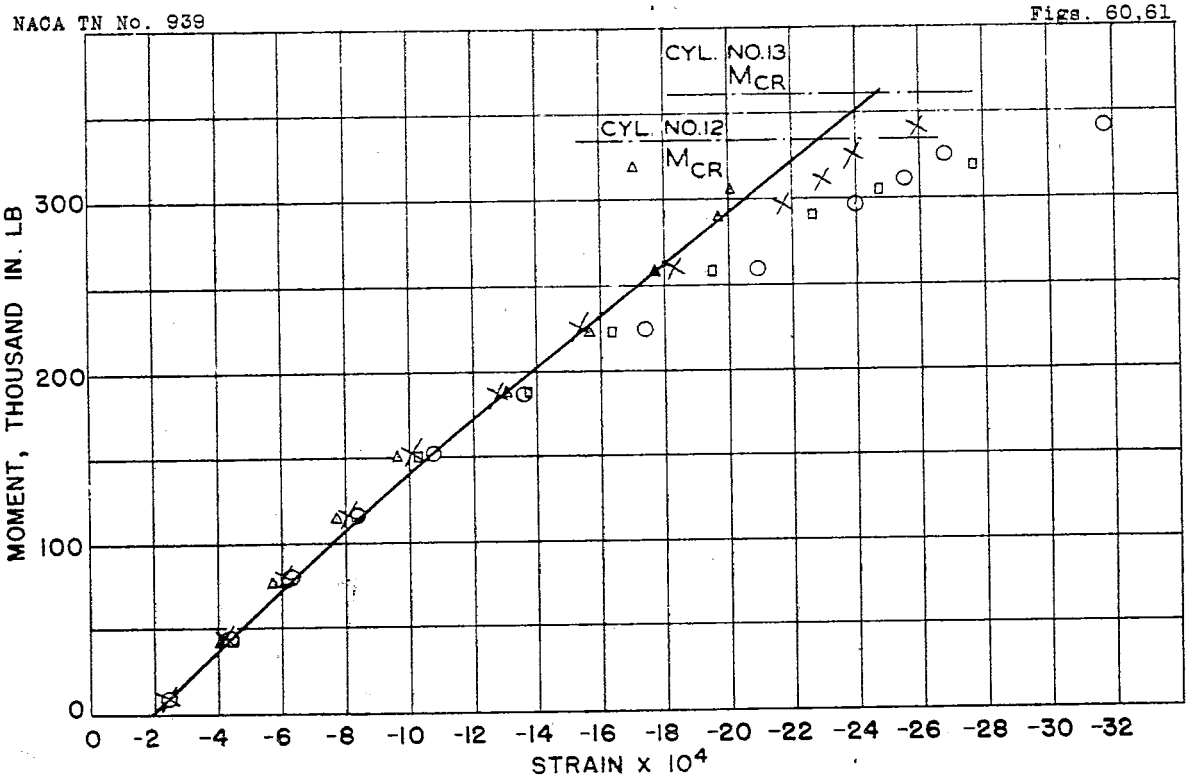

FIG. 60.- MAXIMUM COMPRESSIVE STRINGER STRAIN VARIATION.

COMPRESSIVE FORCE P = 7,250 LB SHEET THICKNESS t = .020 IN.

THEORETICAL

CYLINDER NO. 12 □ BAND A △ BAND B
" " 13 ○ " A X " B

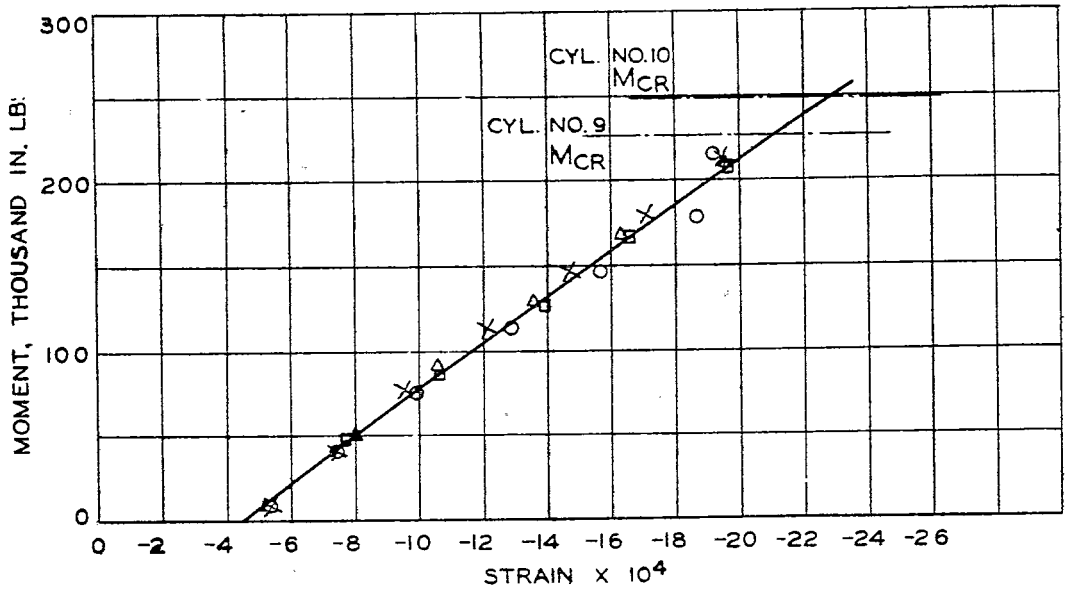

FIG. 61.- MAXIMUM COMPRESSIVE STRINGER STRAIN VARIATION.

COMPRESSIVE FORCE P = 14.000 LB SHEET THICKNESS t = .012 IN.

THEORETICAL

CYLINDER NO 9 —— ○ BAND A X BAND B
" " 10 —— □ " A △ " B

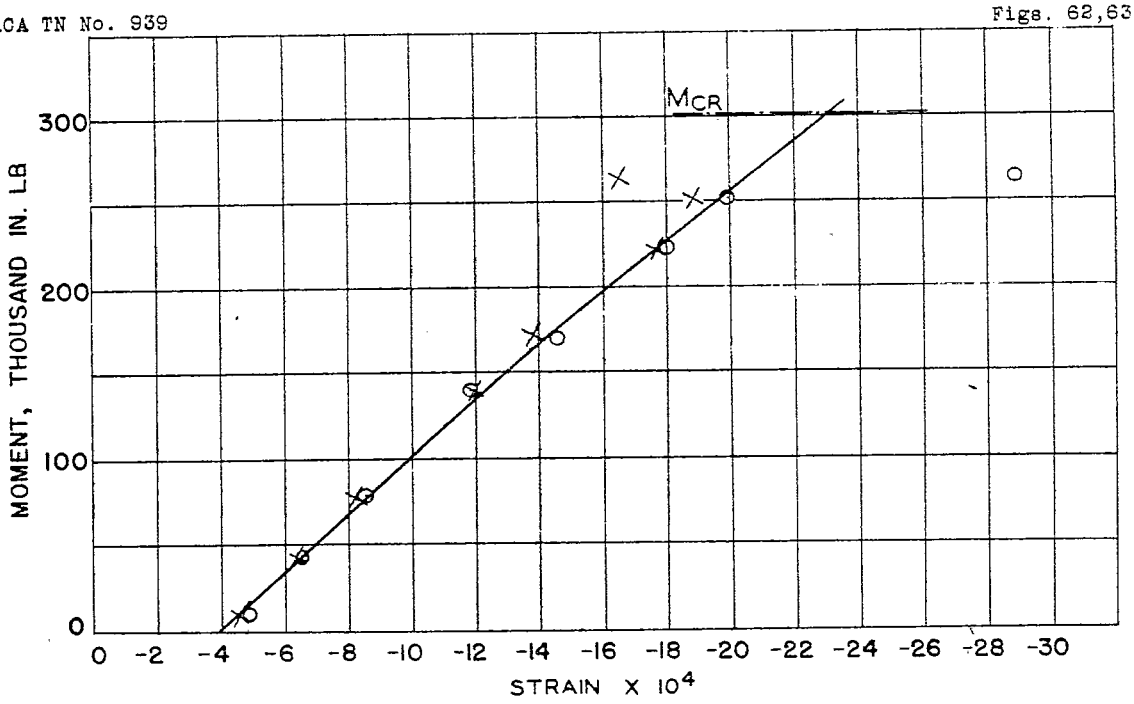

FIG. 62.- MAXIMUM COMPRESSIVE STRINGER STRAIN VARIATION.

COMPRESSIVE FORCE = 14,500 LB SHEET THICKNESS = .020 IN.

THEORETICAL

CYLINDER NO. 8 ——— O BAND A X BAND B

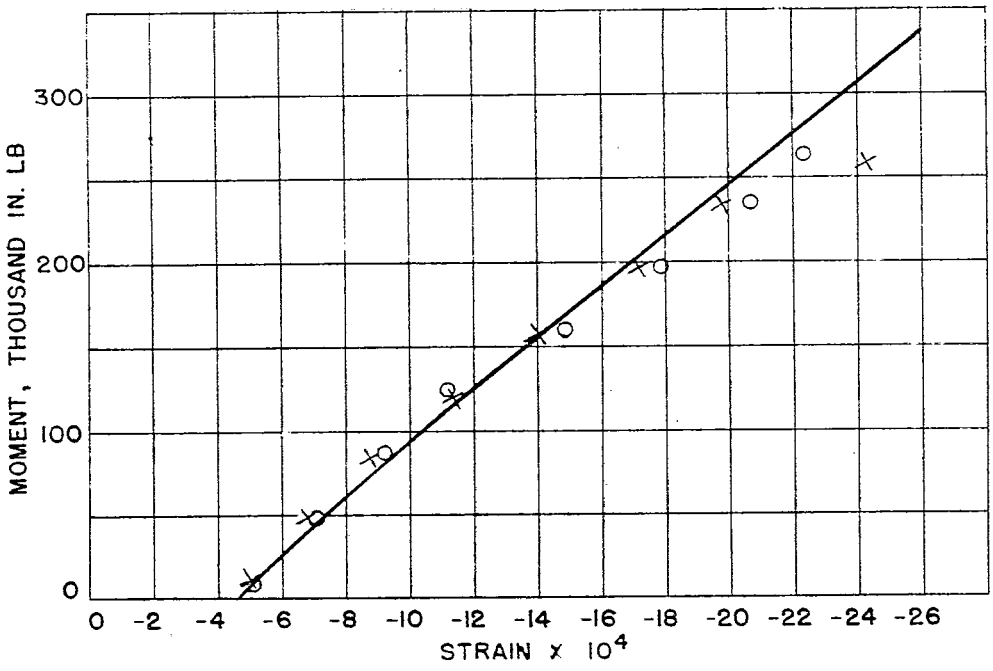

FIG. 63.- MAXIMUM COMPRESSIVE STRINGER STRAIN VARIATION.

COMPRESSIVE FORCE P = 17,000 LB SHEET THICKNESS t = .020 IN.

THEORETICAL

CYLINDER NO. 7 O BAND A X BAND B

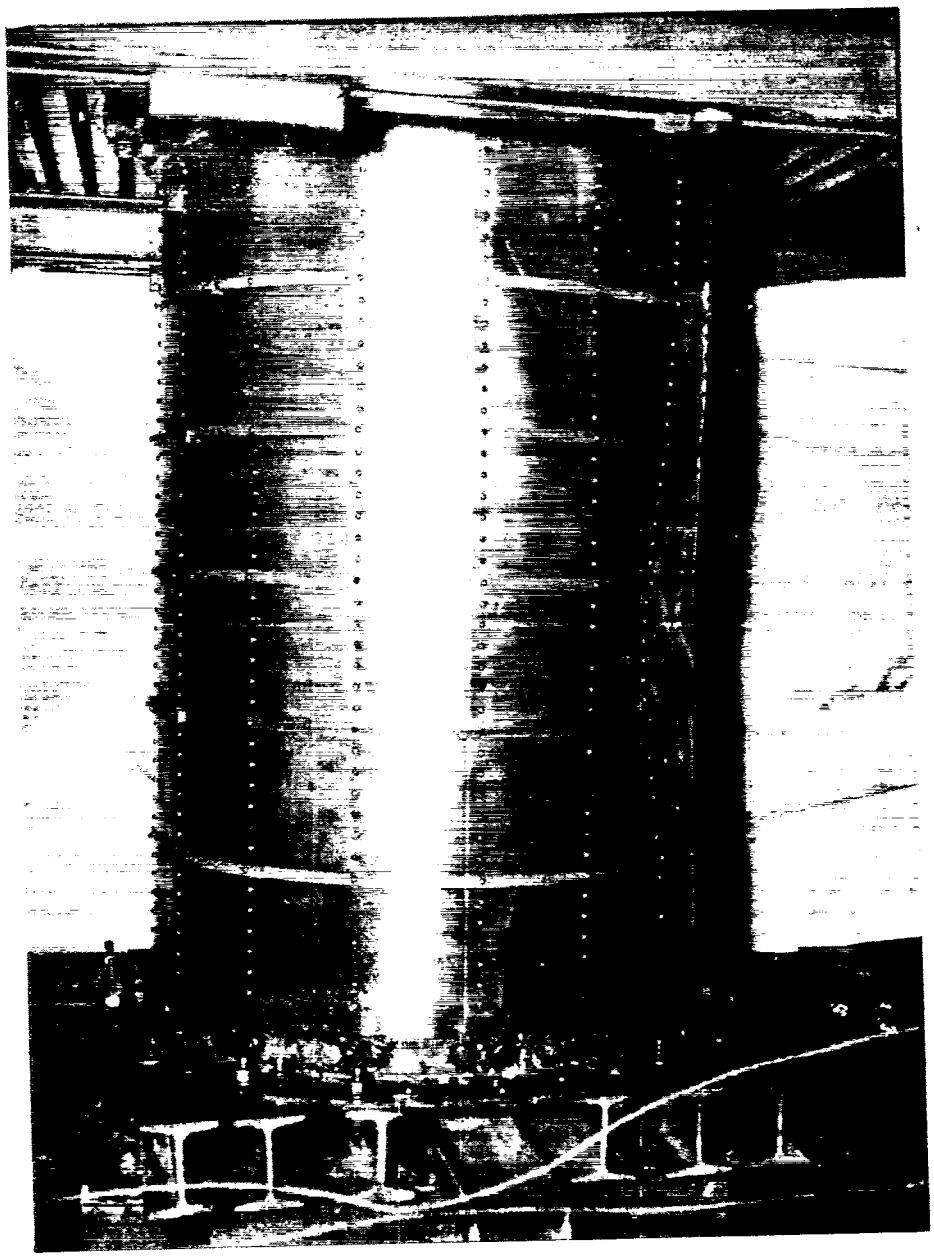

Figure 64. - Test cylinder No. 5 (after buckling).

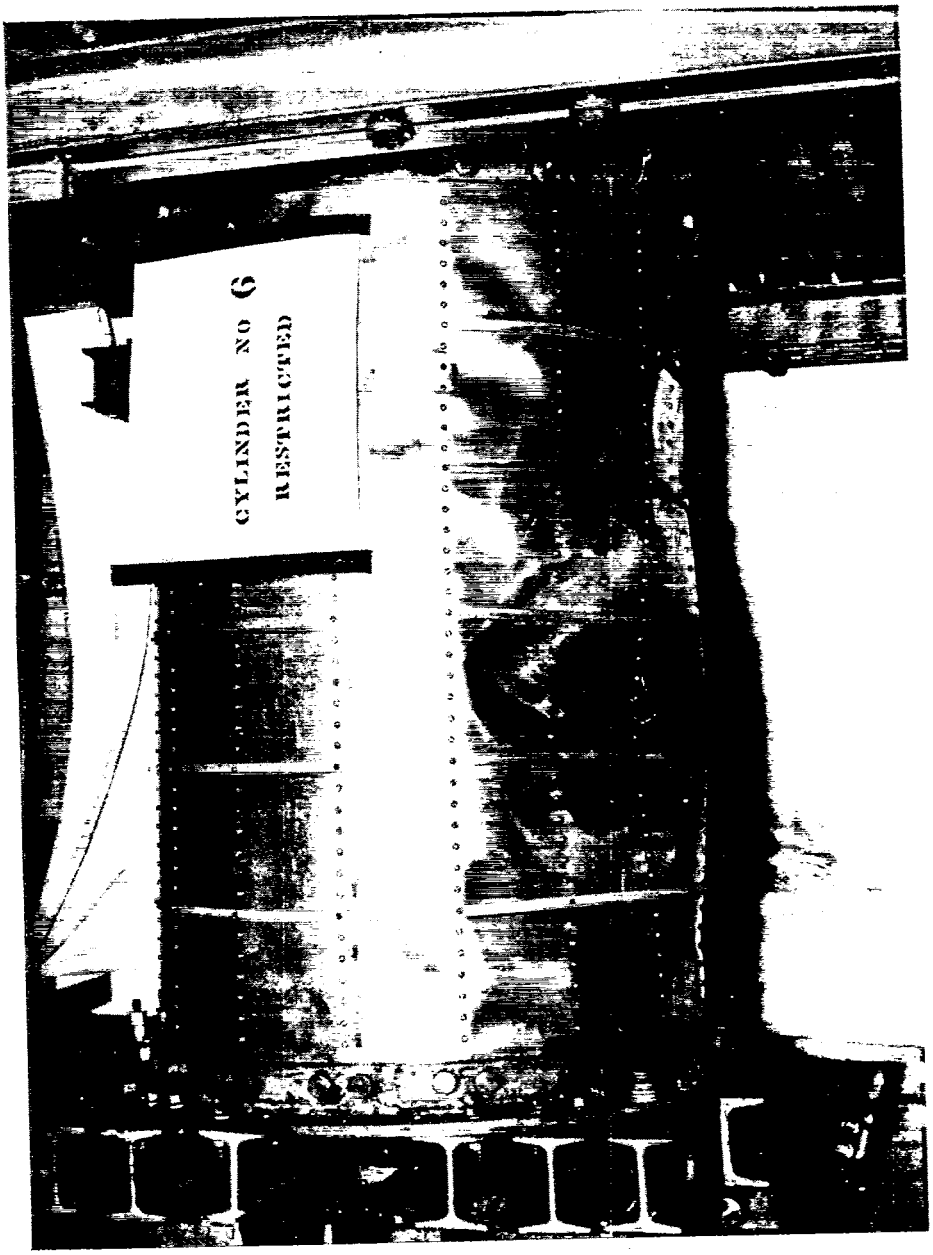

Figure 65. - Test cylinder No. 6 (after buckling).

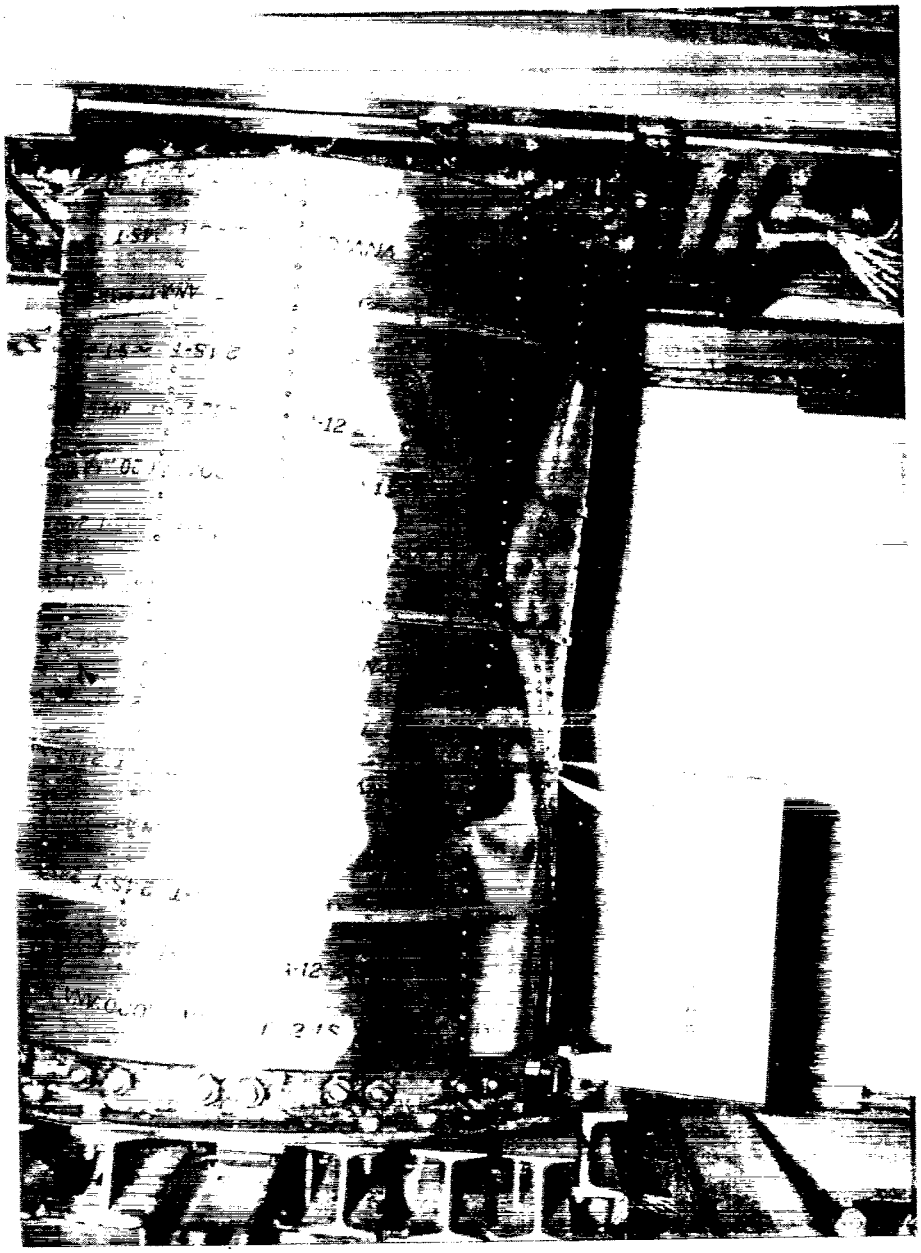

Figure 66. - Test cylinder No. 7 (after buckling).

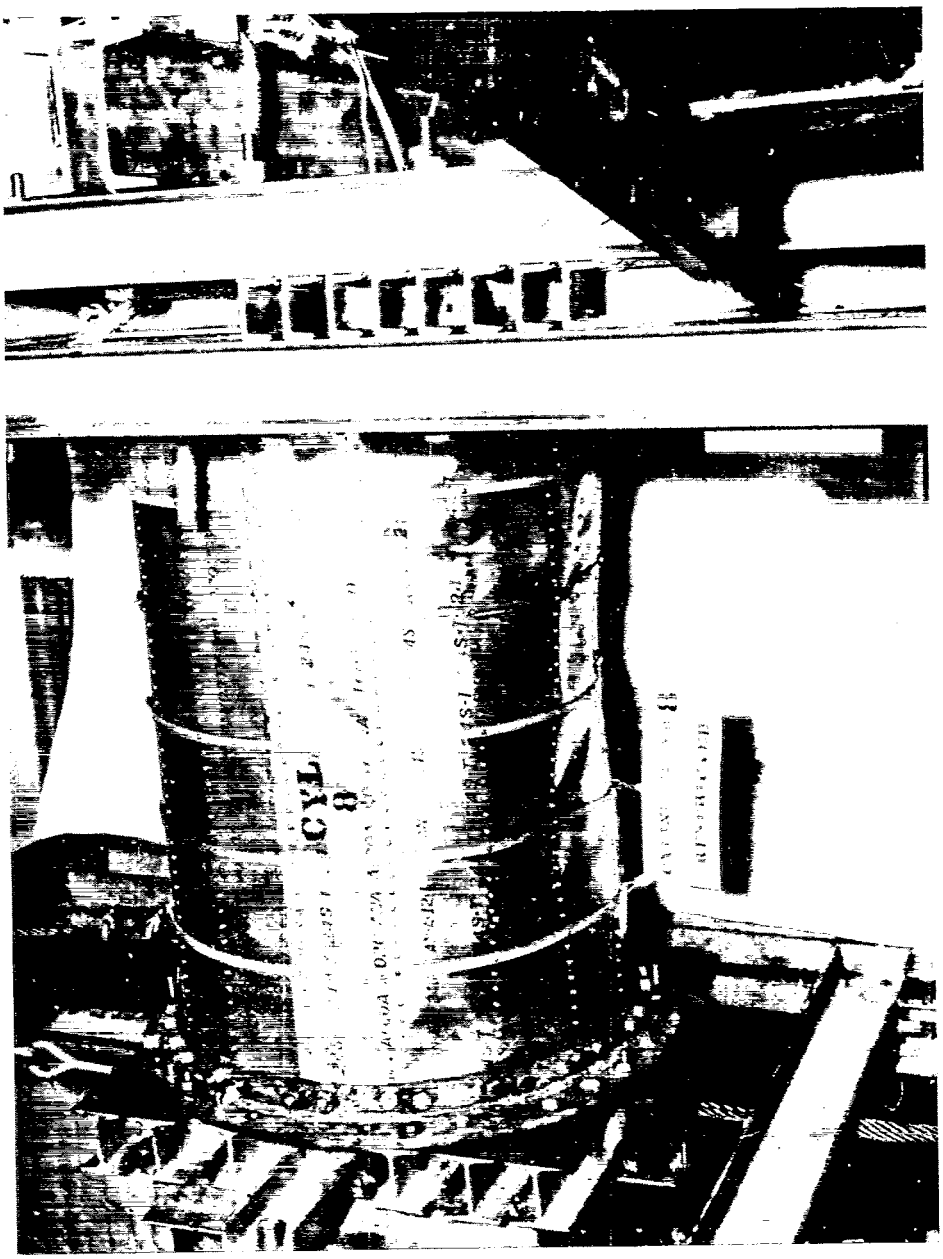

Figure 67. - Test cylinder No. 8 (after buckling).

Figure 68. - Test cylinder No. 9 (after buckling).

Figure 69. - Test cylinder No. 10 (after buckling).

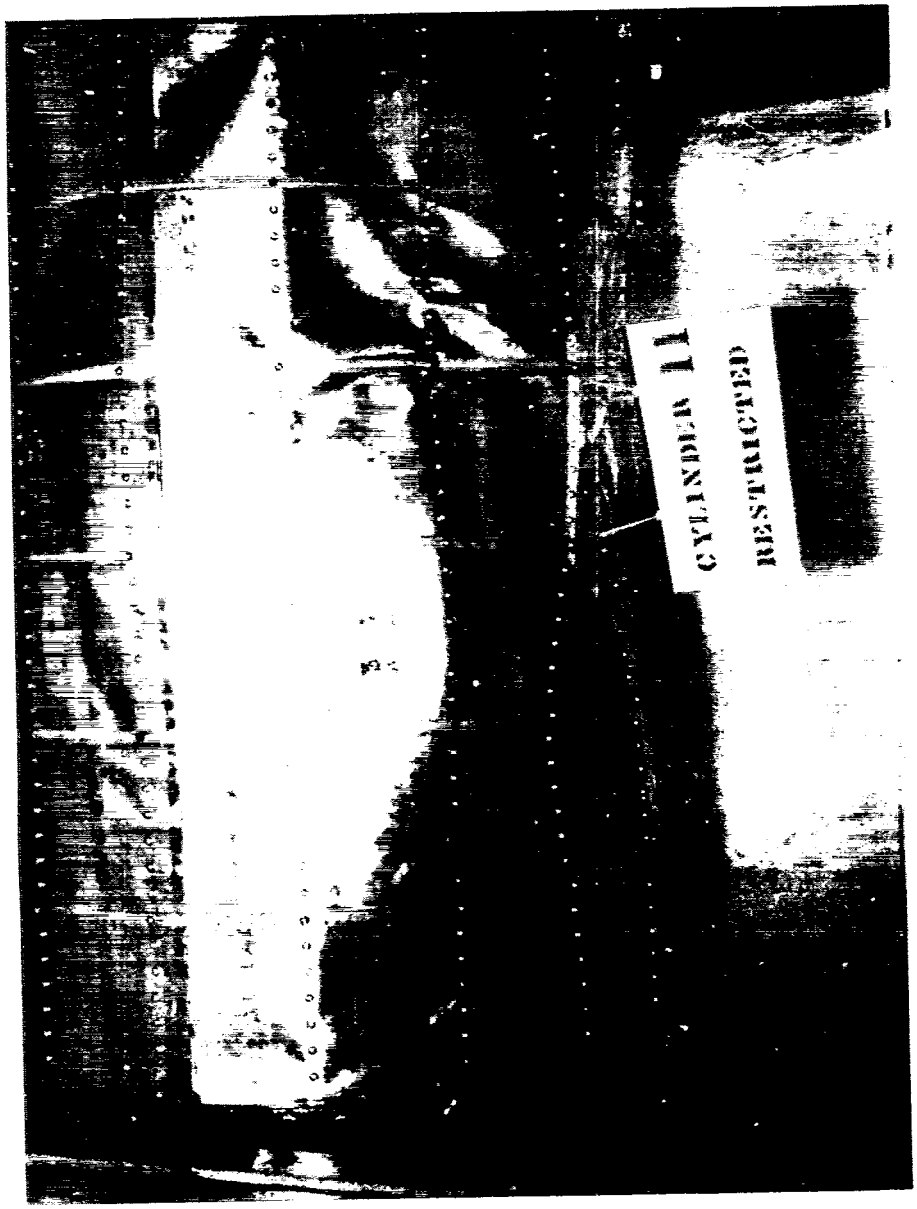

Figure 70. - Test cylinder No. 11 (after buckling).

Figure 71. - Test cylinder No. 11 (after buckling) opposite side.

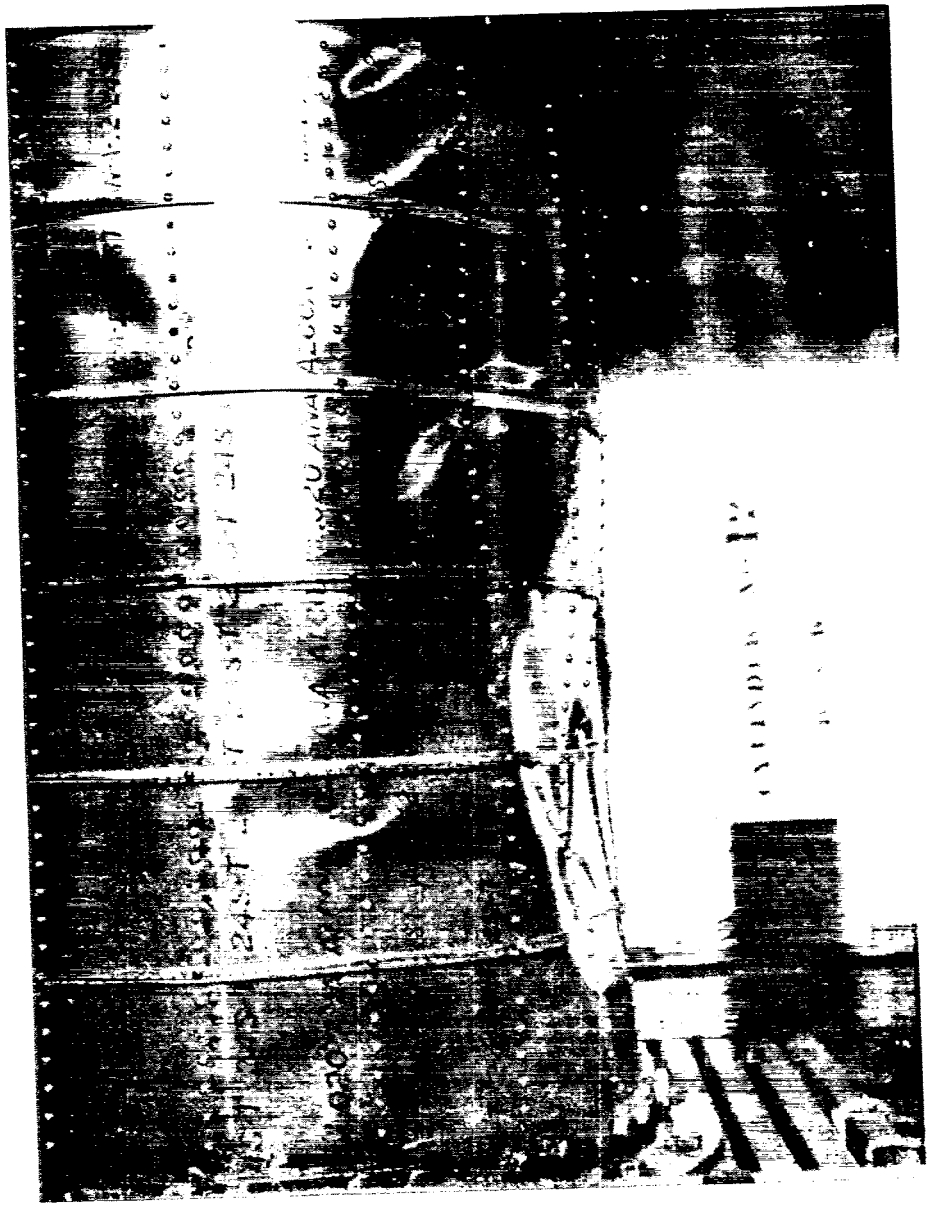

Figure 72. - Test cylinder No. 12 (after buckling).

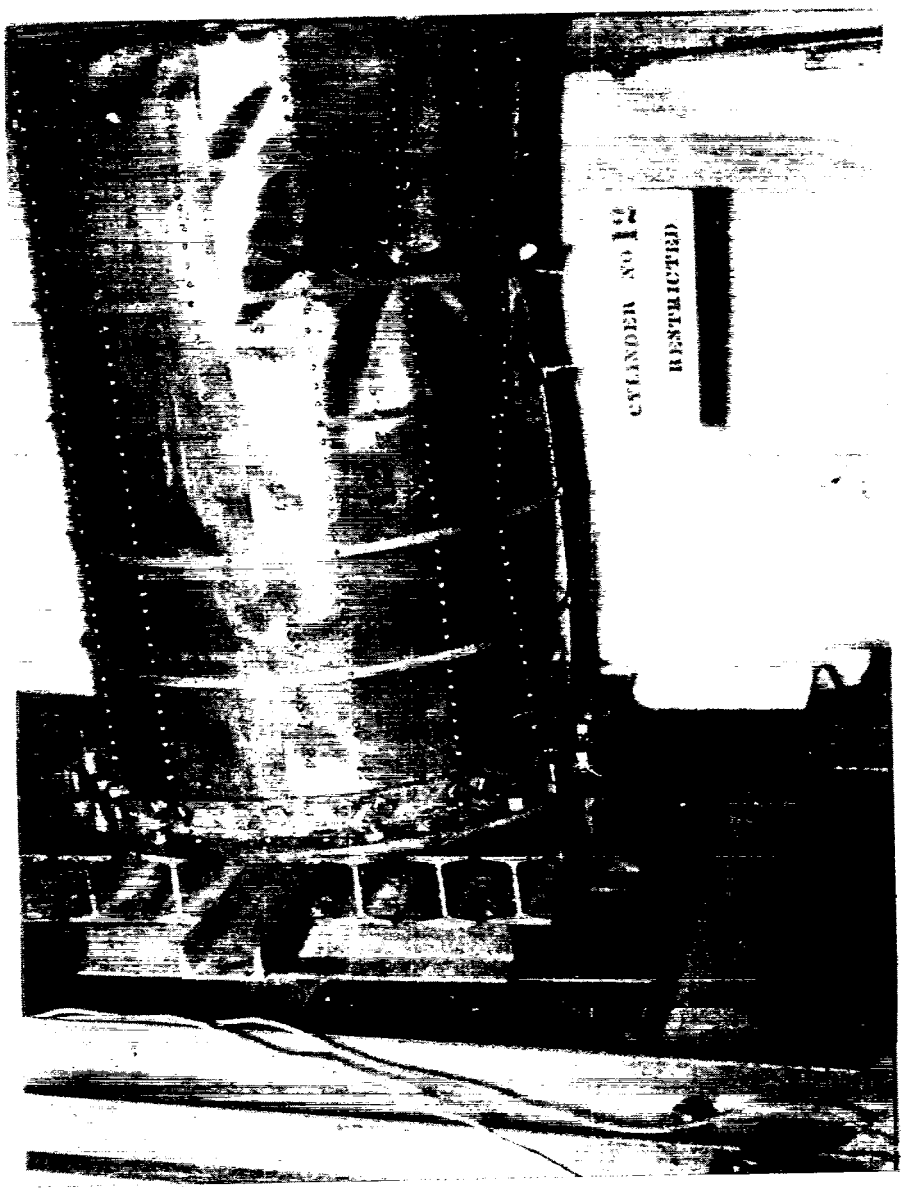

Figure 73. - Test cylinder No. 12 (after buckling) opposite side.

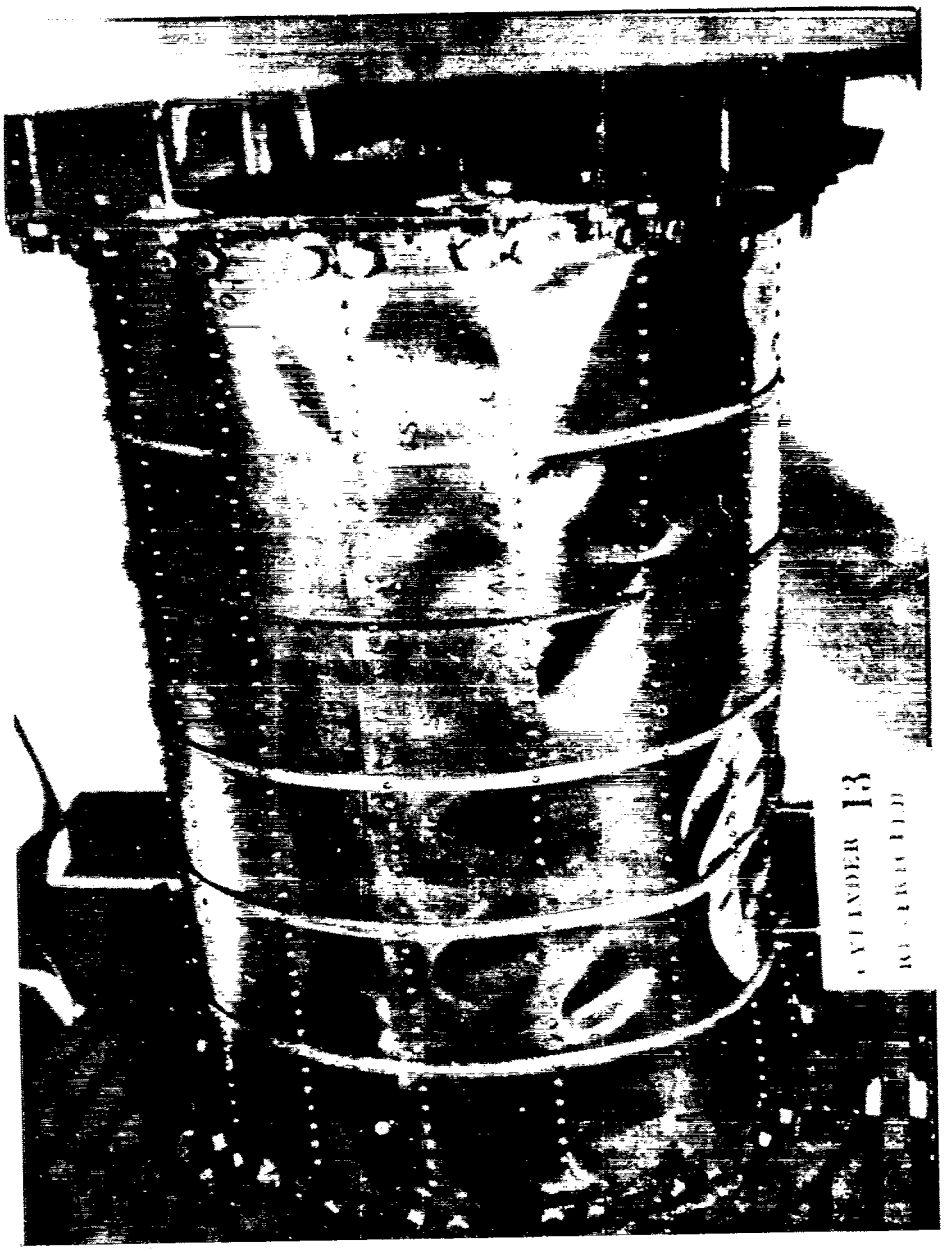

Figure 74. - Test cylinder No. 13 (after buckling).